Addis Ababa University

School of Graduate Studies

Faculty of Technology

Mechanical Engineering Department

FEA For Orthogonal Metal Cutting

By

Dawit Gebreamlak

Advisor

Dr.-Ing Tamrat Tesfaye

A Thesis Submitted to School of Graduate Studies of Addis Ababa University in Partial Fulfillment of the requirement for the Degree of Masters of Science in Mechanical Engineering (Mechanical Design Stream)

April **, 2010**

Addis Ababa University

School of Graduate Studies

Faculty of Technology

Mechanical Engineering Department

FEA For Orthogonal Metal Cutting

By Dawit Gebreamlak

APPROVED BY BOARD OF EXAMINERS:

Dr.-Ing Edassa Dribsa	_____	_____
CHAIRMAN, DEPARTMENT GRATUATE COMMITTEE (DGC)	SIGNATURE	DATE
Dr.-Ing Tamrat Tesfaye	_____	_____
ADVISOR	SIGNATURE	DATE
Dr. Tafesse G/Senbet	_____	_____
INTERNAL EXAMINER	SIGNATURE	DATE
Pro. Idalberto	_____	_____
EXTERNAL EXAMINER	SIGNATURE	DATE

Declaration

I, the undersigned, declare that this project report entitled “FEA For Orthogonal Metal Cutting” is the result of my own research carried out under the supervision of Dr.-Ing Tamrat Tesfaye. It has not been presented as a thesis in any other university and all source of material used for this thesis are duly acknowledged.

Dawit Gebreamlak	_____	_____
Candidate	Signature	Date

This is to certify that the above declaration made by the candidate is correct to the best of my knowledge.

Dr.-Ing Tamrat Tesfaye	_____	_____
Advisor	Signature	Date

ACKNOWLEDGEMENT

I would like to deeply thank my thesis Advisor Dr.-Ing Tamrat Tesfaye for his unconditional support, guidance and understanding, continuous support throughout my work and really will be infinitely profitable for the rest of my life.

I would also like to thank Ato Tefera Shimelis lab-assistance for his encouragement and support throughout the work.

Special thanks go to Ato Tasew Mekuria for his relentless efforts in providing and sharing his profound experience throughout my experiment task which takes place at AAU mechanical workshop.

I am indebted to my fellow post graduate students, staffs and friends for their continuous support and the brainstorming discussions and I strongly believe that what I have learned from them during the study period is worthy to articulate for problem solving.

Lastly, I would like to express my deepest gratitude and respect to my family who made all the things possible. Their support and patience are just making me feel better.

Dawit Gebreamlak

March, 2010

ABSTRACT

The aim of this thesis is to investigate the information regarding the influence of the cutting tool geometry (rake angle) on the main cutting force, the influence of cutting speed on the main cutting force and on the surface texture of the workpiece , and the influence of feed of cut on the main cutting force for orthogonal metal cutting operations was investigated.
The effects of the main cutting force on stress and their distribution around the surface contact of cutting edge of cutter and workpeice by using finite element method (FEM) are analyzed. As simulation tool, commercial Finite Element Method is used. Simulation is one of tools that have been used widely in several manufacturing areas and organizations. Using a valid simulation model gives several benefit and advantages in manufacturing in order to improve productivity. Separation of chip from the workpiece is achieved either only with continuous remeshing or by erasing elements according to the damage accumulated. From the results cutting forces can be estimated. For verification of results several cutting experiments are performed at different cutting conditions, such as rake angle and feed rate. Results show that commercial code is able to simulate orthogonal cutting operations within reasonable limits.

Plain damage model seems not appropriate for separation purposes of machining simulations. On the other hand, although remeshing gives good results, it leads to the misconception of crack generation at the tip of the tool. Therefore, a new separation criterion is necessary to achieve both good physical modeling and prediction of process variables.

Keywords: Finite Element Method, Orthogonal Metal Cutting.

TABLE OF CONTENTS

LIST OF FIGURES

LIST OF TABLES

LIST OF SYMBOLS AND ABBREVIATIONS

θ	Angle of Obliqueness
a_c	Uncut Chip Thickness
a_0	Chip Thickness
γ	Rake Angle
φ	Shear Angle
α	Clearance Angle
V	Relative Velocity Between Tool and Workpiece
Vc	Cutting Speed
B.U.E.	Built-Up Edge
β	Friction Angle
F_f	Frictional Force
Fn	Normal Force
F	Equivalent Force
μ	Friction Coefficient
h_1	Length of Sticking Region
h_1	Length of Sliding Region
Fc	Cutting Force
Ft	Thrust Force
F_{f}	Feed Force
f	Feed
d	Depth of cut
$A_{\mathbf{s}}$	Shear Area
A_{cutting}	Cutting cross sectional area
$t_{\mathbf{c}}$	Chip Thickness
$w_{\mathbf{c}}$	Width of Chip
l_c	Contact Length

CHAPTER 1

INTRODUCTION

1.1 Introduction

Manufacturing technology has been the driving force behind modern economics since the Industrial Revolution (1770). Metal shaping processes, in particular, have created machinery and structures that permeate almost every aspect of human life today. Although manufacturing techniques have become more sophisticated, many processes and tool designs are still based on experience and intuition.

There are mainly two distinct classes of solid-state manufacturing processes. Deformation processes produce the required shape, with the necessary mechanical properties, by plastic deformation in which the material is moved and its volume is conserved. Machining processes produce the required shape by removal of selected areas of the work piece through a machining process. Most machining is accomplished by straining a local region of the work piece by the relative motion of the tool and the work piece. Although mechanical energy is the usual input to most machining processes, some of the newer metal removal processes employ chemical, electrical and thermal energy. Machining is usually employed to produce shapes with high dimensional tolerance, good surface finish and often with complex geometry. Machining is a secondary processing operation since it is usually conducted on a work piece that was produced by a primary process such as hot rolling, forging or casting, etc. More than almost 80 percent of all manufactured parts must be machined before they are completed. There is a wide variety of machining processes and machine tools that can be utilized. Since the development of machine tools is parallel to the industrialization of the society, it is an old field with much specialized terminology.

The majority of industrial applications of machining are in metals. Although the metal cutting process has resisted theoretical analysis because of its complexity, the application of these

processes in the industrial world is widespread. Machining processes are performed on a wide variety of machine tools. The basic machine tools are lathe machines, milling machines, drill presses, grinders, shapers, broaching machines, and saws. Workpieces are held in workholding devices, such as a three-jaw chuck. The tools used to cut metal are in the turrets.

Each of the basic machine tool types has many different configurations. Lathes, for example, may be engine lathes, turret lathes, tracer lathes, or automatic-screw machines. Lathes have followed the trend of other machine tools, and NC lathes can now be routinely purchased.

The primary chip formation processes are listed below, with alternative versions in parentheses. Each process is performed on one or more of the basic machine tools. For example, drilling can be performed on drill presses, milling machines, lathes, and some boring machines:

- Turning (boring, facing, cutoff, taper turning, form cutting, chamfering, recessing, thread cutting).
- Shaping (planing, vertical shaping)
- Milling (hobbing, generating, thread milling)
- Drilling (reaming, tapping, spot facing, counterboring, countersinking)
- Sawing (filing)
- Abrasive machining (grinding, honing, lapping)
- Broaching (internal and surface)

Metal cutting processes are widely used to remove unwanted material and achieve dimensional accuracy and desired surface finish of engineering components. In metal cutting processes, the unwanted material is removed by the cutting tool, which is significantly harder than the work piece. The width of cut is usually much larger than the depth of cut and thus, the chip is produced in a nearly plane strain condition

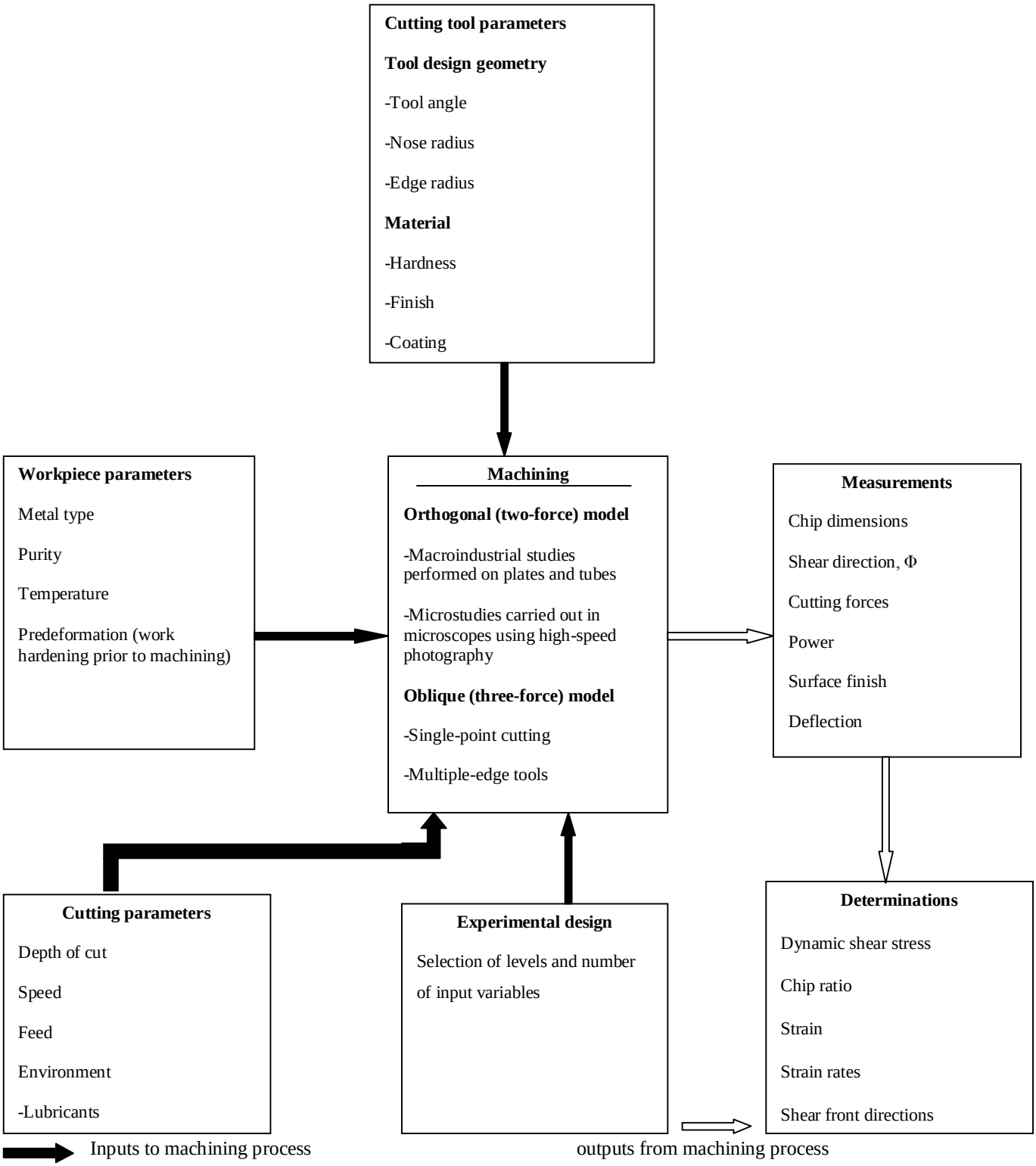

Fig.1. 1 Input/output relationships in metal cutting (machining)

Metal cutting processes can be viewed as consisting of independent (input) variables, dependent variables, and independent-dependent interactions or relationships. The engineer or machine tool operator has direct control over the input variables and can specify or select them when setting up the machining process. Several input variables are described above. Figure 1 summarizes the input/output relationships associated with metal cutting.

A cutting tool is a piece of metal having a single or a number of hardened (or hard) cutting edges, suitably shaped. For a cutting tool to give satisfactory performance work produced should have the desired finish and dimensional accuracy and the cutting tool itself should have adequate life under economical conditions of operation. To have adequate life and give satisfactory performance, the cutting tool must be designed such that it has adequate strength, the point of cutting tool has enough volume to dissipate the heat generated owing to friction, and the material of the cutting tool has adequate wear resistance under normal working temperatures. All these severe requirements call for adequate attention to the cutting tool geometry. The cutting tool geometry refers to the angles provided on the cutting tool face and flanks and the shape of the cutting edge. These angles, except side cutting edge angle, are provided to reduce, to a minimum, the rubbing of the cutting tool against the chips and the work material and to cause the chips to impinge on wider areas.

Importance of metal cutting operations may be understood by considering the total cost associated with this activity. For example, in the USA, the yearly cost associated with metal removal has been estimated at about 10 percent of the gross national product [1]. The importance of the cutting process may be further appreciated by the observation that nearly every device in use in our complex society has one or more machined surface. Therefore, there are several reasons for developing a rational approach to material cutting:

1. Improve cutting: Even minor improvements in increasing production volume and reduce production time are of major importance.
2. Produce products of greater precision and of greater useful life.
3. Increase the rate of production and produce a greater number and variety of products with the tools available.

Metal cutting is a typical irreversible process, comprising large plastic deformation coupled with temperature rise at high strain rates. From a continuum mechanics point of view, suitable constitutive or governing equations that can describe this phenomenon are needed to predict chip flow, cutting forces, cutting temperature, tool wear, etc. However, the solutions of displacement or velocity, stress, strain and temperature fields in metal cutting processes have not easily been obtained since large deformations and temperature rise lead to highly nonlinear and time dependent mechanics of the process.

Cutting processes are quite complex, largely due to the fact that two basic operations occur simultaneously in a close proximity with strong interaction.

1. Large strain and partly extremely large strain-rate plastic deformation in a zone of concentrated shear.
2. Material transport along a heavily loaded region of relative motion between chip and tool.

In general, several simplified models which emphasize different aspects of the problem such as thermal, material and surface considerations are operative simultaneously with varying degrees of importance depending on specific machining conditions. Due to complexities of the problem, a general predictive theory is not possible. Thus, an easier method was to illustrate how fundamental concepts may be used to explain observed results from carefully planned experiments and how solutions to new machining situations may be achieved by application of scientific principles.

The plane-strain orthogonal metal cutting process, for which, the direction of relative movement of wedge-shaped cutting tool is perpendicular to its straight cutting edge, has been extensively studied since it provides a reasonably good modeling of the chip formation on the major cutting edge of many metal removal processes such as turning, facing, milling, drilling, etc.

A computational approach using the finite element method soon became a mainstream for the analysis of machining after it has been developed. Because, it provides a nearly exact displacement and/or velocity field depending on the assumptions made while building the model for orthogonal metal cutting operation. Of course, it is continuing to find even more usage in response to quick and revolutionary developments in computer hardware.

1.2 Aim and Scope of the Study

This work is motivated by the fact that machining is a very common process in the industry and experimental observations with trial and error periods are still needed for the process optimization. Hence, the availability of a successful finite element model for the prediction of process variables cutting speed, feed rate, rake angle are very important in decreasing experimentation, which is quite time consuming and expensive. In addition, simultaneous engineering of product and its machining operations can be achieved by optimizing cutting conditions through modeling.

Cutting forces have considerable effect on machine tool design. The force in the direction of speed is the cutting force acts in a direction tangential to the surface machined. The magnitude of cutting forces to perform a machining operation depends on several factors such as cutting tool geometry, cutting speed, feed and depth of cut, quality of work material and cutting tools. Of these factors, the cutting tool geometry determines, to a large extent, its efficiency relative to the forces exerted. The cutting tool geometry has an important factor on cutting forces and cutting forces are essential sources of information about productive machining.

Thus, in this project the information regarding the influence of the cutting tool geometry (rake angle) on the main cutting force, the influence of cutting speed on the main cutting force and on the surface texture of the workpiece , and the influence of feed of cut on the main cutting force for orthogonal metal cutting operations was investigated. This orthogonal cutting is defined as a cutting operation where, cutting edge of the tool is perpendicular to the relative motion between

the tool and workpiece.Then, observations of the effects of several parameters on the results will be done.

These parameters can be as the variables related with cutting conditions and these cutting conditions can be changed by altering the rake angle of the tool, feed rate, cutting speed, etc.

1.2.1 General Objectives

- The main objective of this project is to determine the effect of cutting tool geometry, especially rake angle on the main cutting force in orthogonal metal cutting operations.
- To observe and analyze the effect of the main cutting force on stress and their distribution around the surface contact of cutting edge of cutter and workpeice by using finite element method (FEM). This will be done through modeling and simulating the hollow cylindrical material with the following condition to have a justified conclusion:-A pre-defined dimension of the hollow cylindrical material will be taken and the stresses and their distributions around the contact surface of cutting edge of cutter and workpeice will be analyzed and discussed.

1.2.2 Specific Objectives

- To develop two dimensional finite element models of orthogonal metal cutting Operations.
- Observing of the effects of several parameters on the results.
- Performing the experiments in AAU workshop for several cutting conditions like different rake angles and feed rates.
- Determination of the effect of cutting speed on the main cutting force for turning.
- Comparison of both experimental and analytical approaches.
- Taking the results from the experiments as input for observing the effect on the modeling.

CHAPTER 2

LITERATURE SURVEY

2.1 Introduction

In this chapter, an overview of the literature related with analytical and numerical solutions of metal cutting and chip formation will be given.

This chapter starts with a section in which fundamental mechanism of metal deformation, cutting tools, nomenclature and mechanics of chip formation is explained. In the second section, analytical solutions of shear angle relationships are given.

Third section explains the friction phenomena on the rake face of the tool which is in contact with the chip. Then, in fourth section, shear stresses observed in the shear zone are mentioned and discussed.

In the last section, Historical review of FEM in metal cutting and numerical models of orthogonal metal cutting are given. The development of models is explained in a historical order.

Fundamental Mechanism of Metal Deformation

Cutting Models. Before the mechanics of machining are presented, a brief discussion of the fundamental nature of the deformation processes is helpful in understanding the assumptions that accompany the mechanics. The machining geometry can be simplified from the three-dimensional (oblique) geometry, which typifies most industrial processes, to a two-dimensional (orthogonal) geometry. Figure 2.1 compares the oblique and the orthogonal cutting geometries. Orthogonal machining can be obtained in practice by:

- End cutting a tube wall by turning (Fig. 2.1b)
- Machining a plate as shown in Fig. 2.2.

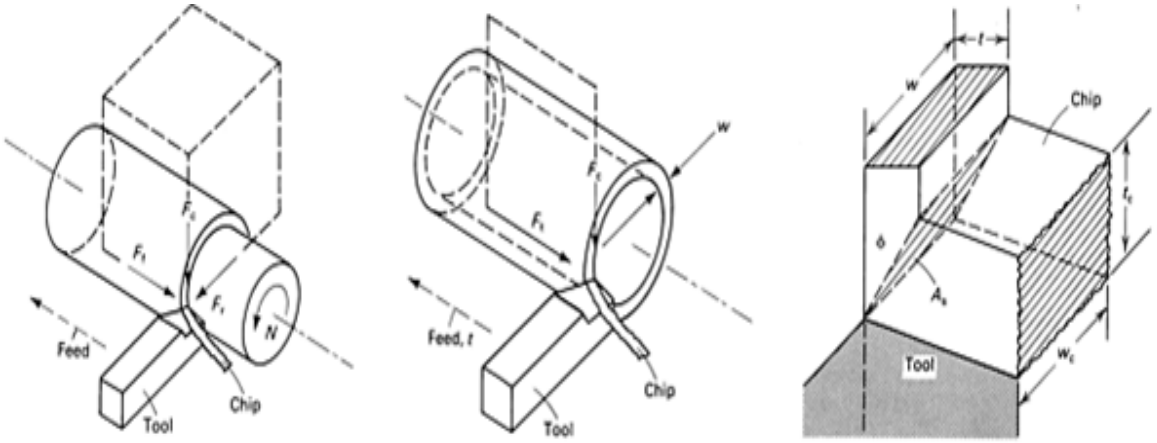

(a) (b) (c)

Fig.2.1 Comparison of oblique and orthogonal geometry machining. (a) Three-force oblique machining. F_c is the primary cutting force, F_f is the feed force, and F_r is the radial or thrust force. (b) Two-force orthogonal machining. F_c is the measured cutting force, and F_t is the feed (tangential) force. A tube-cutting application is shown; the cutting edge of the tool is perpendicular to the direction of motion. (c) For orthogonal cutting, the shear area, A_s occurs for a shear angle Φ, width of cut *w*, and feed *t*.

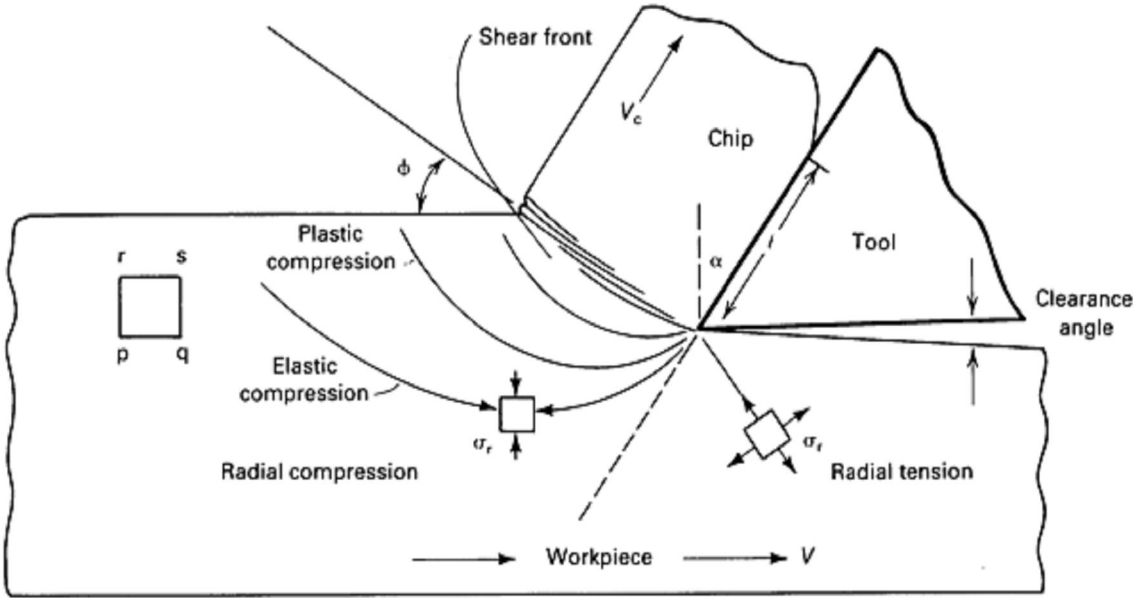

Fig. 2.2 Development of the shear front-lamella structure. As shown by this orthogonal geometry, shear deformation evolves from a radial compression zone.

In the orthogonal cutting of a tube (Fig. 2.1b), the width of the cut is equal to the thickness of the tube wall, *w*. The direction of shear is specified by Φ the shear angle. The cross-sectional area of the chip is given by $t_c \cdot w_c$, where t_c is chip thickness and w_c is the width of the chip. The cutting edge of the tool is perpendicular to the feed direction. The measured horizontal cutting force, F_c, is the force in the direction of the cutting velocity (or cutting speed). The force in the direction of the feed (vertical or tangential) and perpendicular (orthogonal) to F_c is denoted by F_t. With this two-dimensional model of chip formation, the influence of the most critical elements of the tool geometry (rake angle, γ, and the edge radius of the tool) and the interactions that occur between the tool and the chip can be more easily examined.

Oblique cutting is obtained when the cutting edge and the cutting motion are not perpendicular to each other. The oblique machining in Fig.2.3 with the inclination angle i equal to non-zero. The inclination angle i is the angle between the cutting velocity and the normal to the cutting edge measured in the plane of the machined surface.

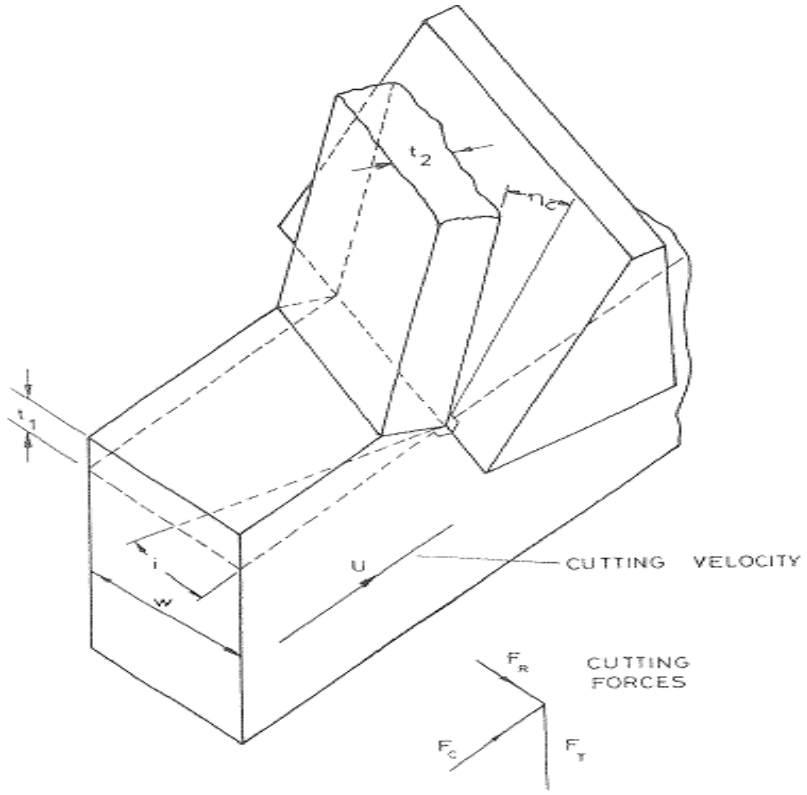

Fig.2.3 Model of oblique machining process.

Cutting Tools

Cutting tools are designed for machining various materials. They are extensively used in engineering, instrument making, mining, woodworking, medical equipment industry, agriculture, etc. In addition quite a number of tool plants built specially to produce conventional tools, tool department of large engineering plants have been given an impetus to expand their production over a broader scale in order to meet the requirements in special tools.

Correct sharpening and lapping of cutting tools is of great importance for attaining their high cutting properties. At an earlier stage of industrial development, tools were sharpened by hand with the aid of primitive grinding appliances. The enlargement of the range of tools, complication of tool shapes, and growing demand for tools have necessitated the employment of special tool-and-cutter grinding machines.

A cutting tool is a piece of metal having a single or a number of hardened cutting edges, suitably shaped. A cutting tool having a single cutting edge is called a single point cutting tool and a cutting tool having a number of edges is called a multipoint cutting tool. Single point cutting tools are used for a wide range of machining operations, such as turning, boring, shaping and planning. Multipoint cutting tools are used for milling, drilling, tapping, reaming, slitting and broaching. Basically, there is no difference between a single point cutting tool and a multi point cutting tool. The type of cutting tool to be used depends on the machine employed and the shape of the work surface required to be produced. It also depends, to an extent, on the quality of the work.

For a cutting tool to give satisfactory performance the work produced should have the desired finish and dimensional accuracy and the cutting tool itself should have adequate life under economical conditions of operation. To have adequate life and to give satisfactory performance, the cutting tool must be designed such that it has adequate strength, the point of the cutting tool has enough volume to dissipate the heat generated owing to friction, and the material of the cutting tool has adequate wear resistance under normal working temperatures. All these stringent requirements call for adequate attention to the cutting tool geometry, cross section, the material from which the cutting tool is made, and the heat treatment.

Cutting Tool Life

As tool damage, by wear or fracture, increases, the surface roughness accuracy of the machined surface deteriorates. Eventually the tool must be changed. Some criteria must be developed to decide when to do this. In factories there is a tendency to adopt flexible criteria according to the needs of a particular operation, while in laboratories inflexible criteria are adopted to evaluate tool and work material machining capabilities. Tool life dependence on the tool (material, geometry, surface integrity and internal defects), the work (hardness, strength, chemical composition, etc), the cutting conditions (speed, feed, depth of cut, cutting fluids), the cutting mode (turning, milling, drilling and others) and the machine tool (for example stiffness, state of maintenance), make a universal life criterion an impossibility.

Cutting Tool Materials

For the cutting element of a tool to plunge into the material of the work and to cut off a stock layer within a long period of time, the material of the cutting element must possess certain properties. First of all, this material should display very high hardness and strength. These features must be retained by cutting tool even after the latter has been heated to rather high temperatures in the process of cutting, in other words, the tool material must show adequate thermal stability, or red hardness.

The cutting element must withstand the abrasive effect of the work material within considerable periods of time and under the conditions of high pressures and temperatures, i.e., tool materials must offer high wear resistance. In addition, tool materials must be machinable in order to ensure the original manufacture of cutting tools and their re-sharpening in operation.

The force exerted by a cutting tool depends on the binding forces holding together the atoms of the work material. For example, the forces holding together lead atoms are much less strong than those holding the atoms of alloy steels. Hence, the forces exerted by the cutting tool to machine alloy steels is much more than that required to machine lead. As such, the force exerted by the cutting tool varies depending on the material to be machined.

All these features depend upon the chemical composition, the structure, and the physical and mechanical properties of the tool materials. Considering all these, it is imperative that due consideration is given to the properties of the cutting tool materials. The selection of the material of the cutting tool is determined by many factors, e.g., cutting variables (speed, feed, and depth of cut), the kind of cut, continuous or intermittent and the wear encountered. Today, cutting tools are made of carbon and alloy tool steels, high-speed tool steels (H.S.S.), cemented carbides, mineral ceramics, diamonds, and abrasive materials.

Comparison of Cutting Tool Materials

Materials available for cutting are many, ranging from plain carbon steels to diamonds and in each of these there are various proprietary brands. The brands available especially in cemented carbides are so large that it is almost impossible to make a choice unless one is aided by the manufacturers who, after extensive tests, specify the applications. However, a general comparison between various materials is possible (Table 2.1).

Characteristic	Plain carbon steels	Low alloy steels	High speed steels	Cast Non-ferrous alloys	Cemented carbides	Ceramics	Diamonds	Remarks
Typical Composition	Carbon 1.2% balance iron	Si 0.25% Cr 0.25% Va 0.25% Mn 1.2% Balance iron	C 0.75-1.5% W 18% Cr 3.15-4.2% Va 1.78-2.0% Balance iron	Mn 0.3% Cr 20% W 14% C 1.7% Co 53%	W & other carbides such as Ta, Li, Co used as binder	Al2O3 95% Co 5%	C 100%	
Relative cost:								
Material	Low	Slightly high	High	Higher	V.High	V.V. High	Prohibitive	
Grinding	Low	Low	High	High	V.High	Not known	Not known	
Hardness	R c55-64	R c60-64	R c62-65	R c62-65	R c87-92	R c90-95	10(Mho's cale)	
Hot hardness temperature	200° C	300° C	500° C	600° C	800° C	1200° C	1500° C	
Cutting speed (Grey cast iron)	20m/min	25m/min	35m/min	70m/min	150m/min	300-400 m/min	500m/min	
Toughness	Good	Good	Fair	Fair	Poor	V .Poor	Poorest	
Wear resistance	Poor	Poor	Fair	Fair	Good	V .Good	Excellent	
Typical Uses	Form tools	Form Tools	Wide use everywhere	Single point cutting tools	Wide use particularly for cast irons	Use will increase with time	Hardly any	

Carbon tools are cheap on weight basis. They also have low fabricating cost. The plain carbon tool steel can be sharpened to a knee cutting edge. On the other hand, these cutting tools loose their hardness at temperature beyond 200^0C and, therefore, the speed of operation is limited. Its use is recommended where low speeds are used such as form tools including threaded cutting tools and parting tools for small quantity manufacture. Besides the above, these cutting tools have little application in modern production.

Low alloy steels are only a small improvement on plain carbon steels. The costs, both for material and for grinding, are higher by about 25 percent. The speeds used are also higher by about 30 percent. They have much the same application as plain carbon steels.

Cutting Tool Geometry

Cutting tool geometry refers to the angles provided on the cutting tool face and flanks and the shape of the cutting edge. One of the simplest and most commonly used kinds of cutting tools is the lathe tool. It consists of cutting point and shank; the latter serves for installing the tool holder.

The principal elements of the tool cutting portion include:

i) Face along which chips flow,
ii) End flank and side flank which face the work-piece,
iii) The intersections of these surfaces forming, side (main) cutting edge and end (auxiliary) cutting edge,
iv) Tool nose which is the point of conjunction of the cutting edges; it is frequently rounded to a radius, lying usually between 0.1 and 2.0 millimeters.

The principal angles of a tool are measured in the main reference plane which is perpendicular to the projection of the side cutting edge onto the basic plane.

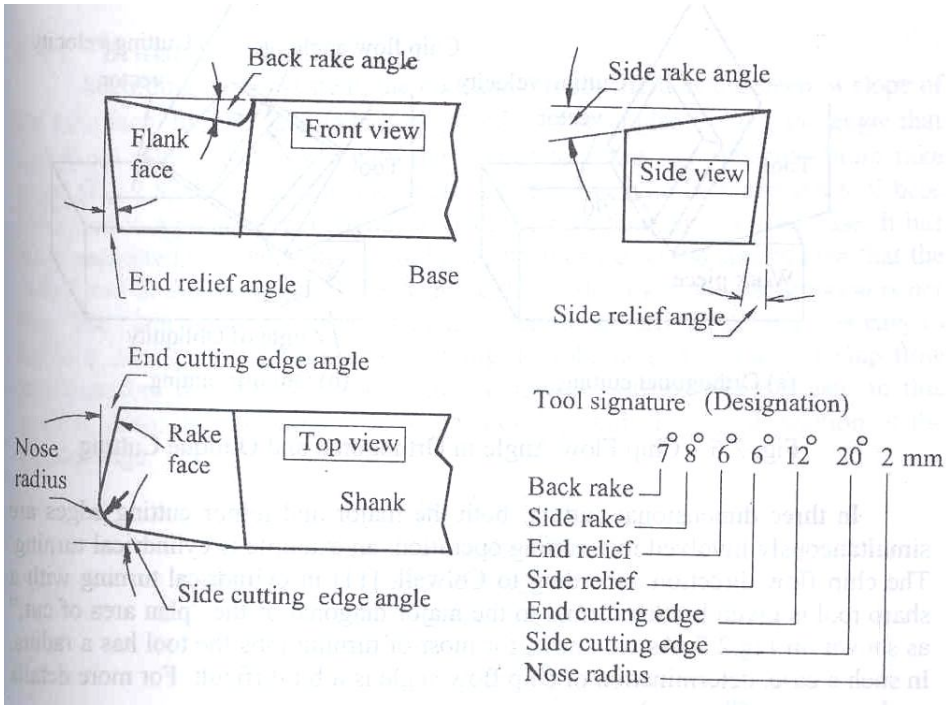

Fig 2.4: A.S.A. (American System) designation of cutting tools

Cutting Tool Signature

The cutting tool signature can be specified in many different ways. American Standard Association describes it in case of single point cutting tools by means of six angles and a nose radius,

i) back rake angle,
ii) side rake angle,
iii) front relief angle,
iv) side relief angle,
v) front cutting edge angle,
vi) side cutting edge angle, and
vii) nose radius

The back and side rake angles are defined in different countries. The other angles, namely, relief and cutting edge angels, are defined in the same way in all countries. It may be added that the

differences in the definitions are merely academic and do not matter at all as far as the working of the cutting tool is considered.

Rake Angle

The rake angle has a complex influence on the temperature, forces and life of a cutting tool. An increase in the rake angle reduces the deformation of chips and, hence, a decrease in the amount of heat generated. Cutting forces also decrease since the wedging action is more concentrated and this further reduces the temperature rise. Consequently, there is an increase in cutting tool life and better surface finish of the work. Increase in the rake angle, on the other hand, decreases the mass of the metal in the immediate vicinity of the cutting edge and, therefore, the effective heat conductivity of the cutting tool is reduced.

Loss of conductivity causes greater temperature rise and, consequently, a decrease in cutting tool life. Taking into account these two contradictory influences, the rake angles used in practice are, by and large, as shown in Table 8.1. The rake angle has the largest single influence on cutting tool life, cutting tool forces, surface finish, and dimensional accuracy. The rake angle can be either positive or negative. It is positive when the face slops downwards from the plane perpendicular to the plane of the cut, zero when the face is in the same plane and negative when the face slops upwards.

The back and side rakes combine to form the slop of the cutting tool face, which governs the cutting forces and the cutting temperature. The two rake angles have, however, their individual effects. The back rake angle controls, to an extent, the direction of the chip flow. With a zero back rake, the chip would flow parallel to the work surface and have a tendency to entangle with the work and cause problem of removal. A proper back rake angle will cause the chip to flow at an angle to the axis of the work and strike the tool holder or a suitable chip breaker, curl and break into small fragments and can be easily disposed of. The side rake angle has a considerable effect on cutting forces. Increase in side rake angle decreases the wedge angle, and therefore, concentrates the forces on the primary deformation zone, thereby reducing the applied force considerably. At the same time, with the decrease in angle, the effective thermal conductivity is reduced and there is a tendency for the edge to crumble due to a decrease in the supporting material.

Relief Angle

A relief angle is the angle between a line perpendicular to the base and passing through any portion of the edge of the cutting tool point and a line in the respective flank perpendicular to the edge. Relief angles are associated with their respective edges, e.g., side cutting edge relief angle, front cutting edge relief angle and nose relief angle. Normally, nose relief angle is not specified. The purpose of the relief angle, also called clearance angle is, as the name indicates, to keep the flanks from rubbing against the shoulder and machined surfaces, thereby eliminating unnecessary heat generation. The side relief angle is necessary to enable the cutting tool to be forced into the work.

The provision of relief angle reduces the mass of the metal and, thereby, the effective conductivity of the cutting tool point. Hence, relief angles should be as small as possible. In normal practice, this angle ranges from 5 to 8^0.

Cutting Edge Angle

A cutting edge angle is the angle between the edge of the cutting tool point and the respective side of the shank measured in a plane parallel to the base. Like clearance angles, the cutting edge angles measured are also associated with their respective edges, e.g., side cutting edge angle and front cutting edge angle.

The front cutting edge angle serves a purpose similar to the front cutting edge relief/clearance angle, namely, to clear the front cutting edge from the machined surface, and like clearance angles it is generally of the same range, viz. 5 to 8^0.

A cutting tool with a large cutting edge angle introduces chatter at the cutting edge. Increased cutting edge angle also increases radial force which gives rise to bending particularly in slender work. With cutting tools having a cutting edge angle up to 25^0, chatter does not present any serious problem in rigid work.

Nose Radius

The junction of the side and front cutting edges of the cutting tools are often blended by a curve called the nose. The radius of this curve is called the nose radius of the cutting tool. In some

cases the junction between the two edges is formed flat. This is done to obtain smooth surface on the work. The cutting speeds for machining with flat nose cutting tool is low, of the order 10 meters per minute. The nose radius plays an important part in the machining of metals. It smoothens the feed marks on the machined surface, strengthens the cutting edge and increases effective conductivity of the cutting tool.

The advantages and disadvantages of having a nose radius are the same having a side cutting edge angle. The effective feed is reduced in the curvilinear portion of the chip and the length of the chip is increased. This increase effective heat conductivity. The longitudinal and the radial forces increase, making the use of cutting tools difficult on slender work. Chatter is also increased. In general, a nose radius of 1.5mm is provided. On rigid work and on cast iron, a generous nose radius is used to advantage. Nose radius increases abrasion to an extent.

Table 2.2 Advantage and limitation of geometry.

Geometry	**Advantages**	**Limitations**
Rake Angles -5 to 20	Control chip flow, Reduce Cutting Force, Reduce Temperature, Improve surface finish	Weakens edges, Difficult to grind, Decrease cutting angles
Relief (about 6)	Reduce friction, Less flank wear	High stresses on the edge
Side cutting (about 15)	Reduce the heat , Improve surface finish	Separate the tool and workpiece, Tool chatter
End cutting (about 15)	Reduce heat	Reduce surface finish[1], Chatter
Nose radius (about 1/8")	Improve cutting speed , Improve surface finish	Separate tool and work, Tool chatter

2.2 Chip Formation and Nomenclature

Since the cutting process involves separation of metal, historically it was first believed to be a fracture process, involving crack formation and propagation. Later there was doubt whether or not a crack existed ahead of the tool. Mallock [2], who took some of the first photomicrographs of chip formation, claimed that a crack could be observed. However, Degarmo [3] opposed the interpretation of the original photographic evidence and claimed that no crack existed. Improved photomicrograph techniques have indicated that metal cutting is basically a plastic-flow process and there is no crack formation at the tool tip.

Most practical cutting operations, such as turning or milling, involve two or more cutting edges inclined at various angles to the direction of cut. However, the basic mechanism of cutting can be explained by analyzing cutting with a single cutting edge. The simplest case of this is known as orthogonal cutting, in which the cutting edge is perpendicular to the relative cutting velocity between tool and workpiece, as shown in Figure 2.5-a. A single cutting edge inclined to the cutting velocity as in Figure 2.5-b gives oblique cutting.

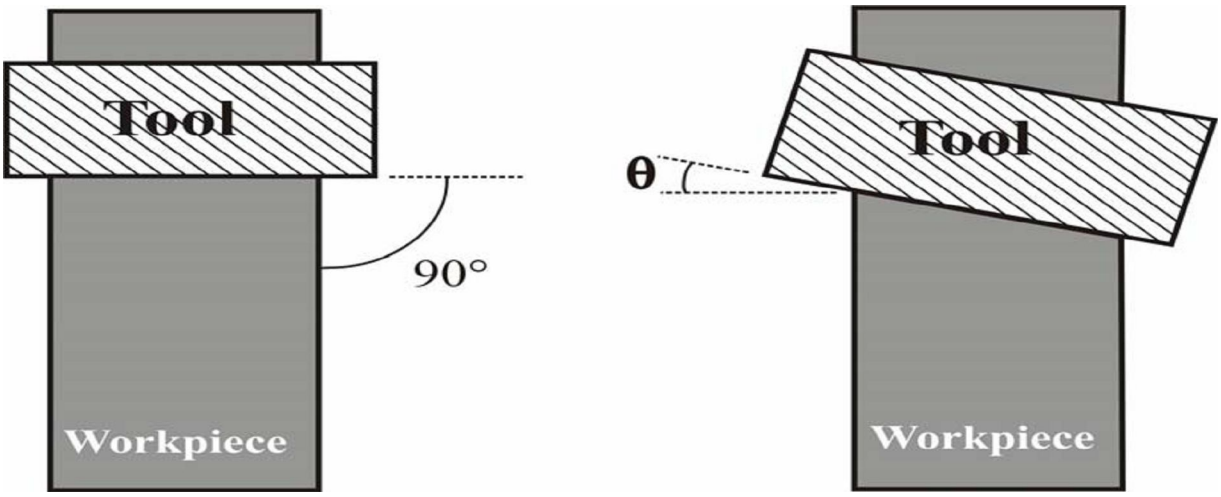

(a) (b)

Figure 2.5 (a) Orthogonal cutting (b) Oblique cutting

The nature of chip formation is approximately the same for orthogonal or oblique cutting with one or more cutting edges. Three basic types of chip formation are generally recognized:

1. Discontinuous-chip formation, which involves periodic rupture so that the chip forms as small separate segments
2. Continuous-chip formation
3. Continuous chip with built-up edge, where, a strain-hardened nose of material periodically builds up and breaks away from the cutting edge of the tool.

Figure 2.6 shows the photo-micrographs of chip samples produced by quick-stop techniques. The mentioned chip forms can be seen clearly.

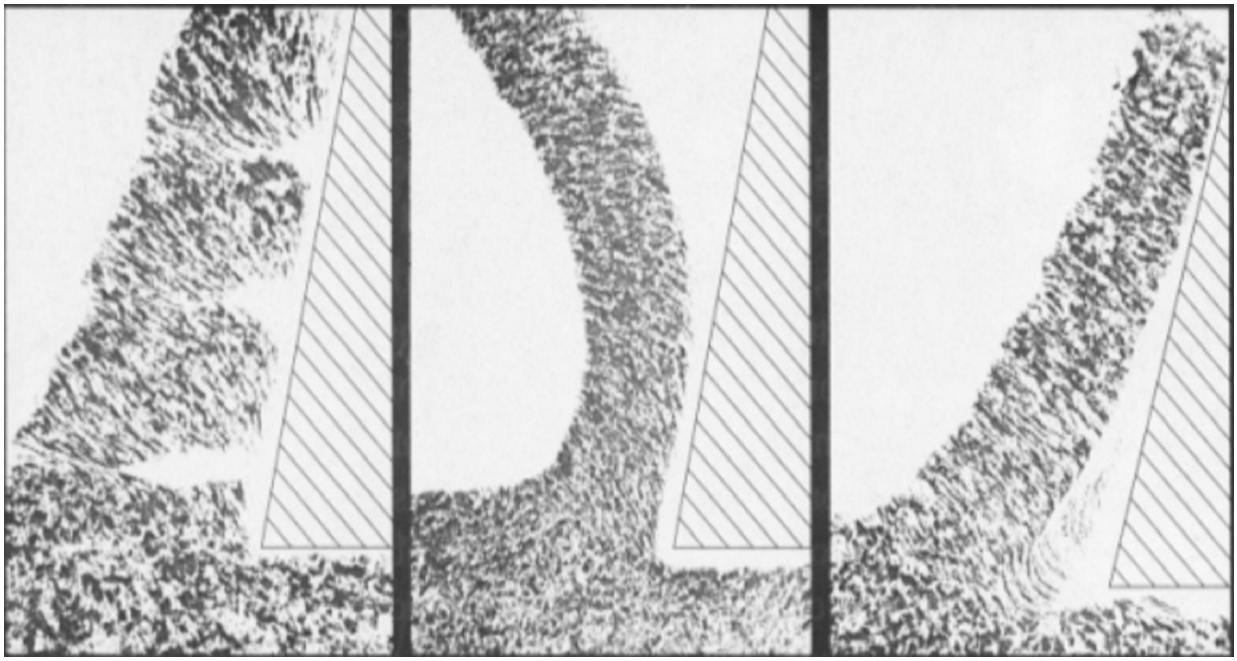

(a) (b) (c)

Figure 2.6: Chip samples produced by quick stop techniques. (a) Discontinuous (b) Continuous chip (c) Continuous chip with build-up edge [4]

In Figure 2.7, rake angle γ, undeformed chip thickness a_0, and chip thickness a_c are indicated for an orthogonal cut.

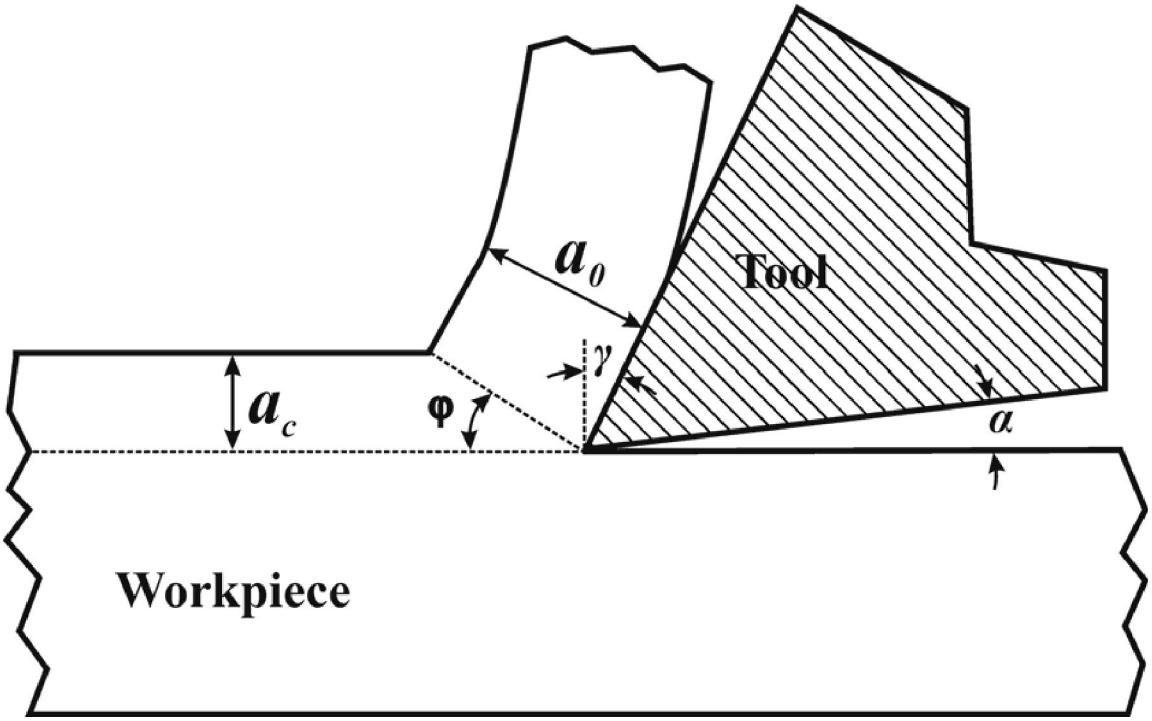

Figure 2.7 Some of the variables in orthogonal cutting: γ is the rake angle, a_0 is the undeformed chip thickness, a_c is the chip thickness and α is the clearance angle

Chip formation, at least with a continuous chip, is a plastic-flow process due to shear. There is, and has been for some time, considerable controversy about the shape of the plastic-flow region. Merchant [4] proposed a cutting model as in Figure 2.8-a. They claimed that the chip is formed by simple shear on a plane running from the tool tip to a point on the free surface workpiece. No plastic flow takes place on either side of this shear plane. Palmer and Oxley [5], and others, have suggested the deformation zone somewhat like that shown in Figure 2.8-b.

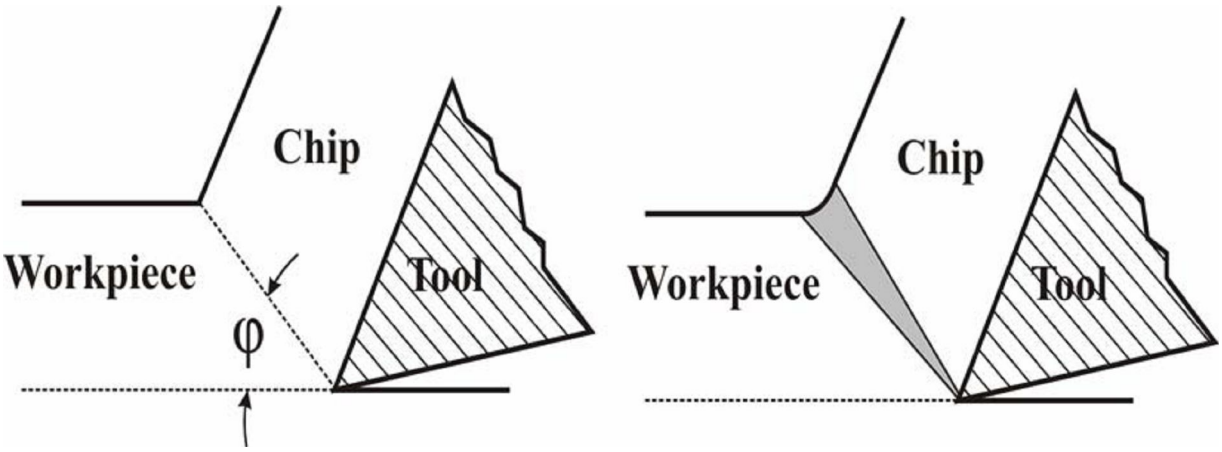

(a) (b)

Figure 2.8 Assumed shape of deformation zone in cutting:
(a) thin shear-plane model, where φ is known as shear angle (b) thick shear zone.

Careful examination of motion picture films and photomicrographs indicates that under different conditions the deformation approximates to one or the other of the above shear models. At low cutting speeds, particularly when cutting metals which are in the annealed condition, the thick-zone model is usually the most realistic. At high speeds, the thin-shear-plane model is approached (Figure 2.8).

The dependence of the plastic zone on cutting conditions can be illustrated by cutting wax. In tests with wax, it has been shown that at small, or negative, rake angles the plastic zone is very thin with a sharp transition between the top of the workpiece and the chip. On the other hand, at very large rake angles there is a gradual curvature from the workpiece into the chip, and a thick plastic zone.

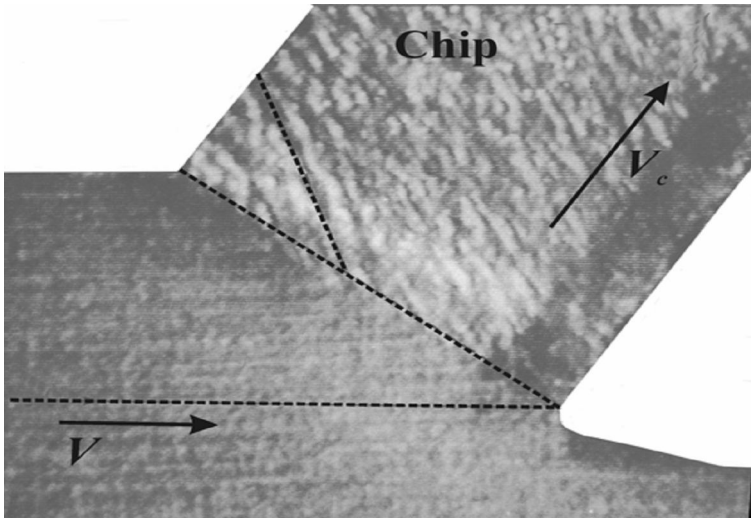

Figure 2.9: A photomicrograph of orthogonal cutting operation where thin shear plane is approached

Discontinuous chip formation, on the other hand, does involve some fracture. However, it is a non-steady-state process and between the fracture cycles there is some plastic flow as in continuous chip formation. This probably takes on a form as indicated in Figure 2.10. No doubt the plastic zone may at times approach to a thin plane. As the plastic zone spreads forward, the shear strain increases and fracture occurs. The properties of the material, as well as the cutting conditions, play a part in causing discontinuous chip formation.

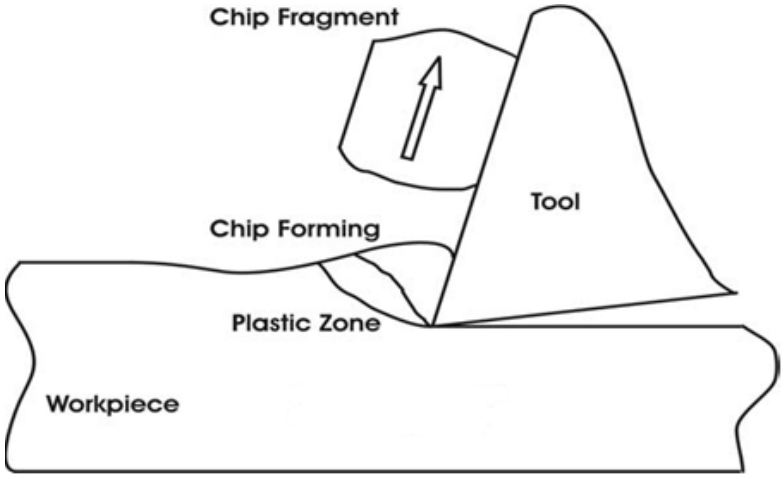

Figure 2.10: An illustration of the mechanism of discontinuous chip formation.

It must be realized that the change from one type of chip to the other is gradual and sometimes the chip fragments may not be completely separated. This is sometimes referred to as a semi-discontinuous chip, but it may be classified as discontinuous.

The formation of a built-up edge on the tool is brought about by high normal loads on the tool rake face, leading to adhesion between the chip and tool. This adhesion may be so severe that instead of sliding of chip over the tool rake face, rapture occurs within the chip after a considerable amount of plastic flow. Further layers build up, until a large nose of material may project from the cutting edge as shown in Figure 2.11.

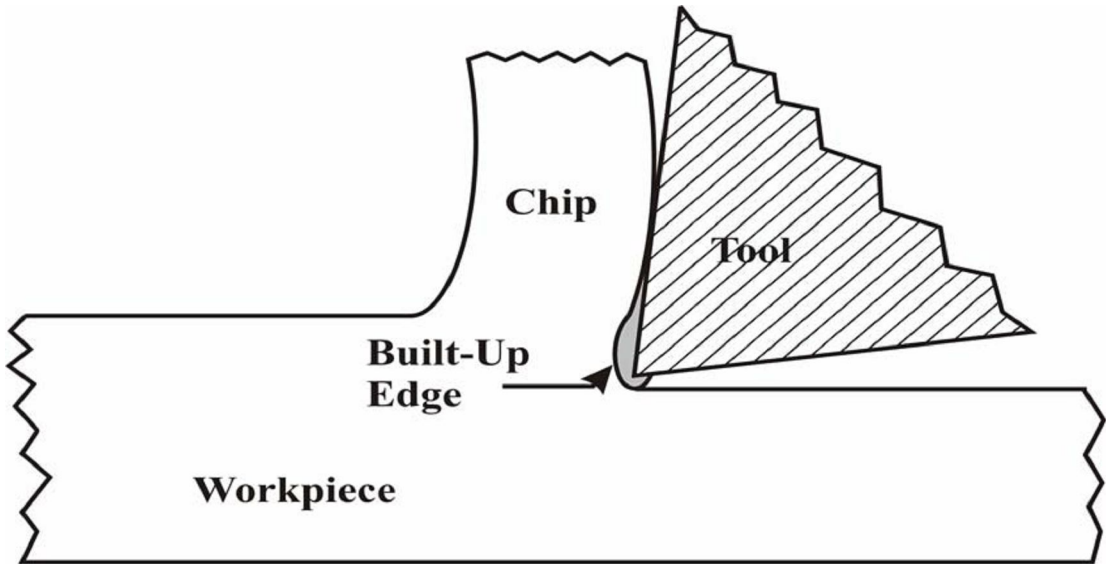

Figure 2.11. Idealized picture of built-up edge (B.U.E) formation.

Periodically, this nose fractures and the fragments are welded onto the chip and the workpiece. This mechanism is repeated with a frequency of the order of several cycles per a second.
The conditions in metal cutting are more extreme than in most of other deformation processes. The distinguishing features of the metal cutting process are the following:

1. It is a plastic-flow process with exceptionally large strains. There is a high compressive stress acting on the plastic zone and this prevents rupture from occurring until the strain is well above the rupture value in, say, a tensile test.

2. The deformation is localized to an extremely small plastic zone. Thus, the strain rate is unusually high.

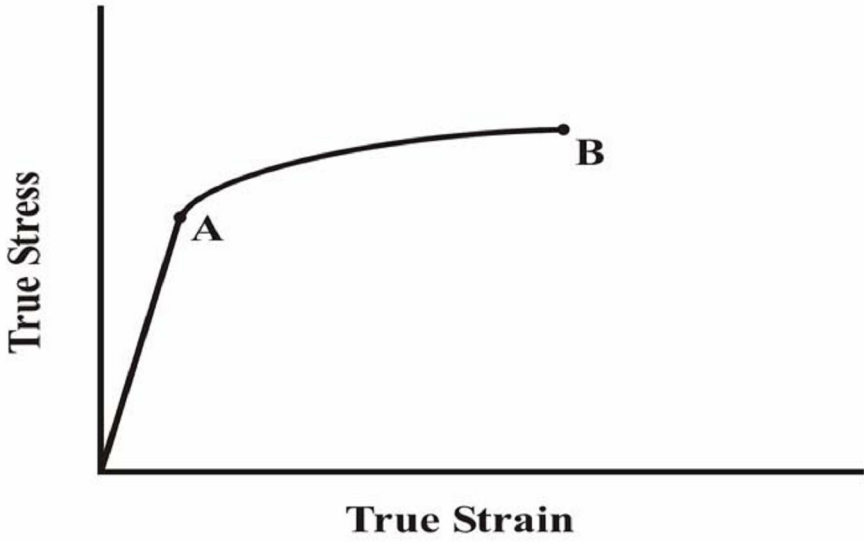

Figure 2.12. Typical shape of the stress-strain relationship for a metal under the action of a tensile stress.

The high values of strain and strain-rate mentioned in 1 and 2 mean that the material properties in cutting are considerably different from the properties of the same material when deformed in other ways, such as by metal forming processes. Consider Figure 2.12; the high strain-rate modifies the plastic flow process so that the whole curve between A and B in Figure 2.12 is raised up along the true stress axis. The point A where plastic deformation is begin and point B where before rupture is occuring. In addition, high temperatures, attained especially at the deformation zones, soften the material. These changes in material behavior have led to some of the major difficulties in relating metal cutting mechanics to conventional plastic deformation theory.

2.3 Shear Zone Models

In the last thirty years many papers on the basic mechanics of metal cutting have been written. Several models to describe the process have been developed; some have been fairly successful in describing the process, but none can be fully substantiated and definitely stated to be the correct solution. Thus, while none of the analyses can precisely predict conditions in practical cutting situations, the analyses are worth examining because they can qualitatively explain phenomena observed and indicate the direction in which conditions should be changed to improve cutting performance.

There is conflicting evidence about the nature of the deformation zone in metal cutting. This has led to two basic approaches in the analysis. Many workers, such as Merchant [4] has favored the thin-plane (or thin zone) model, as shown in Figure 2.13(a). Others such as Palmer and Oxley [5], have based analyses on a thick deformation region as in Figure 2.13(b).

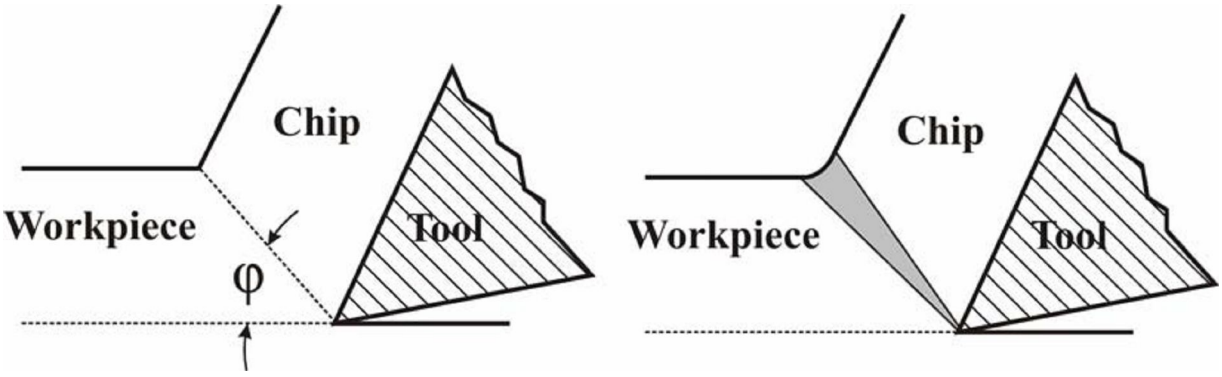

(a) (b)

Figure 2.13: Shear zone types.
(a) thin shear plane (b) thick shear zone

Available experimental evidence indicates that the thick-zone model may describe the cutting process at very low speeds, but at higher speeds most evidence indicates that a thin shear plane is approached. Thus it seems that thin-zone model is likely the most realistic for practical cutting conditions.

In addition, it leads to far simpler mathematical treatment than does the thick-zone model. For these two reasons the analysis of the thin zone has received far more attention and is more complete than that of the thick zone.

2.4 The Shear-Angle Relationships

The shear angle is of particular importance in metal cutting. In fact, the shear angle is a measure of the plastic deformation in cutting and is an essential quantity for predicting the forces in cutting. Because of this, a considerable amount of work has been done by many investigators to establish a shear-angle relationship. An examination of research publications in the metal cutting field reveals a big array of relationships. A review of these shows that many can be reduced to the form

$$\varphi = C_1 - C_2.(\beta - \gamma) \qquad 2.1$$

Where C_1 and C_2 are constants, φ is the shear angle, β is the friction angle (Figure 2.14) and γ is the rake angle.

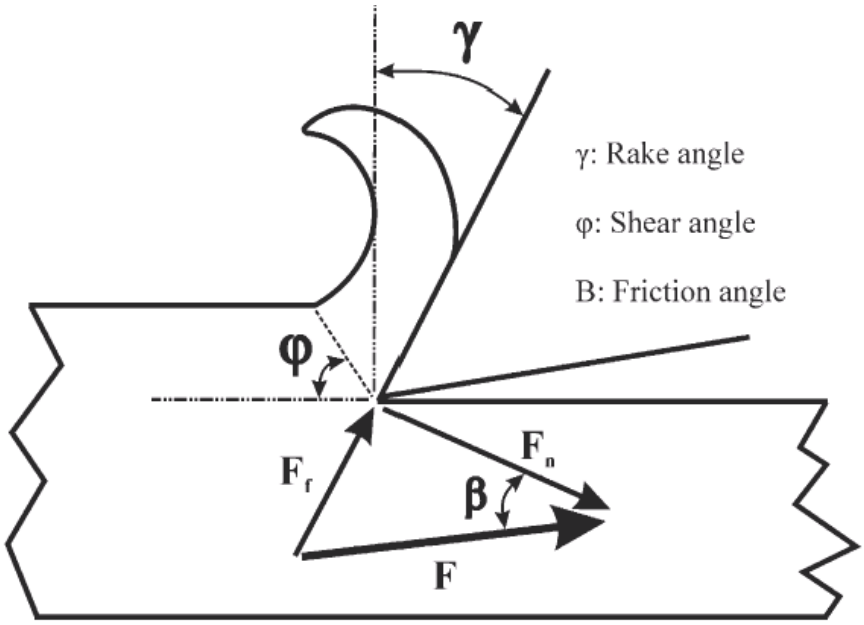

Figure 2.14: Variables used in shear angle relationships.

2.4.1 Merchant's Relationship

This is one of the earliest and possibly the best known shear-angle relationship, which suggests that material will choose to shear angle that minimizes the required energy[4].The relationship is given in Equation (2.2) as:

$$\varphi = \frac{\pi}{4} - \frac{1}{2} \cdot (\beta - \gamma) \qquad (2.2)$$

2.4.2 Lee and Shaffer's Relationship

Lee and Shaffer [6] applied the theory of plasticity for ideal rigid-plastic material, and assumed that deformation occurred on a thin-shear plane. They considered that there must be a stress field within the chip to transmit the cutting forces from the shear plane to the tool face. They represented this by a slip-line field in which no deformation occurs although it was stressed up to yield point. Resulting equation is given as:

$$\varphi = \frac{\pi}{4} - (\beta - \gamma) \qquad (2.3)$$

2.5 Friction on the Rake Face of a Cutting Tool

The laws of friction have been shown to be invalid for conditions where plastic deformation is occurring close to the sliding interface, i.e. under the conditions of very high normal load. In this situation the real area of contact approaches to the apparent area (in the extreme case the real area of contact become equal to the apparent area). Hence the proportionality between the real area of contact and the applied normal load is constant and equal to the apparent area. Under these conditions the friction force is independent of normal load [7] as shown on Figure 2.15.

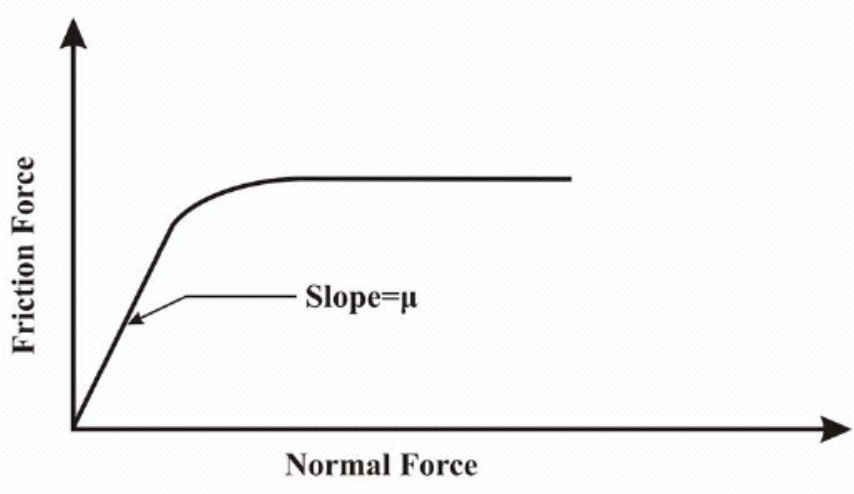

Figure 2.15: Dependence of friction force to the normal force.

In metal cutting we have a sliding situation under the conditions of exceptionally high normal force, which can explain some of the departures from the usual laws of friction depended on normal force.

An important factor to consider in discussing the friction in metal cutting is that the measured forces; some account should be taken of this before calculating the value of friction on the rake face. One way of deducting this rubbing component is to plot the measured cutting forces against depth of cut and extrapolating back to zero depth [8]. The force intercept is then taken as the rubbing or edge force. When this intercept is removed, the friction parameter is still high and may vary with the cutting conditions. The dependence of friction parameter on the cutting conditions can be explained by considering the distribution of stress on the rake face of the tool.

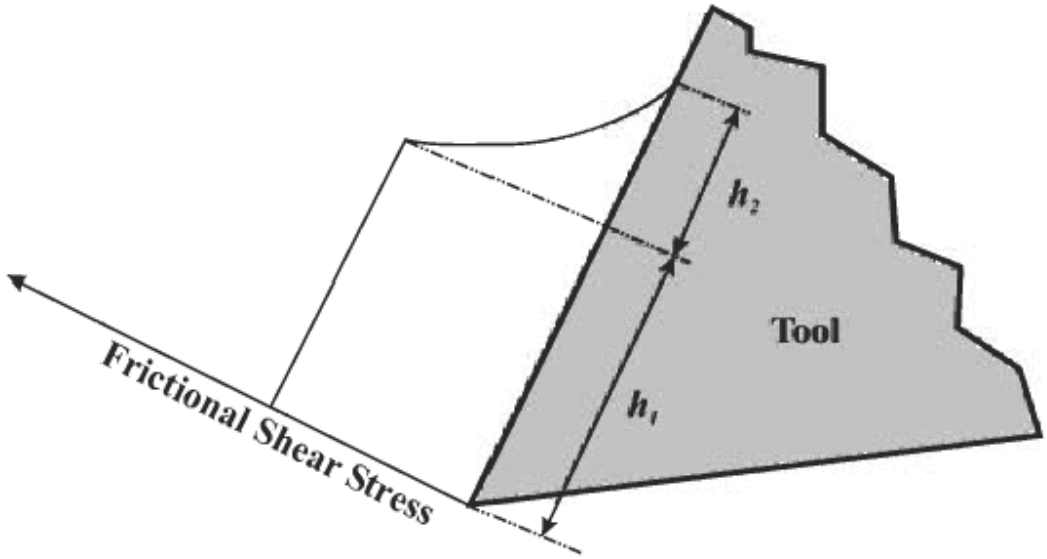

Figure 2.16: Frictional shear stress distribution on rake face of the tool.

Merchant have shown that the stress distribution on the rake face is of the form shown in Figure 2.16. Over the length h_1, the normal stress is very high and the metal adheres to the rake face;

plastic flow occurs in the work material. In this region the shearing stress (or friction stress) is independent of the normal load and generally equal to the shear yield stress of the material. This is known as the sticking region of friction. On the length h_2, smaller normal stresses exist and the usual condition of sliding friction applies.

It is to be expected that any changes in the cutting conditions which change the relative length of h_1 and h_2 will alter the measured value of the friction. For example, an increase in the rake angle reduces the overall normal load on the rake face causing a decrease in ratio of h_1 and h_2.

2.6 The shear stress in shear zone during metal cutting

The shear stress in the shear zone is found to be higher than the yield stress determined from tensile tests on the work material. One immediate explanation for the high yield-stress value is that two extraneous effects have been included in the calculation. These are, first the effect of

rubbing on the clearance face of the tool. This introduces a force which is measured, but does not contribute to the shearing process in the shear zone. Secondly there exists a pre-flow region (Figure 2.17) for many cutting conditions which has the effect of extending the length of the shear plane or shear zone beyond that assumed in the analysis

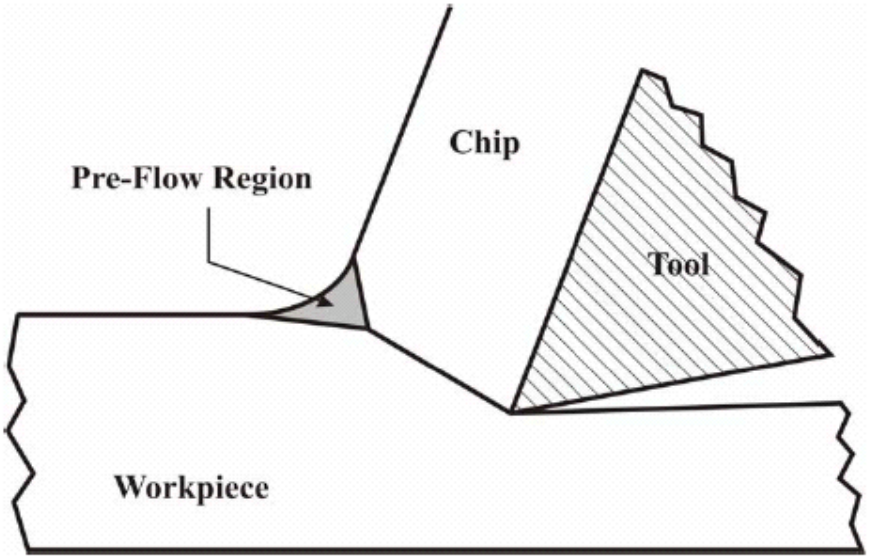

Figure 2.17: Pre-Flow region.

The effect of rubbing and the pre-flow region can be taken into account approximately. When this is done the value of the shear stress is still found to be higher compared with the yield stress for the material being cut. A number of explanations have been presented to explain the high stress values, even though some do not now seem likely to be fully justified.

1. It was proposed by Merchant [4], that the yield shear stress on the shear plane was increased due to high values of the normal stress on this plane.

2. It has been suggested by Backer, Marshall and Shaw [9] that the size of the deformation region may influence the shear-stress value. This follows from the theory of size effect for single crystals which is based on the concept that at small sizes the probability of finding dislocation sources are reduced and hence the yield stress of a material rises. The existence of the latter effect has been demonstrated by the growth of very fine single crystal whiskers.

3. Strain rate and temperature are normally considered to have opposing effects on the value of yield stress for a material. Because the temperature in the shear zone and the strain rate are both high in metal cutting, it has been argued that the two effects cancel each other [10].

On the other hand, Cotrell [10] has described a mechanism of yield at high rates of strain, which suggests that above a certain critical strain rate the yield stress is independent both of the strain rate and of temperature. He considers that the obstacles preventing slip of dislocations (other dislocations, alloy precipitates, and grain boundaries) may be represented by an undulating internal stress field. When the applied stress is less than the internal stress, the dislocations cannot pass the obstacles unless thermal vibrations of the lattice provide sufficient additional energy. Since the probability of obtaining sufficient thermal energy is dependent on both time and temperature, the yield stress will depend both on strain rate and temperature. If, however, the applied stress is greater than the internal stress, rapid slip will occur and the yield stress will be independent of strain rate. By this theory, the yield stress at high rates of strain will be higher than the static yield, but above a certain rate it will be independent of the rate of strain. The straining will be sudden and catastrophic at any applied stress level, hence work-hardening effects will not be observed.

2.7 Finite element methods

The finite element method is a natural tool for handling the non-linearities involved. There are, in fact, several finite element methods, not just one. There is a coupling of thermal and mechanical analysis methods. In the mechanical domain, different approaches have been tried and are still in use. The differences cover how material stress–strain relations are described (modeling elasticity as well as plasticity, or neglecting elastic components of stress and strain); how flow variations are described (relative to fixed axes, or convecting with material elements the Eulerian and Lagrangian views of fluid and solid mechanics); how the elements are constructed (uniform, or structured according to physical intuition, or allowed to remesh adaptively in response to the results of the calculations);and how some factors more specific to metal machining (for example the separation of the chip from the work) are dealt with.

Historical review of FEM in metal cutting: In metal cutting, use of FEM has increased considerable since the late 1970s, 1980s, and 1990s. This trend suggests that the application of FEM will continue to grow. This is primarily because the ‘’classical shear angle approach [Merchant, 1945,[4]]’’ and the ‘’slip line field solution [Lee, and Schaffer,, 1951, [6]]’’ are based on oversimplistic assumptions and cannot account for some important features, such as flow stress characteristics of workpiece material, chip tool interface friction, strain hardening, and build up edge (BUE). In addition, rapid improvement of computer hardware and software makes the previously complicated finite element calculations feasible.

The machining analyses based on the finite element method have found varying degree of success depending upon the numerical methods, material models, and specific assumptions that were made to calculated the temperature distribution of the chip and tool based on experimental data for the flow field’’. ‘’[Iwata 1984[13]] used an elastic-plastic material model based on the assumptions of the chip shape and flow field’’. ‘’[Komvopoulos and Erpenbeck, 1991,[15]] studied the machining process with a rigid build-up edge using the elastic-perfectly plastic and elastic-plastic material models’’.

Understanding the cutting process/ Application: The purpose of FEM modeling is to obtain a more complete understanding of the metal cutting process, but the reverse is also true. A good understanding of the metal cutting process is one of the key factors for a successful FEM. The metal cutting process is so complex that it is very difficult to understand completely. It is necessary to make some reasonable assumptions based on current process knowledge to make the problem manageable. Currently, most FEM builders focus their attention only on the 2-D orthogonal process, which is ideal and simplified by homogenous assumptions. Although all, the orthogonal cutting is still unusually complex since there are very large strain and plastic deformations operating at very high strain rates, and heavily loaded friction along the tool-chip interface occur simultaneously with strong interactions. These characteristics make the metal cutting process unique.

A variety of specializations under the umbrella of the mechanical engineering discipline (such as aeronautical, biomechanical, and automotive industries) commonly use integrated FEM in design

and development of their products. Several modern FEM packages include specific components such as thermal, electromagnetic, fluid, and structural working environments. In a structural simulation, FEM helps tremendously in producing stiffness and strength visualizations and also in minimizing weight, materials, and costs.

FEM allows detailed visualization of where structures bend or twist, and indicates the distribution of stresses and displacements. FEM software provides a wide range of simulation options for controlling the complexity of both modeling and analysis of a system. Similarly, the desired level of accuracy required and associated computational time requirements can be managed simultaneously to address most engineering applications. FEM allows entire designs to be constructed, refined, and optimized before the design is manufactured.

This powerful design tool has significantly improved both the standard of engineering designs and the methodology of the design process in many industrial applications. The introduction of FEM has substantially decreased the time to take products from concept to the production line. It is primarily through improved initial prototype designs using FEM that testing and development have been accelerated. In summary, benefits of FEM include increased accuracy, enhanced design and better insight into critical design parameters, virtual prototyping, fewer hardware prototypes, a faster and less expensive design cycle, increased productivity, and increased revenue.

FEM application in metal machining: Finite Element Method (FEM) based modeling and simulation of machining processes is continuously attracting researchers for better understanding the chip formation mechanisms, heat generation in cutting zones, tool-chip interfacial frictional characteristics and integrity on the machined surfaces. Predictions of the physical parameters such as temperature and stress distributions accurately play a pivotal role for predictive process engineering of machining processes. The FEM modeling studies conducted in the past and to develop.FEM models for most satisfying simulation of the physical cutting process and most reasonable predictions for cutting forces, temperatures and residual stresses on the machined surface.

In continuum-based FEM modeling, there are two types of analysis in which a continuous medium can be described: Eulerian and Lagrangian. In a Lagrangian analysis, the computational grid deforms with the material where as in a Eulerian analysis it is fixed in space. The Lagrangian calculation embeds a computational mesh in the material domain and solves for the position of the mesh at discrete points in time. In those analyses, two distinct methods, the implicit and explicit time integration techniques can be utilized. The implicit technique is more applicable to solving linear static problems while explicit method is more suitable for nonlinear dynamic problems.

A vast majority of research has relied on the Lagrangian formulation, which allows the chip to be modeled from incipient to steady state where as some of the studies also used the Eulerian formulation. However, using the Lagrangian formulation requires a criterion for separation of the undeformed chip from the work piece. Several chip separation criteria (e.g. strain energy density, effective strain criteria) have been developed and implemented. Updated Lagrangian implicit formulation with automatic remeshing without using chip separation criteria has also been used in simulation of continuous and segmented chip formation in machining processes.

Arbitrary Lagrangian Eulerian (ALE) technique combines the features of pure Lagrangian analysis in which the mesh follows the material, and Eulerian analysis in which the mesh is fixed spatially and the material flows through the mesh. ALE formulation is utilized in simulating machining to avoid frequent remeshing for chip separation. Explicit dynamic ALE formulation is very efficient for simulating highly non-linear problems involving large localized deformations and changing contact conditions as those experienced in machining. The explicit dynamics procedure performs a large number of small time increments efficiently.

Mesh Separation Criteria in Finite Element Simulation: Several mesh separation criteria used for the finite element simulation of the metal cutting. In real machining process, several chip separation criteria that correspond to the mesh separation criteria in the finite element analysis were proposed by Merchant, Lee and Palmer. Merchant [4] considered chip formation as a process of shear which was illustrated as displacement of cards in a stack. An alternative theory

of chip separation suggested by Palmer [5] is based on the microcrack mechanism. Lee [6] explained the process of chip separation in terms of shear front. However, none of them clearly explained the real mechanism when the material is being cut. Therefore, most of the mesh separation criteria in the finite element machining simulation highly depend on trial-and-error. The mesh separation criteria for the finite element simulation of the metal cutting are energy, stress, total effective plastic strain, effective plastic strain, distance, strain energy density.

2.8 Numerical Approach

In the two past decades, the finite element method based on Eulerian and updated Lagrangian formulation has been developed to analyze the metal cutting processes. Several special finite element techniques, such as element separation, modeling worn cutting tool geometry, mesh rezoning, friction modeling etc. have been implemented to improve the accuracy and efficiency of the finite element modeling. Detailed workpiece material modeling with the coupling of temperature, strain rate and strain hardening effects, has been applied to model the material deformation.

The literature for the numerical approach is classified so that the steady state solutions, in which separation is not included, will first be mentioned. Later, the models, which are including separation, will be explained. The latter one is also divided into two sections according to whether they simulate the chip formation from incipient to continuous stage or they simulate the chip formation at the continuous stage only.

2.8.1 Steady -State Solutions

In steady-state solutions the metal cutting problem is modeled at the steady-state conditions. These are generally one increment solutions. The chip form and the needed data are obtained from experimental and theoretical results for the definition of the model and for the boundary conditions.

Strenkowski and Kyoung-Jin Moon [11] presented an Eulerian finite element model that simulates orthogonal metal cutting and predicts chip geometry and temperature distribution in the workpiece, chip and tool without the need for empirical cutting data. They showed that the characteristics of the flow field in the vicinity of the tool can be determined such as the material velocity and the stress and strain rate distributions. They found out that the shearing occurs over a finite region in front of the tool, rather than a single shear plane.

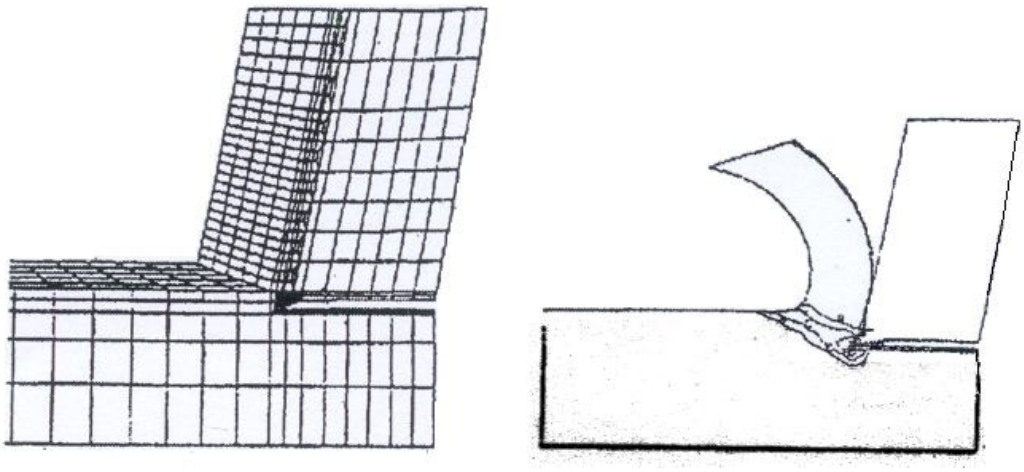

Figure 2.18: Model by Strenkowski and Kyoung-Jin Moon.
(a) initial chip form (b) strain-rate distribution after solution.

Tyan and Yang [12] simulated the orthogonal metal cutting process for a controlled contact tool using a limit analysis theorem. The basic principles are in the form of a primal optimization problem with an objective function subjected to constraints of equilibrium equation, its static boundary conditions and a constitutive inequality. An Eulerian reference coordinate is used to describe the steady state motion of the workpeice relative to the tool. The results are obtained for a wide range of control parameters including cutting depth, rake angle, rake length and friction.

The converged solution provides information on cutting force, chip thickness, chip flow angle and shear angle.

The temperature distributions in the workpiece and chip during orthogonal machining are obtained numerically using the Galerkin approach of finite element method for various cutting conditions. The effect of a number of process variables such as speed, feed, rake angle, and tool material on the temperatures has been investigated. The finite element solution of the problem takes into account the actual geometries of the chip and the tool, experimentally obtained velocity and heat source distribution within the primary and secondary deformation zones and the variation of density, thermal conductivity specific heat with temperature. It also takes into consideration the variation of the flow stress with strain, strain rate and temperature and heat generation due to boundary friction on the rake face and along the flank face of the tool.
Iwata, Osakada and Terasaka [13] developed a rigid-plastic finite element model for orthogonal cutting in a steady state condition. The methods for determining the material and frictional properties to be used in the model are discussed. The shape of chip and distributions of stress and strain are calculated. Fracture of chip is predicted by combining the present model with the criteria of ductile fracture. In this work, an initial model is generated by giving the cutting condition and the shape of the cutting tool, and then the model is modified by using the result of the plane strain finite element analysis. The modification is repeated until the obtained shape of the chip and distribution of strain (flow stress) coincide with the assumed one. The boundary conditions are given according to the assumption of moving workpiece with a constant velocity to unmoving tool. The shear force F_s acting on the chip surface due to frictional stress is a function of normal force F_n.

Liu and Lin [14] used the finite element method to investigate the effect of shear boundary conditions on the stress field in workpiece during machining. The length of the shear plane is found to be a major parameter governing the stress field in the workpiece in machining, confirming a previous experimental study. In this work, separation of chip from the workpiece is not simulated. Force boundary conditions were used and the model is solved for one increment at the assumed cutting conditions.

2.8.2 Solutions for Continuous Chip Formation

In this type of modeling, incipient stage of chip formation is not included and the model is generated for continuous chip formation stage. Generally, a separation criterion is needed for the formation of chip.

Komvopoulos and Erpenbeck [15] modeled orthogonal chip formation process by using finite element method. They analyzed the effect of important factors, such as plastic flow of the workpiece material, friction at the tool-workpiece interface and wear of the tool on the cutting process. To model separation of chip from the workpiece, distance tolerance criterion was used by super positioning two nodes at each nodal location of a parting line of the initial mesh.
Elastic - perfectly plastic and elastic plastic with isotropic strain hardening and strain rate sensitivity constitutive laws was used in the analysis. For simplicity, the tool material and the built-up edge were modeled as perfectly rigid. The dimension of the crater, assumed in the finite element involving a created tool, was also determined from the experiments. Steady state magnitudes of the cutting force, shear plane angle, chip thickness and chip-tool contact length are estimated. The initial mesh configuration was based on the preliminary estimates of the shear angle and chip thickness.

2.8.3 Solutions for Transient Chip Formation

Lin and Lin [16] constructed an orthogonal cutting coupled model of thermoelastic- plastic material under large deformation. A chip separation criterion based on the critical value of the strain energy density is introduced into the numerical model. The flow stress is taken as a function of strain, strain rate and temperature in order to reflect realistic behavior in metal cutting. The cutting tool is incrementally advanced forward from an incipient stage of tool-workpiece engagement to a steady-state chip formation. The chip geometry, residual stresses in the machined surface, temperature distributions within the chip and tool, and tool forces are obtained. It has also been verified that the chip separation criterion value based on the strain energy density is a material constant and is independent of uncut chip thickness.

2.8.4 Solutions for Transient and Continuous Chip Formation

Caroll and Strenkowski [17] reviewed two finite element models of orthogonal metal cutting. From the models, the detailed stress and strain fields in the chip and workpiece, chip geometry and cutting forces can be estimated. The first model is based on a specially modified version of large deformation updated Lagrangian, which employs an elastic-plastic material model. The second model treats the region in vicinity of the cutting tool as an Eulerian flow field. Material passing through this field is modeled as viscoplastic.

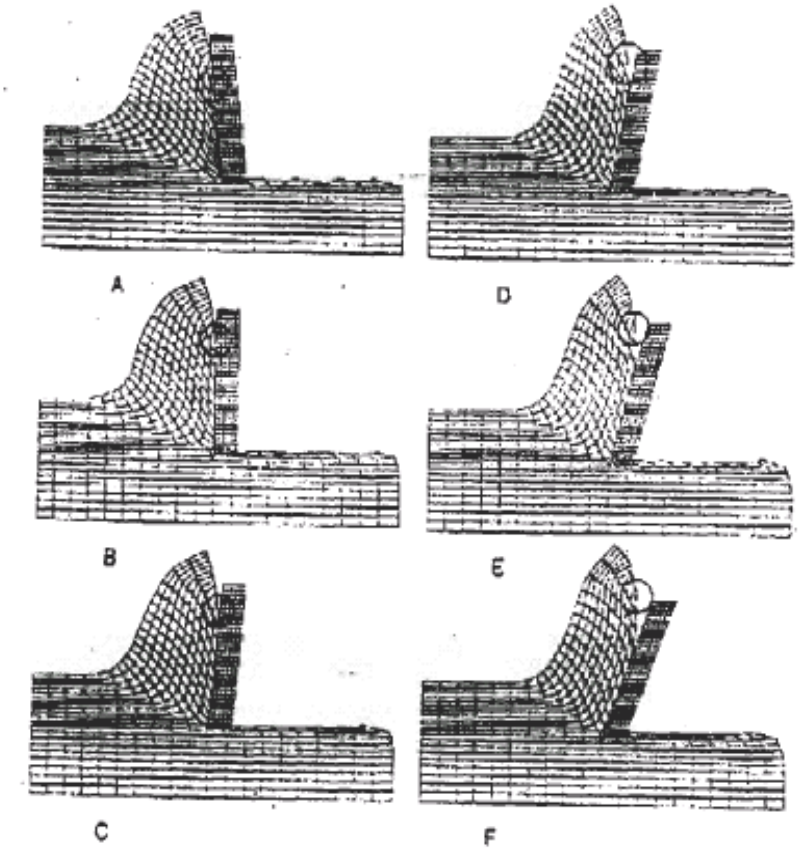

Figure 2.19: Estimated chips at different rake angles by Carroll and Strenkowski.

To allow for separation of the chip formation from workpiece, the model employs a material parting (or separation) criterion based on the effective plastic strain at the tool tip region of the workpiece.

CHAPTER 3

EXPERIMENTAL WORK

3.1 Experimental Equipment Description

3.1.1 Machine Tool

In order to carry out this experiment of cylindrical material was used a center lathe with the cutting speed and feed rate being selected from the available options, which can be supplied automatically by the machine. A center lathe is the mother of all machine tools and there are many references to it in the technical literature of the world. It is the most widely used machine tool for machining of metals. It is a versatile machine tool and more than half the machine tools operating in the manufacturing industries in the country are of the lathe family. The work produced is mostly of a cylindrical shape. In its operation, a center lathe holds the work by a suitable device, usually a chuck mounted on the spindle which rotates the chuck at varying speeds. The cutting tool is clamped in the tool-post and travels in a suitable direction-parallel, at right angles and at any other angle in between to the axis of rotation of the spindle. Other cutting tools such as drills, reamers or taps can also be mounted on the tailstock, but mover by hand.

The maximum power utilization of the machine is 15kw. The speed ranges are from 120 up to 1500 rpm. These speeds can be varied with the help of gears. The machine can run in automatic mode by specifying the depth and feed of cut.

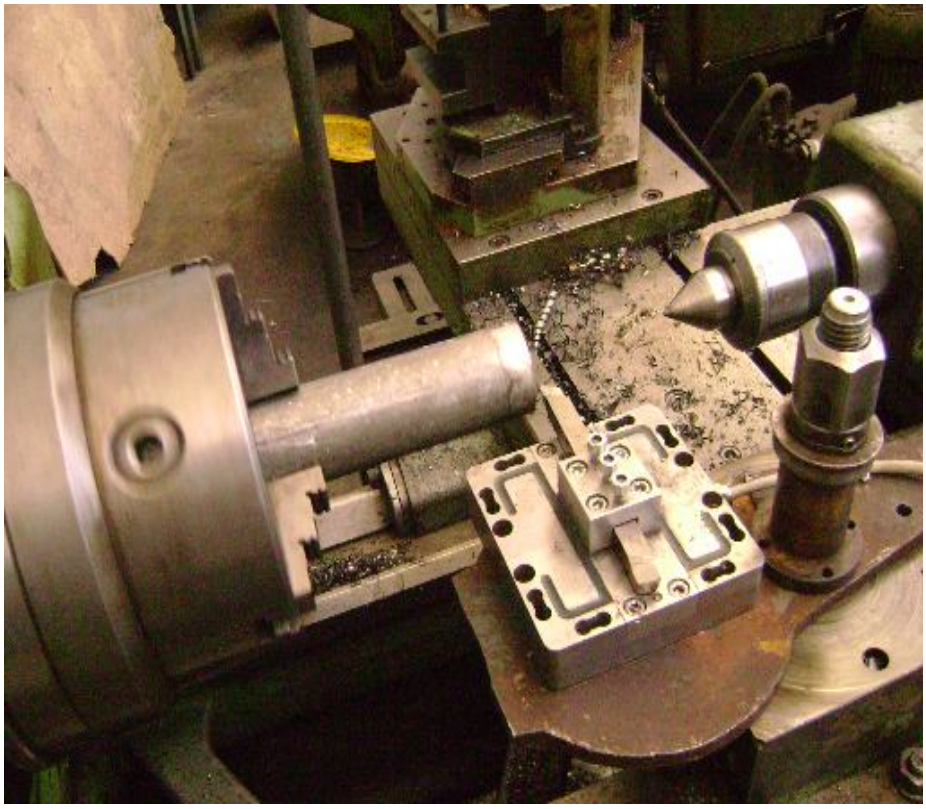

Figure 3.1 Center lathe

3.1.2 Force Sensor

The FT102 Three-Component Electronic Cutting Force Measuring Device for Lathe Tool experiments with electronic display enables numerous experiments to be performed on the evaluation of the force relationships on lathe tools during the orthogonal cutting operation.

The Three-Component Electronic Force Measuring Device for Lathe Experiments comprises a force sensor and display unit.

The force sensor uses strain gauges and measures the forces in three directions that are orthogonal to each other.

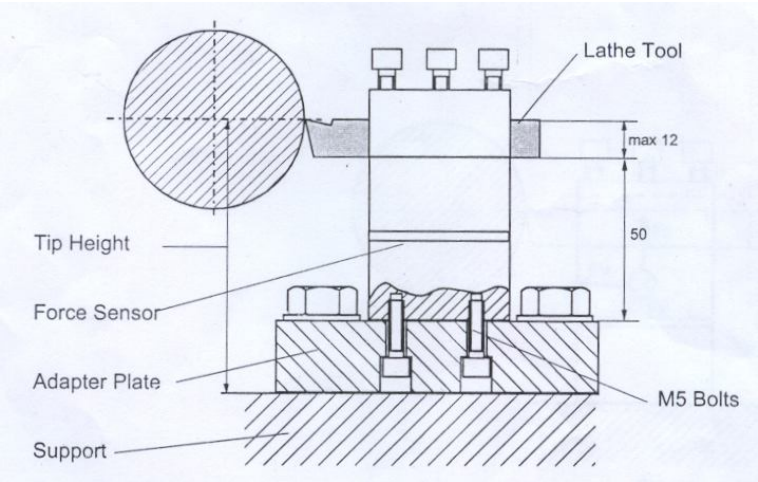

Figure 3.2: Layout of Force Sensor on Lathe

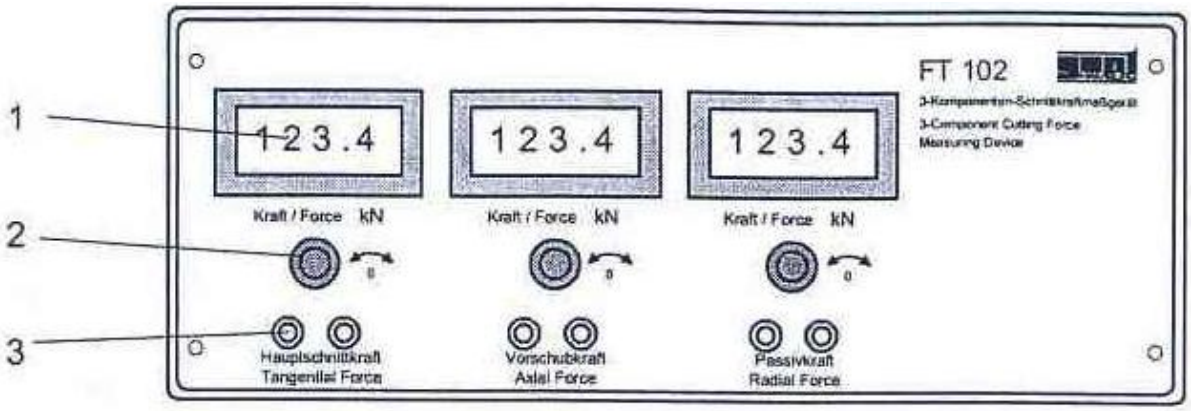

Figure 3.3: The Display Unit

The display unit contains the measuring amplifier for the strain gauge bridges, digital displays (1) and the power supply. Zero adjusters (2) enable the zero point to be set for the measuring bridges. The forces are fed to laboratory sockets (3) as analogue voltages in the range of 10V. In this way it is possible to feed the forces to a recording device for logging.

Table 3.1: Technical Description of Force Measuring Device

Technical Data

Display Unit	
Dimensions:	365 x 315 x 150 mm
Weight:	5 Kg
Power Supply:	230 V / 50Hz
Digital Displays	LCD, 3 ½ digits
Frequency Bandwidth:	0-0.5 Hz
Analogue Output:	1 V/KN
Temperature Range:	10 – 40°C
Force Sensor	
Number of Force Axes:	x, y, z
Measuring Range	± 5 KN
Can Be Overloaded up to	± 6.25 KN
Fracture Load	± 7.5 KN
Supply Voltage	10 V
Temperature Range:	10 – 70 C
Dimensions without Tool Holder	45 x 45 x 50 mm
Tool Holder	12 x 12 mm
Fastening	4 x M5

3.2 Orthogonal Cutting

Orthogonal cutting, Figure 3.4, is defined as a cutting operation where, cutting edge of the tool is perpendicular to the relative motion between the tool and work piece. A cutting operation on a shaping or a planning machine with single point cutting tool is an example of simple orthogonal metal cutting.

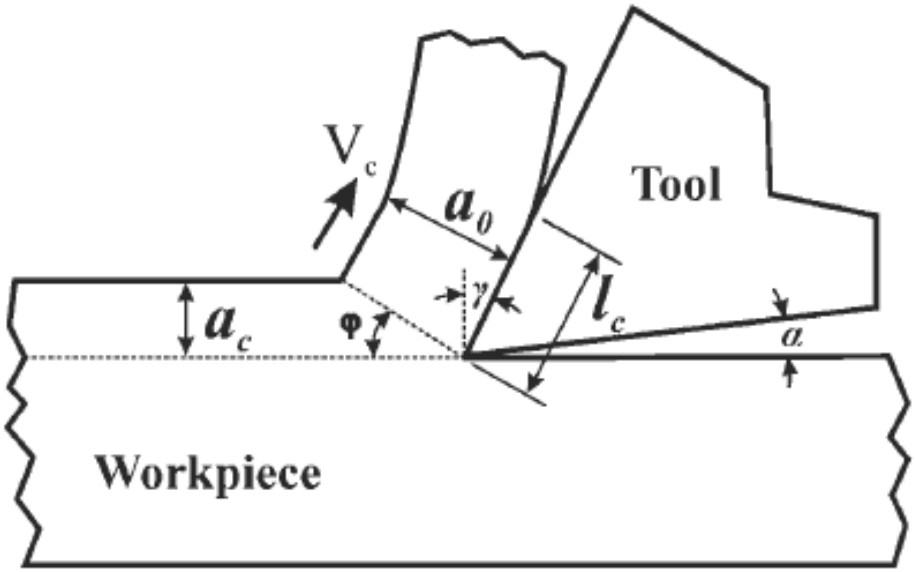

Figure 3.4: Schematic representation of orthogonal cutting

There are other methods to do experiments where orthogonal metal cutting is studied. For example, machining a hollow cylinder, which has a large diameter and small thickness, on a lathe from the end is also an example of practical orthogonal metal cutting operation (Figure 3.5). The other reason choosing hollow cylinder material is that because of the tool post that hold the cutter is 12 x 12 mm^2 means smaller than the standard size 20 x 20 mm^2. Using a cutter size of 12 x 12 mm^2 on solid cylinder is difficult to get result because the cutter repeatedly slipped.

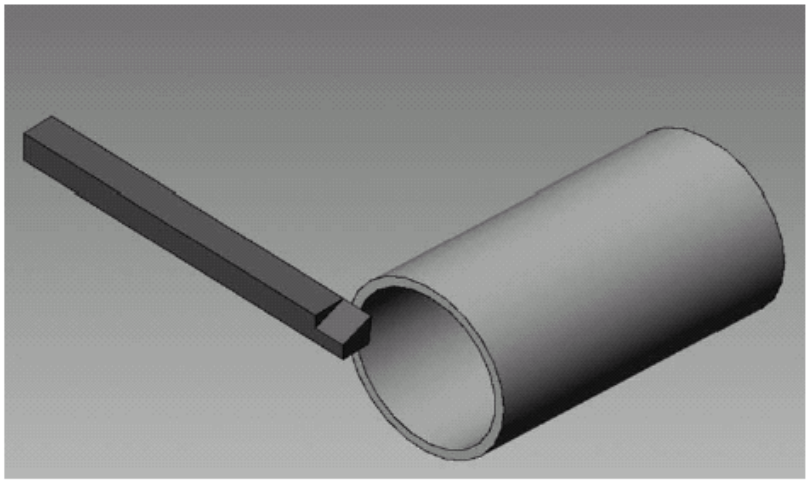

Figure 3.5 Orthogonal turning operation on a lathe.

In this work, the latter one is used. The important thing here is that, wall thickness, which is depth of cut in this case, must be significantly larger than the feed rate (undeformed chip thickness when side cutting edge angle is 0°) to satisfy the plane-strain assumption of finite element model.

3.3 Workpiece Material

Workpiece is a hollow cylinder made of mild steel. This is a low carbon steel (carbon percentage 0.15 to 0.25) whose corresponding St. Standard designation is 37. These steel do not respond to heat treatment because of their low carbon content. Typical uses of this steel are nails, chains, rivets, motorcar bodies, structural steels, screws, tin plate, drop forging, stampings, free-cutting steels. The outer and inner diameters of the workpiece are 40 and 37 millimeters respectively. Therefore, the depth of cut is 1.50 millimeter.

Table 3.2: Chemical Composition, Mechanical and Physical Properties of Test Material

Chemical composition	**%**
C	0.15
Si	0.22
Mn	0.45
P	0.08
S	0.06
Fe	99.04
Mechanical properties	
Tensile Strength (kg/mm^2)	42
Yield Strength (kg/mm^2)	21
Poisson,s ratio	0.3
Modulus of elasticity (Gpa)	210
Shear modulus (Gpa)	80
Physical properties	
Density (g/cm^3)	7.85

3.4 Cutting tool material

High speed steels: The high speed steels are alloy steels with about 0.75% to 1.5% carbon (C), 4% to 4.5% chromium (Cr), between 10% and 20% tungsten (W) and molybdenum (Mo); they can also have vanadium (V), up to 5%, and cobalt (Co), up to 12%. They are strengthened by heating to high temperature (around 1150 to 1250˚C), just below the solidus; then quenching in

two stages (to avoid thermal cracking) – to the range 500˚C to 600˚C and then to room temperature; and then tempering typically between 500˚C and 560˚C. Tempering causes hardening by the precipitation of fine carbides.

There are two series of materials, the T series which is based on W (with no Mo), and the M series which substitutes Mo for some of the W. There are no major technical advantages of one series over the other. The choice is one of cost, varying with the availability of these two elements. The basic grades in each series contain 0.75% to 0.85% C and 4% to 4.5% Cr, with a small amount of V (<2%) but no Co. The addition of extra V, with extra C as well, results in the formation of hard vanadium carbides on tempering. These increase the alloy's room temperature hardness and abrasion resistance but at the expense slightly of its toughness. The addition of Co improves hot hardness, also at the expense of toughness. Table 3.3 gives the nominal compositions of a range of grades.

Table 3.3 Sample compositions of some high speed steels.

Grade	**Composition (wt. %, balance Fe)**					
	C	**Cr**	**W**	**Mo**	**V**	**Co**
T 1	0.75	4	18	-	1	-
M 2	0.85	4	6.5	5	2	-
T 6	0.8	4	20.5	-	1.5	12
T 15	1.5	4.5	13	-	5	5
M 42	1.05	4	1.5	9.5	1	8

3.5 Parameters Used in the Experiment

The cutting tool used in the experiment was H.S.S. which is made in Czechoslovakia. The cutting tools which selected are to be grounded to the required tool angles. For the sake of this

experiment which are considered three cutters. Each has different rake angles (15, 20 and 25). These different rake angles are the cutting tool parameters that were used in the experiment.

The cutting parameters are the speed, feed and depth of cut. In this experiment feed and depth of cut were taken to be fixed. The cutting speed *v* was assigned five different levels (21, 34, 41, 49, 58 m/min); feed rate *f* and depth of cut *d* were kept constant as (0.05 & 0.1 mm/rev) and 1.50 mm, respectively. The values of cutting parameters selected are recommended by the tool manufacturer for general purpose and finish turning operations of low carbon steels. Each experiment was carried out with new sharp tools in order to keep the cutting conditions unchanged. Totally, 30 experiments (3(angles) * 5 (speeds) * 2(feed rate)) were performed by the combinations of cutting parameters.

3.6 Experimental Setup

- The test setup in the lathe is shown in fig. 3.6.
- Before beginning of the cutting process, fasten the force sensor to the support on the lathe (see fig. 3.7)
- The force sensor itself has a height of 50mm. To obtain the required tip height the adapter must be adjusted in height.

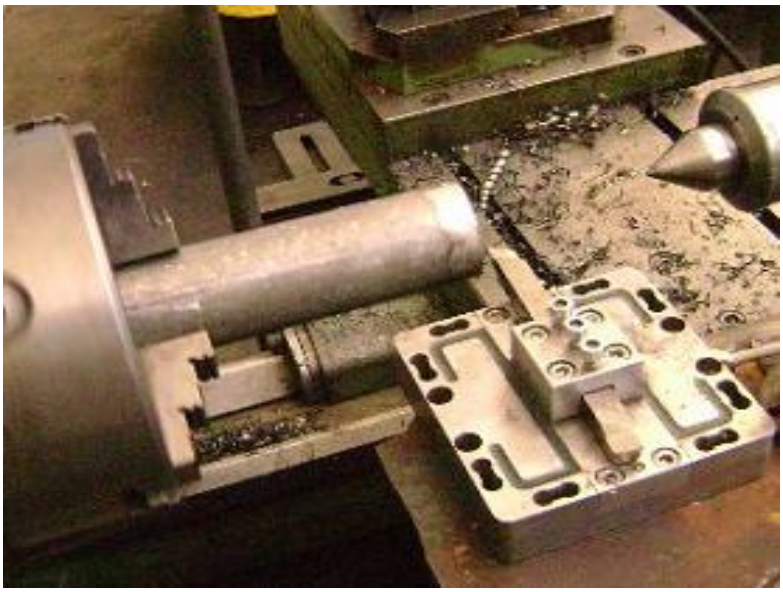

Fig.3.6 Cutting operation on lathe

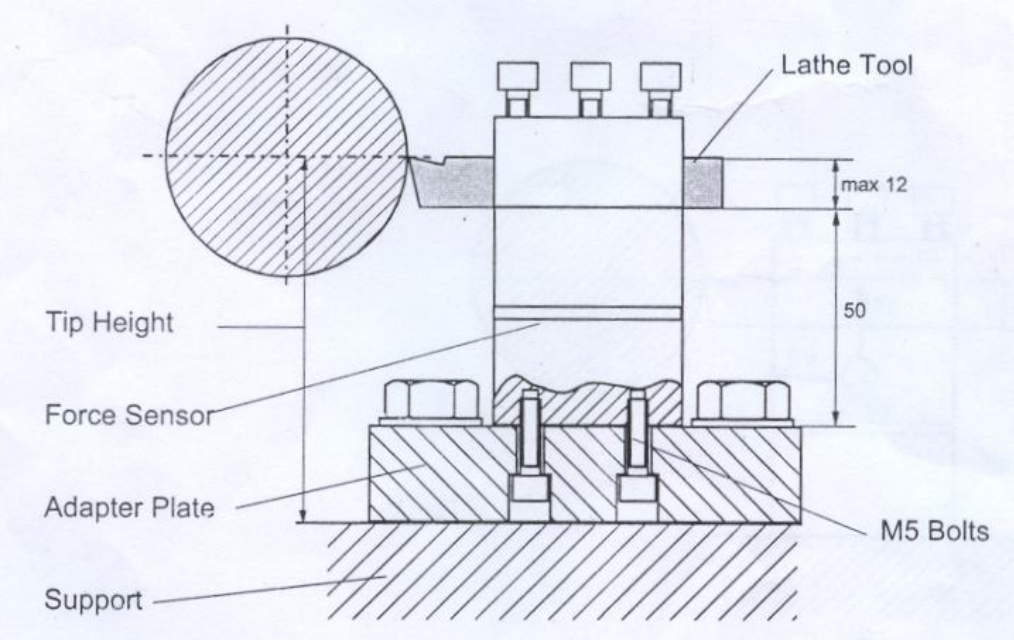

Fig. 3.7 Force Sensor on Lathe

- A tool holder is integrated in to the top of the force sensor (see fig. 3.8)
- The force sensor is connect to the display unit via a cable.

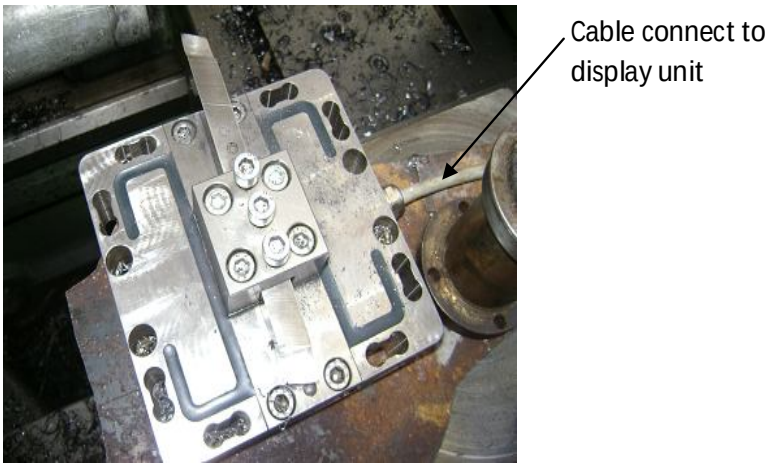

Figure 3.8 Tool holder

- After switch on the display unit it was left to warm up for approximately 30 minutes, to avoid measurement errors due to thermal drift.
- After the warm up phase has been completed, the displays are to be set to zero. Once the displays have been zeroed, the measurement can be started.

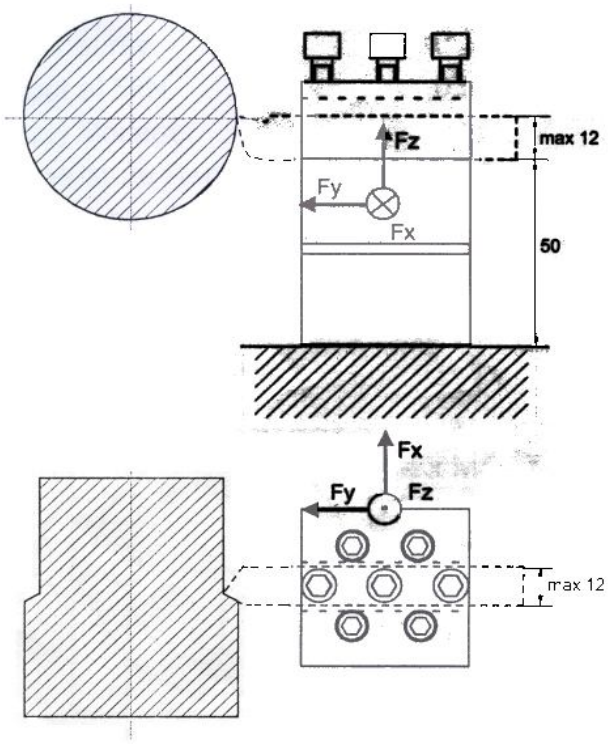

Fig. 3.9 Force sensor with Force Directions

Furthermore, the experiments were carried out with the following setup parameters: V_c (Cutting Speed) are 21, 34, 41, 49, 58m/min, feed f=0.05mm/rev, 0.1mm/rev,& depth of cut is 1.5mm. The specimen was an extruded mild steel profile with internal diameter 37mm and external diameter of 40mm. The cutting force was measured with a FT102 3-component cutting force measuring device.

In order to satisfy statistical demands, the experimental settings were made with three repetitions of each measure- Cycle. When the measured raw-data was filtered, the average value was calculated. Each of these average values represents a measure-value. The three repetitions of the measured forces from the experiment are shown in Table 3.3. The average value of the three

measured values was calculated in the direction of cutting force. The measured cutting forces were compared with force output from the analysis.

Experimental data collected when turning (St. 37) mild steel.

Table 3.4: Cutting conditions at which experiments were performed and predicted force.

No of test	Feed rate (mm/rev) 0.05	Rake Angle 15°	Cutting Speed (m/min)	Measured Cutting Force (N)			Average Measured Cutting Force (N)	Predicted Force (N)
				Case 1	Case 2	Case 3		
1			21	700	693	702	698.3	306.16
2			34	670	665	662	665.67	
3			41	640	642	641	641	
4			49	620	615	617	617.3	
5			58	650	643	646	646.3	

Table 3.4 (a) Results for experiment.1

No of test	Feed rate (mm/rev) 0.1	Rake Angle 15°	Cutting Speed (m/min)	Measured Cutting Force (N)			Average Measured Cutting Force (N)	Predicted Force (N)
				Case 1	Case 2	Case 3		
1			21	717	720	722	719.67	612.32
2			34	675	683	680	679.3	
3			41	650	652	651	651	
4			49	638	640	641	639.67	
5			58	660	662	661	661	

Table 3.4 (b) Results for experiment.2

No of test	Feed rate (mm/rev) 0.05	Rake Angle 20°	Cutting Speed (m/min)	Measured Cutting Force (N)			Average Measured Cutting Force (N)	Predicted Force (N)
				Case 1	Case 2	Case 3		
1			21	540	538	541	539.67	306.16
2			34	520	520	522	520.67	
3			41	521	520	519	520	
4			49	580	585	582	582.3	
5			58	588	590	591	589.67	

Table 3.4 (c) Results for experiment.3

No of test	Feed rate (mm/rev) 0.1	Rake Angle 20°	Cutting Speed (m/min)	Measured Cutting Force (N)			Average Measured Cutting Force (N)	Predicted Force (N)
				Case 1	Case 2	Case 3		
1			21	660	665	662	662.3	612.32
2			34	635	640	642	639	
3			41	600	598	602	600	
4			49	727	728	730	728.3	
5			58	782	780	782	781.3	

Table 3.4 (d) Results for experiment.4

No of test	Feed rate (mm/rev) 0.05	Rake Angle 25°	Cutting Speed (m/min)	Measured Cutting Force (N)			Average Measured Cutting Force (N)	Predicted Force (N)
				Case 1	Case 2	Case 3		
1			21	665	670	667	667.3	306.16
2			34	640	638	640	639.3	
3			41	620	625	622	622.3	
4			49	702	700	703	701.67	
5			58	770	765	765	767.67	

Table 3.4 (e) Results for experiment.5

No of test	Feed rate (mm/rev) 0.1	Rake Angle 25°	Cutting Speed (m/min)	Measured Cutting Force (N)			Average Measured Cutting Force (N)	Predicted Force (N)
				Case 1	Case 2	Case 3		
1			21	680	678	677	678.33	612.32
2			34	658	660	662	660	
3			41	635	640	644	639.67	
4			49	715	710	720	715	
5			58	810	830	820	820	

Table 3.4 (f) Results for experiment.6,

3.7 Forces and power in cutting

In most machining operations, forces and power consumption are secondary by themselves. But, because of the impact of forces (and power) on the size and accuracy of work, they are considered important. Moreover, forces and power have considerable effect on machine tool design. Cutting forces also affect cutting tool life. Hence, the importance of cutting forces and power.

The magnitude of cutting forces and power required to perform a machining operation depends on several factors such as shape of the cutting tool, cutting speed, feed and depth of cut, quality of the work material and cutting fluids. The shape of the cutting tool determines, to a large extent, its efficiency relative to the forces exerted and the power supplied.

The cutting speed, feed, and depth of cut are the factors determining the amount of material to be removed in a given time. Therefore, the magnitude of the forces required and the power expended may vary in direct proportion to the amount of metal removed per unit time. The composition and physical properties of the work material also have its influence on these forces and power. Besides, coolants and lubricants tend to reduce frictional force and hence forces and power are also reduced.

Power in machining

In general, four terms are used to specify the power consumed in machining, (i) gross power (P_g), (ii) net power (P_n), (iii) specific power (P_s), and (iv) metal removal factor (M_v).

Gross power (P_g). This is the power supplied to the machine tool. The gross power supplied to the machine tool operating under 'no-load' power. No-load power is a function of the speed of operation of the machine tool.

Net power (P_n). This is the power available at the cutting tool and is consumed in cutting. The net power, rather than the gross power, is significant in cutting force and specific power calculations. The net power is less than the gross power by the amount used in overcoming friction and other losses in the operation of the machine tool,

Specific power consumption (P_s). It is the amount of power (net) required to remove a unit volume of metal in unit time and is usually expressed in terms of horse power per cubic centimeter per minute. It is related to power consumption in cutting and the rate of metal removal in the following manner:

$$P_s = P_n/U$$

Where U = cubic centimeters of metal removed per minute.

Metal removal Factor (M_v). It is the volume of metal removed per unit of power (net) in a unit of time. It is, as can be seen, the reciprocal of specific power consumption, i.e

$$M_v = 1/P_s = U/P_n$$

Both the metal removal factor, or its reciprocal, i.e., the specific power consumption, are useful quantities for expressing the power requirements for metal removal in a given machining operation. They remain relatively constant in value for small changes in the cutting conditions and are, therefore, to some extent characteristics of the material being machined and serve as a criterion of machinability.

Forces in Machining

The cutting force F_c (the component of the resultant cutting force in the direction of cutting) is of considerable practical importance as it determines the power consumed in cutting. The other components, namely, the longitudinal and radial forces, F_l and F_r respectively, do little or no work. For this reason only the cutting force F_c will be considered here.

The manufacturing process of turning can be considered a model machining case with geometrically defined cutting. Thus knowledge of machining during turning can also be applied to other processes such as milling and drilling.

Important for economical turning is the power used for machining. This can be calculated from the cutting force and the cutting speed.

$$P=F_c.V_c$$

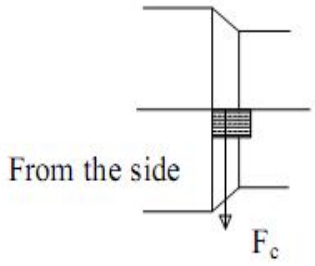

Fig.3.10 Forces on the lathe tool

The cutting force F_c is dependent on the cutting cross-section A comprising the cutting depth h and the cutting width b.[Chandiramani, 1975 [18]]

$$F_c=b.h^{(1-mc)}.k_{c1.1}$$

The expression $1-m_c$ and the constant $k_{c1.1}$ are dependent on the material and can be found in tables. For mild steel of St37, the following are applies:

$1-m_c=0.83$

$K_{c1.1}=1780N/mm^2$

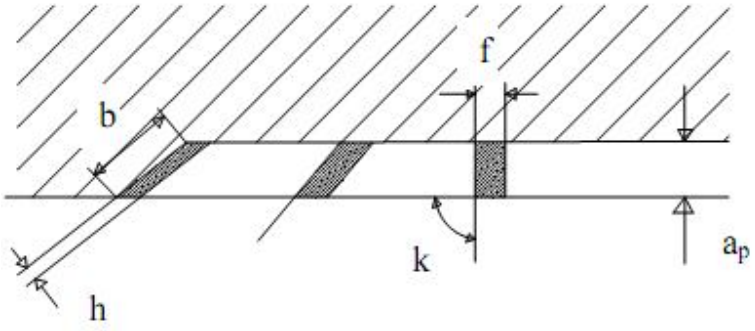

Fig.3.11 Cutting Cross-Section for Various Adjustment Angles k.

As the cutting force is heavily dependent on the cutting thickness h, for a given cutting power, that is constant cutting cross-section A, this can be changed by means of the cutting width b. This is in turn, for a given cutting depth a_p dependent on the adjustment angle k of the cutting edge. However, in this case the other forces at the cutting edge such as axial force F_f and radial force F_p also change. The other angles such as cutting angle γ and clearance angle α at the cutting edge have a greater effect on the formation of surface finish.

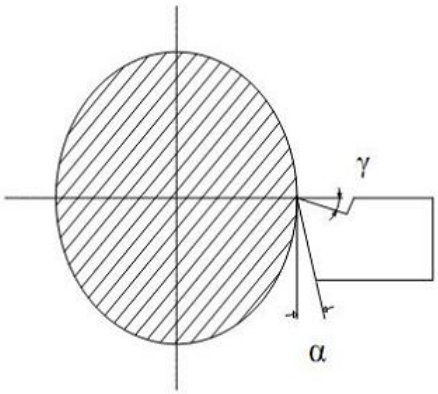

Fig.3.12 Angles at the lathe tool

CHAPTER 4

MODELLING OF THE ORTHOGONAL METAL CUTTING

4.1 Constitutive equations for numerical modeling

Most plasticity calculations are formulated to obtain stresses from strain increments (or strain rates) Thomas Childs [19]. The flow rules must be inverted. This can review how this may be done, first for a rigid plastic material, then for combined elastic and plastic deformation.

Rigid plastic flow rule inversion

The Levy Mises flow rules may be written more generally as

$$\frac{d\varepsilon_x}{\sigma'_x} = \frac{d\varepsilon_y}{\sigma'_y} = \frac{d\varepsilon_z}{\sigma'_z} = \frac{d\varepsilon_{xy}}{\tau_{xy}} = \frac{d\varepsilon_{yz}}{\tau_{yz}} = \frac{d\varepsilon_{zx}}{\tau_{zx}} = \frac{3\, d\bar{\varepsilon}}{2\, \bar{\sigma}_x} \quad \text{or} \quad \frac{3\, d\bar{\sigma}}{2\, H'\bar{\sigma}} \tag{4.1}$$

Rearranging the equations gives

$$\sigma'_{ij} = \frac{2}{3} \frac{\bar{\sigma}}{d\bar{\varepsilon}} d\varepsilon_{ij} \tag{4.2}$$

In principle, this can be used directly to determine the deviatoric stress field from a given strain increment field. However, the right-hand side is nonlinear in the strain increments as both $\bar{\sigma}$ and $d\bar{\varepsilon}$ depend on them. Practical rigid plastic finite element methods seek actual strain increment fields from initial guesses, by iteration. For efficiency of operation, they use a linearized form of equation (4.2), to calculate variations of σ'_{ij} caused by variations in strain increment. They must also find some way to estimate hydrostatic stresses, not involved in yielding. Both these practical matters are introduced in this section.

Linearization

The sensitivity of σ'_{ii} to variations in strain increments about a base value $(\mathrm{d}\varepsilon_{ii})_0$ may be expressed, to a first approximation, in a linear way as

$$\mathrm{d}\sigma'_{ij} = \frac{\partial \sigma'_{ij}}{\partial(\mathrm{d}\varepsilon_{kl})}\,\mathrm{d}(\mathrm{d}\varepsilon_{kl}) = \frac{2}{3}\,\frac{\bar{\sigma}_0}{\mathrm{d}\bar{\varepsilon}_0}\,\mathrm{d}(\mathrm{d}\varepsilon_{ij}) + \frac{2}{3}\,\frac{\partial\bar{\sigma}}{\partial(\mathrm{d}\bar{\varepsilon})}\,\frac{\partial(\mathrm{d}\bar{\varepsilon})}{\partial(\mathrm{d}\varepsilon_{kl})}\,\frac{\mathrm{d}(\mathrm{d}\varepsilon_{kl})(\mathrm{d}\varepsilon_{ij})_0}{\mathrm{d}\bar{\varepsilon}_0} - \frac{2}{3}\,\frac{\bar{\sigma}_0}{(\mathrm{d}\bar{\varepsilon}_0)^2}\,\frac{\partial(\mathrm{d}\bar{\varepsilon})}{\partial(\mathrm{d}\varepsilon_{kl})}\,\mathrm{d}(\mathrm{d}\varepsilon_{kl})(\mathrm{d}\varepsilon_{ij})_0 \tag{4.3}$$

For a material whose flow stress depends only on $\bar{\varepsilon}$, for example whose flow stress does not depend on strain rate,

Furthermore,
$$\frac{\partial\bar{\sigma}}{\partial(\mathrm{d}\bar{\varepsilon})} = 0 \tag{4.4}$$

$$\frac{\partial(\mathrm{d}\bar{\varepsilon})}{\partial(\mathrm{d}\varepsilon_{kl})} = \frac{2}{3}\,\frac{(\mathrm{d}\varepsilon_{kl})_0}{(\mathrm{d}\bar{\varepsilon})_0} \tag{4.5}$$

Substituting equations (4.4) and (4.5) into equation (4.3), and slightly rearranging, gives

$$\mathrm{d}\sigma'_{ij} = \frac{2}{3}\,\frac{\bar{\sigma}_0}{\mathrm{d}\bar{\varepsilon}_0}\,\mathrm{d}(\mathrm{d}\varepsilon_{ij}) - \frac{4}{9}\,\frac{\bar{\sigma}_0}{(\mathrm{d}\bar{\varepsilon}_0)^3}\,(\mathrm{d}\varepsilon_{ij})_0(\mathrm{d}\varepsilon_{kl})_0\mathrm{d}(\mathrm{d}\varepsilon_{kl}) \tag{4.6}$$

Elastic–plastic flow rules

Introducing elastic deformation creates advantages and disadvantages relative to rigid plastic modelling. There is no problem with respect to including hydrostatic stress effects (the material is elastically compressible). However, immediate linearization of the flow rules, after the manner of equation (4.2), is no longer possible. First, one must separate the elastic from the total strain increment, to isolate the plastic strain increment.

Elastic strains

Consider the geometrical representation of the stress state in Figure 4.1. If the point P lies within the yield cylinder, only elastic strains occur. The relation between strain and stress is commonly given as (Hooke's law)

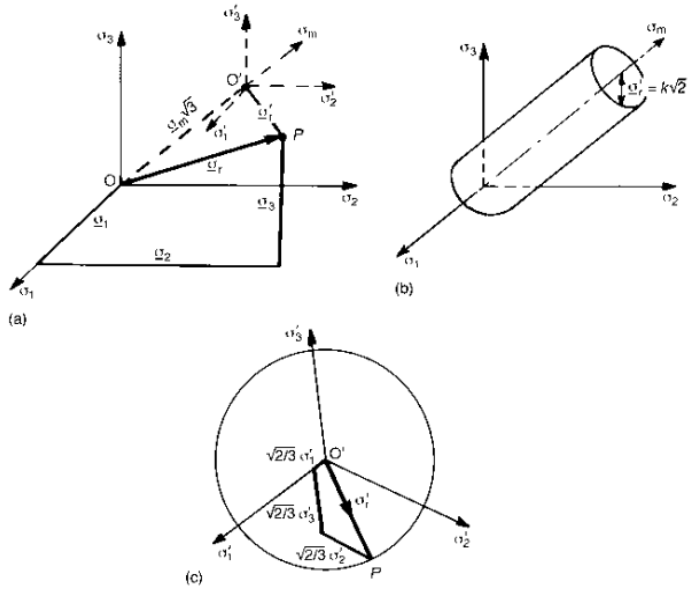

Fig.4.1 Geometrical representations of principal stresses and yielding

$$\varepsilon_{xx} = \frac{1}{E}\left[\sigma_{xx} - \nu(\sigma_{yy} + \sigma_{zz})\right]$$

$$\varepsilon_{yy} = \frac{1}{E}\left[\sigma_{yy} - \nu(\sigma_{zz} + \sigma_{xx})\right]$$

$$\varepsilon_{zz} = \frac{1}{E}\left[\sigma_{zz} - \nu(\sigma_{xx} + \sigma_{yy})\right]$$

$$\varepsilon_{xy} = \varepsilon_{yx} = \frac{1+\nu}{E}\sigma_{xy};$$

$$\varepsilon_{yz} = \varepsilon_{zy} = \frac{1+\nu}{E}\sigma_{yz}; \qquad \varepsilon_{zx} = \varepsilon_{xz} = \frac{1+\nu}{E}\sigma_{xz} \tag{4.7}$$

where E and υ are Young's modulus and Poisson's ratio. The strains have deviatoric and hydrostatic parts έ and ε_m ($\varepsilon_m = \varepsilon_v/3$). More compactly, in tensor notation

$$\varepsilon_{ij} \equiv \varepsilon'_{ij} + \delta_{ij}\varepsilon_m = \frac{1+\nu}{E}\sigma'_{ij} + \delta_{ij}\frac{1-2\nu}{E}\sigma_m \tag{4.8}$$

The inversion of this relation is

$$\sigma_{ij} \equiv \sigma'_{ij} + \delta_{ij}\sigma_m = \frac{E}{1+\nu}\varepsilon'_{ij} + \delta_{ij}\frac{E}{1-2\nu}\varepsilon_m \tag{4.9a}$$

or in incremental terms

$$d\sigma_{ij} \equiv d\sigma'_{ij} + \delta_{ij}d\sigma_m = \frac{E}{1+\nu}d\varepsilon'_{ij} + \delta_{ij}\frac{E}{1-2\nu}d\varepsilon_m \tag{4.9b}$$

Plastic and elastic strains

When the point P lies on the yield cylinder (Figure 4.1), and a stress increment causes further yielding, the total strain change has an elastic part proportional to it, and a plastic part normal to the yield locus:

$$\begin{aligned}(d\varepsilon_{ij})_{total} &\equiv (d\varepsilon'_{ij})_{total} + (\delta_{ij}d\varepsilon_m)_{elastic} \equiv (d\varepsilon'_{ij})_{plastic} + (d\varepsilon'_{ij})_{elastic} + (\delta_{ij}d\varepsilon_m)_e \\ &= \frac{3}{2}\frac{d\bar{\sigma}}{H'\bar{\sigma}}\sigma'_{ij} + \frac{1+\nu}{E}d\sigma'_{ij} + \delta_{ij}\frac{1-2\nu}{E}d\sigma_m\end{aligned} \tag{4.10}$$

The complexity in inverting this flow rule is caused by the presence in the right-hand side of both total stress and stress increment terms.

Elastic–plastic flow rule inversion

The elastic deviatoric strain increment of equation (4.10) is the difference between the total deviatoric and the plastic strain increment. It causes a deviatoric stress increment given by the deviatoric part of equation (4.9b):

$$\mathrm{d}\sigma'_{ij} = \frac{\mathrm{E}}{1+\nu}\left[(\mathrm{d}\varepsilon'_{ij})_{\text{total}} - \frac{3}{2}\,\frac{\mathrm{d}\bar{\sigma}}{H'\bar{\sigma}}\,\sigma'_{ij}\right] \tag{4.11a}$$

This may be substituted into the first of this equations

$$\mathrm{d}\bar{\sigma} = \frac{3}{2}\,\frac{\sigma'_{kl}}{\bar{\sigma}}\,\mathrm{d}\sigma'_{kl} \tag{4.11b}$$

$$\mathrm{d}\bar{\sigma} = \frac{3}{2}\,\frac{E}{1+\nu}\left[\frac{\sigma'_{kl}}{\bar{\sigma}}(\mathrm{d}\varepsilon'_{kl})_{\text{total}} - \frac{3}{2}\,\frac{\mathrm{d}\bar{\sigma}}{H'\bar{\sigma}}\,\frac{\sigma'_{kl}\sigma'_{kl}}{\bar{\sigma}}\right] \tag{4.12a}$$

After simplifying and rearranging, an expression for $\mathrm{d}\bar{\sigma}$ is found:

$$\mathrm{d}\bar{\sigma} = \frac{\frac{3}{2}\,\frac{E}{1+\nu}\,\sigma'_{kl}(\mathrm{d}\varepsilon'_{kl})_{\text{total}}}{\bar{\sigma}\left(1+\frac{3}{2}\,\frac{E}{1+\nu}\,\frac{1}{H'}\right)} \tag{4.12b}$$

Finally, substituting this back into the elastic deviatoric stress equation (4.11) and adding the hydrostatic stress term (equation (4.9b)), the total stress increment becomes (after dropping the subscript total , so $\mathrm{d}\varepsilon'_{kl}$ is the total deviatoric strain)

$$\mathrm{d}\sigma_{ij} = \frac{E}{1+\nu}\,\mathrm{d}\varepsilon'_{ij} + \delta_{ij}\,\frac{E}{1-2\nu}\,\mathrm{d}\varepsilon_{\mathrm{m}} - \frac{\frac{9}{4}\left(\frac{E}{1+\nu}\right)^{2}\sigma'_{ij}\sigma'_{kl}\mathrm{d}\varepsilon'_{kl}}{\bar{\sigma}^{2}\left(H'+\frac{3}{2}\,\frac{E}{1+\nu}\right)} \tag{4.13}$$

Because the sum of deviatoric stress terms $\delta_{kl}\sigma'_{kl}$ is zero, the total deviatoric strain increment $d\varepsilon'_{kl}$ in the last term may be replaced by the total strain increment $d\varepsilon_{kl}$.

Matrix notation

Tensor notation with the summation convention enables the most compact writing and analysis of relations between stress and strain. When it comes to applying the results, a different representation is more useful. The stress tensor σ_{ij} has nine components but, because $\sigma_{ij} = \sigma_{ji}$, only six are independent. The same applies to the strain tensor. The six independent stress components, regarded as a vector, may be obtained from the six independent strain components, also regarded as a vector, by matrix multiplication:

$$\begin{Bmatrix} \sigma_{xx} \\ \sigma_{yy} \\ \sigma_{zz} \\ \sigma_{xy} \\ \sigma_{yz} \\ \sigma_{zx} \end{Bmatrix} = \begin{bmatrix} \quad \mathbf{D} \quad \end{bmatrix} \begin{Bmatrix} \varepsilon_{xx} \\ \varepsilon_{yy} \\ \varepsilon_{zz} \\ \varepsilon_{xy} \\ \varepsilon_{yz} \\ \varepsilon_{zx} \end{Bmatrix} \quad \text{or} \quad \{\sigma\} = [\mathbf{D}]\{\varepsilon\} \tag{4.14}$$

Here, [D] is a 6 × 6 matrix. The values of its elements (as well as the detail of whether the vectors should be stress or stress increment, strain or strain increment) depend on whether the relation between stress and strain is elastic, elastic–plastic, or rigid–plastic.

Elastic conditions

Equation (4.14) can be written either in total or increment form:

$$\{\sigma\} = [\mathbf{D}^e]\{\varepsilon\} \quad \text{or} \quad \{d\sigma\} = [\mathbf{D}^e]\{d\varepsilon\} \tag{4.15a}$$

Where, from equation (4.9)

$$[\mathbf{D}^{e}] = \frac{E}{1+\nu}\begin{bmatrix} \frac{1-\nu}{1-2\nu} & \frac{\nu}{1-2\nu} & \frac{\nu}{1-2\nu} & 0 & 0 & 0 \\ \frac{\nu}{1-2\nu} & \frac{1-\nu}{1-2\nu} & \frac{\nu}{1-2\nu} & 0 & 0 & 0 \\ \frac{\nu}{1-2\nu} & \frac{\nu}{1-2\nu} & \frac{1-\nu}{1-2\nu} & 0 & 0 & 0 \\ 0 & 0 & 0 & 1 & 0 & 0 \\ 0 & 0 & 0 & 0 & 1 & 0 \\ 0 & 0 & 0 & 0 & 0 & 1 \end{bmatrix} \quad (4.15b)$$

Elastic–plastic conditions

Equation (4.14) must be used in incremental (or rate) form:

$$\{d\sigma\} = [\mathbf{D}^{e-p}]\{d\varepsilon\} \qquad \text{or} \qquad \{\dot{\sigma}\} = [\mathbf{D}^{e-p}]\{\dot{\varepsilon}\} \quad (4.16a)$$

where, from equation (4.13), after noting that the shear modulus G = 0.5E/(1 + n)

$$[\mathbf{D}^{e-p}] = [\mathbf{D}^{e}] - \frac{9G^2}{\bar{\sigma}^2(H'+3G)}\begin{bmatrix} \sigma'_{xx}\sigma'_{xx} & \sigma'_{xx}\sigma'_{yy} & \sigma'_{xx}\sigma'_{zz} & 2\sigma'_{xx}\sigma'_{xy} & 2\sigma'_{xx}\sigma'_{yz} & 2\sigma'_{xx}\sigma'_{zx} \\ \sigma'_{yy}\sigma'_{xx} & \sigma'_{yy}\sigma'_{yy} & \sigma'_{yy}\sigma'_{zz} & 2\sigma'_{yy}\sigma'_{xy} & 2\sigma'_{yy}\sigma'_{yz} & 2\sigma'_{yy}\sigma'_{zx} \\ \sigma'_{zz}\sigma'_{xx} & \sigma'_{zz}\sigma'_{yy} & \sigma'_{zz}\sigma'_{zz} & 2\sigma'_{zz}\sigma'_{xy} & 2\sigma'_{zz}\sigma'_{yz} & 2\sigma'_{zz}\sigma'_{zx} \\ \sigma'_{xy}\sigma'_{xx} & \sigma'_{xy}\sigma'_{yy} & \sigma'_{xy}\sigma'_{zz} & 2\sigma'_{xy}\sigma'_{xy} & 2\sigma'_{xy}\sigma'_{yz} & 2\sigma'_{xy}\sigma'_{yz} \\ \sigma'_{yz}\sigma'_{xx} & \sigma'_{yz}\sigma'_{yy} & \sigma'_{yz}\sigma'_{zz} & 2\sigma'_{yz}\sigma'_{xy} & 2\sigma'_{yz}\sigma'_{yz} & 2\sigma'_{yz}\sigma'_{zx} \\ \sigma'_{zx}\sigma'_{xx} & \sigma'_{zx}\sigma'_{yy} & \sigma'_{zx}\sigma'_{zz} & 2\sigma'_{zx}\sigma'_{xy} & 2\sigma'_{zx}\sigma'_{yz} & 2\sigma'_{zx}\sigma'_{zx} \end{bmatrix} \quad (4.16b)$$

Rigid–plastic conditions

The basic relation between stress and strain increment, for a base set of stresses so and strain increments $d\varepsilon_o$ leads to

$$\{\sigma_o\} = [\mathbf{D}_o^{r-p}]\{d\varepsilon_o\} \tag{4.17a}$$

with

$$[\mathbf{D}_o^{r-p}] = \frac{2\bar{\sigma}_o}{3d\bar{\varepsilon}_o}\begin{bmatrix} 1+a & a & a & 0 & 0 & 0 \\ a & 1+a & a & 0 & 0 & 0 \\ a & a & 1+a & 0 & 0 & 0 \\ 0 & 0 & 0 & 1 & 0 & 0 \\ 0 & 0 & 0 & 0 & 1 & 0 \\ 0 & 0 & 0 & 0 & 0 & 1 \end{bmatrix} \tag{4.17b}$$

where

$$a = \frac{1}{3}\left(\frac{1}{g} - \frac{1}{3}\right)$$

Linearization about the base σ_o and $d\varepsilon_o$ leads to

$$\{d\sigma\} = [\mathbf{D}^{r-p}]\{d(d\varepsilon)\} \tag{4.18}$$

Where $[D^{r-p}]$ can be extracted from equations (4.6).

4.2 Finite element formulations

The basic ideas of the finite element method are given in many general texts, for example Zienkiewicz (1989), as well as in Kobayashi et al. (1989). A continuum throughout which the solution to some problem is required is divided into an assembly of finite-sized elements, filling

the continuum without leaving any gaps. Each element is identified by the positions of its nodes. The nodes are the vertices of the elements and for some elements additional points too.

Instead of seeking an exact solution to a problem, over the whole continuum, an approximate solution is sought at the positions of the nodes, with some form of interpolation of the solution between the nodes. First, the governing equations of a problem are applied to each element alone, to obtain relations between the problem variables at the element nodes. These element nodal equations are then assembled to describe the whole continuum. The global assembly of all equations is finally solved numerically.

In mechanics problems, the nodal displacements, changes in displacements, or velocities,{u},{du} or {ů}, are usually the unknowns. They cause element strains, strain increments or strain rates {ε}, {dε} or {έ}, which depend on the element geometry. Transformation of the nodal displacement quantities to the element strain quantities may be carried out by a matrix multiplication operation: the transformation matrix is known as the [B] matrix. Once element strain expressions are created, they may further be transformed to stress quantities by operating with the [D] matrix. Finally, once element stress expressions are created, external force quantities on the element's nodes may be obtained either by direct consideration of force equilibrium or by virtual work methods. For the special cases of 3-node triangular or 4-node tetrahedral elements (for which stress and strain quantities are constant throughout an element), the transformation from stress to force is achieved by multiplication by the product of the element's volume, V_e, and the transpose of the [B] matrix; the chain of activities that relates nodal displacement and force quantities may be summarized as

$$\{u,\ \mathrm{d}u,\ \text{or } \dot{u}\} \xrightarrow{[\mathbf{B}]} \{\varepsilon,\ \mathrm{d}\varepsilon,\ \text{or } \dot{\varepsilon}\} \xrightarrow{[\mathbf{D}]} \{\sigma,\ \mathrm{d}\sigma,\ \text{or } \dot{\sigma}\} \xrightarrow{V_e[\mathbf{B}]^{\mathrm{T}}} \{F,\ \mathrm{d}F,\ \text{or } \dot{F}\} \tag{4.19}$$

and the resulting finite element assembly of equations to be solved becomes

$$\{F,\ \mathrm{d}F \text{ or } \dot{F}\} = [\mathbf{K}]\{u,\ \mathrm{d}u \text{ or } \dot{u}\} \tag{4.20}$$

Where $$[\mathbf{K}] = V_e[\mathbf{B}]^{\mathrm{T}}[\mathbf{D}][\mathbf{B}] \tag{4.21}$$

In general, for any shape of finite element, $[\mathbf{K}] = \int_{v_e} [\mathbf{B}]^{\mathrm{T}} [\mathbf{D}][\mathbf{B}] \mathrm{d}V$. [K] is known as the stiffness matrix and equation (4.21) as the stiffness equation.

It is not the purpose of this appendix to develop all aspects of the finite element method applied to metal machining problems, but only to indicate differences that arise from the differences in the [D] matrix between elastic, elastic–plastic and rigid–plastic formulations.

Elastic conditions

The coefficients of [D^e], equation (4.15b), are material constants. There is therefore a linear relation between the nodal forces and displacements, and force and displacement change. From equation (4.15a),

$$\{F\} = [\mathbf{K}]\{u\} \quad \text{or} \quad \{\mathrm{d}F\} = [\mathbf{K}]\{\mathrm{d}u\} \quad \text{or} \quad \{\dot{F}\} = [\mathbf{K}]\{\dot{u}\} \tag{4.22}$$

Elastic–plastic conditions

The coefficients of [De–p], (equation (4.16b)) include deviatoric stress terms. Integration of equation (4.16a) to obtain current total stresses and strains depends on the path by which the current state has been reached. Thus, after creating, from equation (4.16a),

$$\{\mathrm{d}F\} = [\mathbf{K}]\{\mathrm{d}u\} \quad \text{or} \quad \{\dot{F}\} = [\mathbf{K}]\{\dot{u}\} \tag{4.23}$$

displacement increments are calculated in steps along the problem's loading path. After each increment has been obtained, the accompanying strain and stress increments are calculated. The stress increments are added to the stresses that existed at the start of the step, to update [D^{e-p}] and hence [K]. The new value is used for the next step. The non-linearity of the calculation requires each step to be very small. Elastic–plastic calculations for large strain problems, as in metal machining, are inherently lengthy and time consuming.

Rigid–plastic conditions

Larger steps than in the elastic–plastic case can be taken with the rigid–plastic formulation; and hence the computing effort is less. However, it is not possible to simulate some aspects of chip formation, for example the elastic contact region of the chip/tool contact.

Suppose that over some time interval dt, the velocity of a plastic flow is guessed to be $\{\mathring{u}_o\}$, and a better guess is $\{\mathring{u}_o + \delta\mathring{u}\}$. The stiffness equation for the better guess is

$$\{F\} = [\mathbf{K}_o]\{\dot{u}_o\}dt + [\mathbf{K}]\{\delta\dot{u}\}dt \tag{4.24}$$

Where $[\mathbf{K}_o] = V_e[\mathbf{B}]^T[\mathbf{D}_o^{r-p}][\mathbf{B}]$ and $[\mathbf{K}] = V_e[\mathbf{B}]^T[\mathbf{D}^{r-p}][\mathbf{B}]$. $[\mathbf{D}_o^{r-p}]$ and $[\mathbf{D}^{r-p}]$ are given by equations (4.17b) and (4.18) (from equations (4.6)). Their coefficients are known in terms of the initial guess.

Equation (4.24) may be rearranged to

$$\{F\} - [\mathbf{K}_o]\{\dot{u}_o\}dt = [\mathbf{K}]\{\delta\dot{u}\}dt \tag{4.25}$$

The left-hand side is known in terms of the applied forces and the initial guess of velocities. Equation (4.25) may be solved for the unknown velocities $\{\delta\mathring{u}\}$. If they are significant relative to $\{\mathring{u}_o\}$, they may be added to $\{\mathring{u}_o\}$ to create a better initial guess; and the cycle of calculation is repeated until $\{\delta\mathring{u}\}$ becomes negligibly small. This approach to calculating flows, and hence stresses, in plastic problems, ignoring elastic deformation, with the modification of the yield criterion and flow rules to include a small amount of compressibility, to enable hydrostatic stresses to be calculated. It has been chosen because of the easy physical interpretation that can be given to the method of introducing hydrostatic stresses. Other methods, based on Lagrange multipliers and penalty functions give the same results.

4.3 Finite Element Modeling

In recent years, finite element method became the main tool for the analysis of metal cutting. Because it has important advantages, which can be counted as follows.

• Material properties can be handled as a function of strain, strain-rate, and temperature.

• Nonlinear geometric boundaries, such as free surfaces, can be modeled.

• Other than global variables like cutting force, thrust force; local variables like strains,

Strain-rates, stresses, etc. can be obtained.

• Interaction of chip and tool can be modeled in different forms.

In this work one commercial finite element code used to model three dimensional plain-strain orthogonal metal cutting operations.

The finite element method (FEM) has undoubtedly become the most popular and powerful analytical tool for studying the behaviour of a wide range of engineering and physical problems. Several general purpose finite element softwares have been developed, verified and calibrated over the years and are now available to almost anyone. One of the important applications of FEM is the analysis of metal cutting problems. The ANSYS software is one of the finite element method packages available to analyze metal cutting process problems which have different elements for discretization and modelling isotropic materials. Among them SOLID186 is a higher order 3-D 20-node solid element that exhibits quadratic displacement behavior. The element is defined by 20 nodes having three degrees of freedom per node: translations in the nodal x, y, and z directions. The element supports plasticity, hyperelasticity, creep, stress stiffening, large deflection, and large strain capabilities.

Figure 4.2 SOLID186 structural solid Geometry

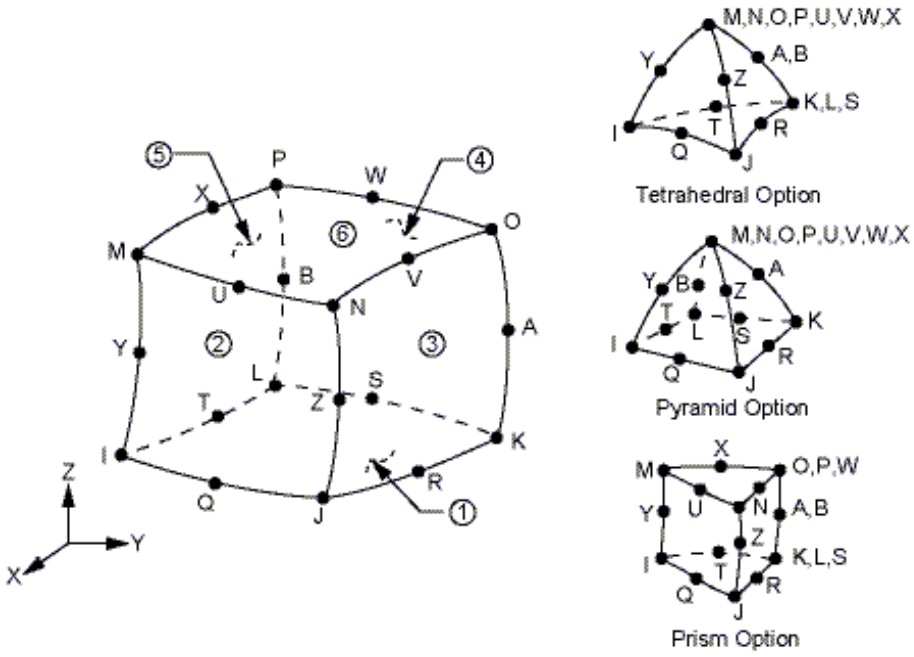

SOLID186 Structural Solid is well suited to modeling irregular meshes (such as those produced by various CAD/CAM systems). The element may have any spatial orientation. This element supports all nonlinear features allowed for an explicit dynamic analysis.

4.4 Modeling of cylindrical hollow material with chip flow in ANSYS

The cylindrical hollow material is modeled using ANSYS, which is used for pre and post-processing of model with FEA as the solver. The model is created in the preprocessing stage of the model generation and the results are viewed in the post processing stage. The cylindrical hollow material is created using SOLID186 (3-D 20-Node Structural Solid) element. The properties of the material are given as input using ANSYS material library and the real constant command is used for defining the cylindrical material structure.

The chip flow in a cylindrical hollow material is generated by cutting out a half/semi circular cylinder volume with the rake angle on the outer face of hollow material structure having with wedge shape and oriented in upward direction.

The chip is described schematically as seen in figure 4.3, which is modeled by removing semi-circular cylindrical volume from the cylindrical hollow material end section/face.

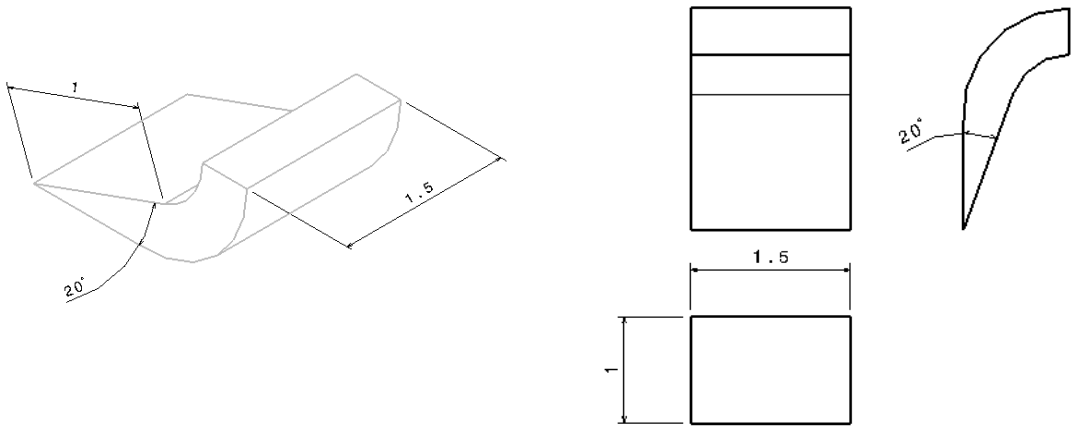

Figure 4.3 Model of chip

4.5 Description of the parameters of the model

Chip description

As seen in figure 4.3 a wedge shape chip is generated by removing out a semi-circular cylindrical volume from the hollow cylindrical material having a rake angle 20 degrees, width of chip $c=1.50*10^{-3}$ m, and a length of $f=1.0*10^{-3}$m.

The hollow cylinder material with the chip model structure is shown in figures 4.4 & 4.5.

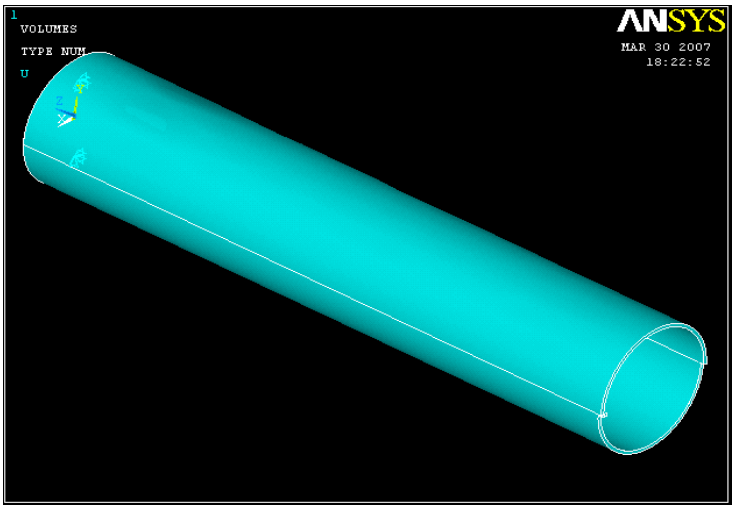

Figure 4.4 Model of cylindrical hollow material with chip flow.

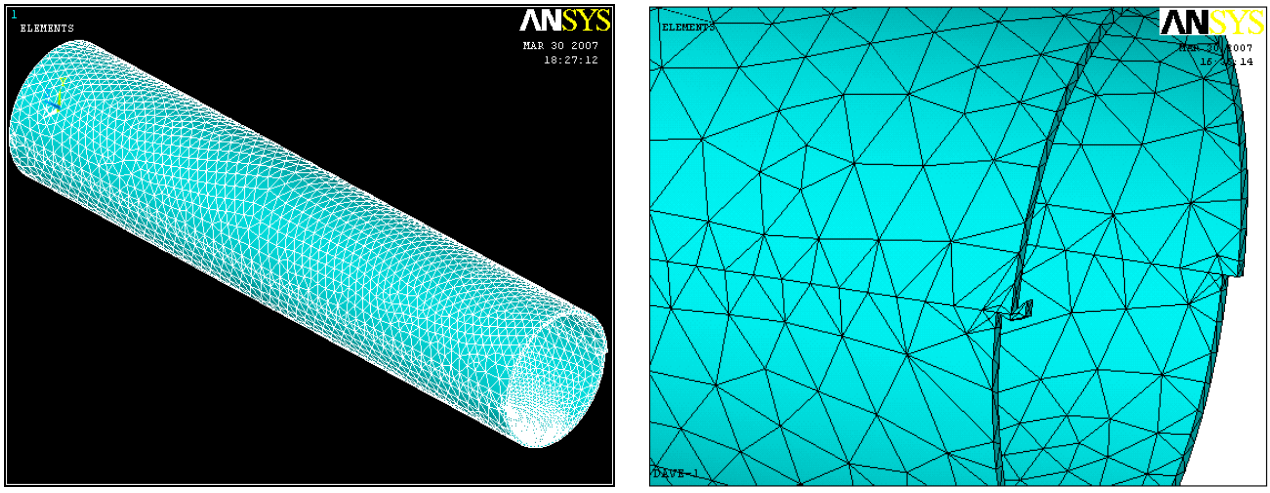

Figure 4.5 Model of meshed hollow material with chip flow.

Meshing the model

The model is meshed with automatic mesh generation command “Auto Mesh Generation”. As can be seen from figure 4.5, the model is meshed with more refined elements in the chip and coarsely meshed in areas away from the chip flow model to economize the computation time.

Geometric parameters of the model

Outer diameter=40mm

Inner diameter=37mm

Length of the hollow cylinder material=200mm.

The material of the hollow cylinder is made of linear elastic isotropic material with the following properties.

Material = mild steel

Poison's ratio = 0.3

Modulus of elasticity = 210Gpa

Density = 7.85 g/cm^3

4.6 Loading and boundary conditions

The hollow material is constrained as shown in figure 4.6. The material is constrained at Z = 0, Y =0, & X = 0 by assuming it is fixed, but in reality it rotates with specified or mentioned in the experimental work. Since it is difficult to model the material having with rotational speed by ANSYS, so it is better to put an assumption. The force/load is the cutting forces which are taken from the experimental work are applied at a distance of less than 200mm from the fixed boundary condition.

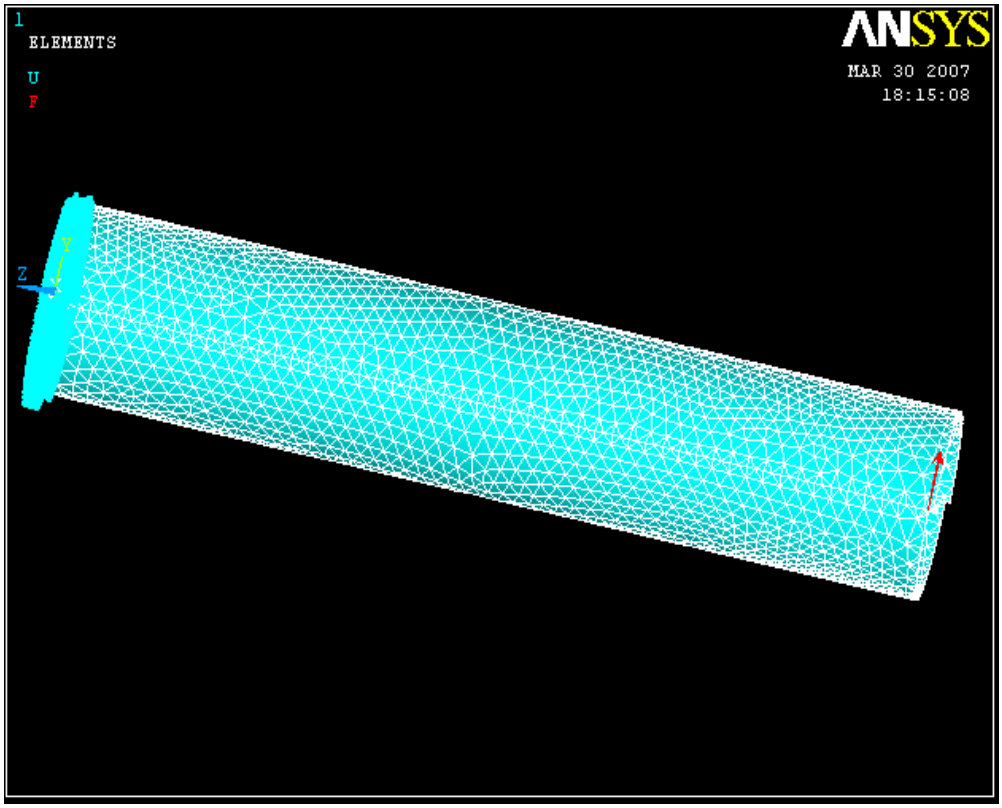

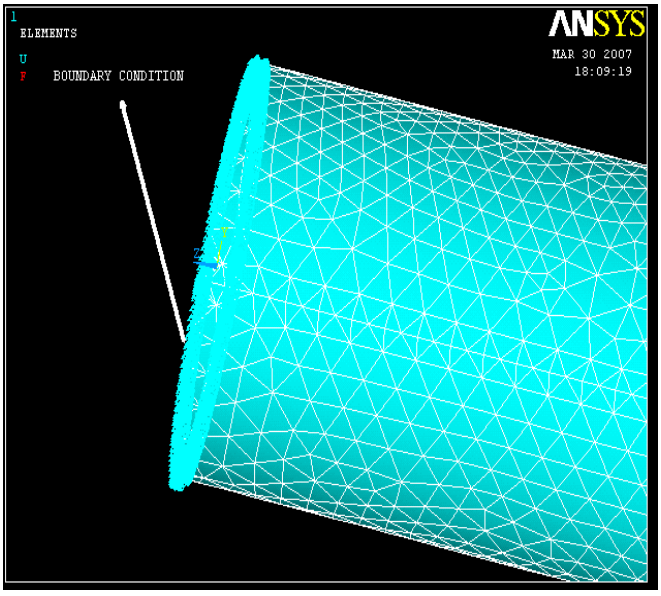

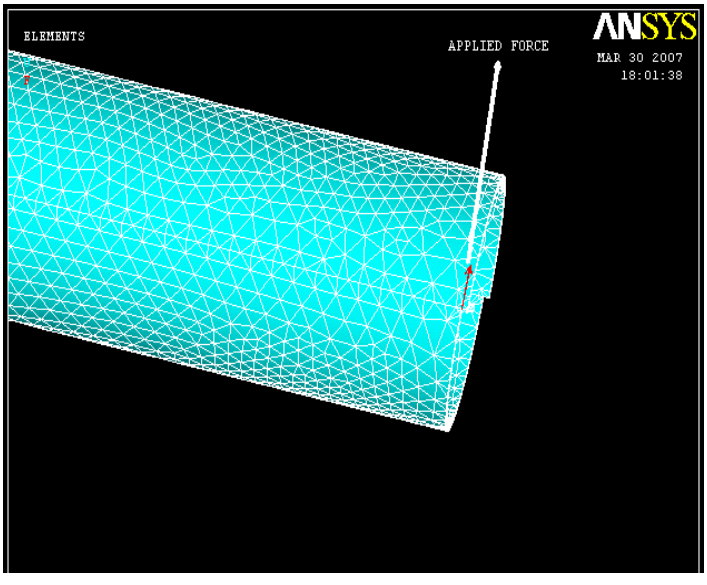

Figure 4.6 Model with loading & boundary condition

Chapter 5

Results and Discussion

5.1 Experimental Results

Experimental data was collected when cutting mild steel material. The cutting speed and rake angle were varied at a time keeping one variable constant.

Rake angle, which is one of geometry constituted components, has considerable effect on the main cutting force, which has a great influence on the surface finish, dimensional accuracy and quality of work. There usually an optimum value for the rake angle. Increasing the rake angle more than its optimum value negatively affects tool resistance and this effect accelerates tool wear mechanisms. Excessive wear causes wider clearance face contacting to machined surface, as a result cutting forces increase. However, increase of rake angle until certain value through positive direction causes reduction of tool/chip contact length, so cutting forces expected to be reduced. Particularly, increasing of contact area in negative angles and machining chip volume considerably cutting forces and heat generation too much.

5.1.1 The effect of cutting speed on main cutting force (F_c)

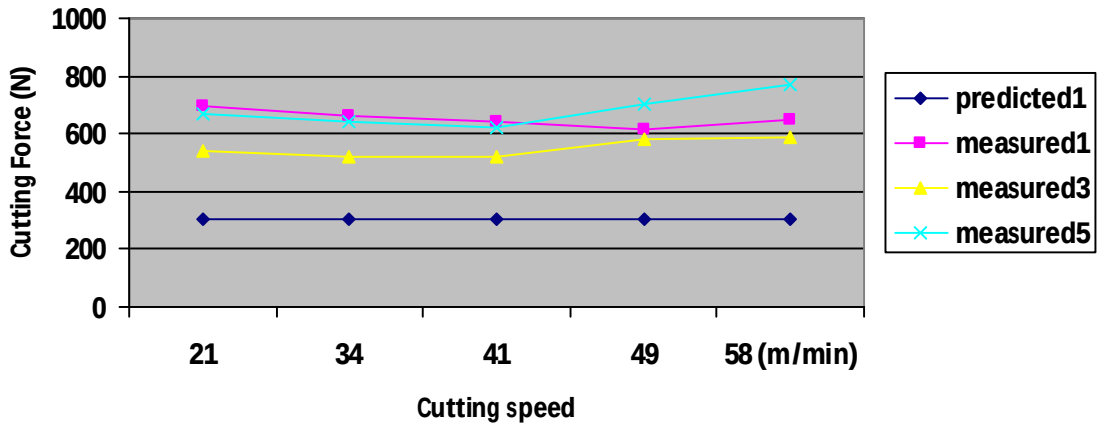

Figure 5.1: Cutting speed versus main cutting force & comparison of cutting force between experiments & analysis

In this section the results are presented by taking the force output from the analysis and the force output measured from experiments are compared.

The cut was orthogonal with feed of 0.05mm/rev, depth of cut 1.5mm, and cutting speeds of 21, 34, 41, 49, 58m/min. When average values of the measured force from the experiments are compared with the force from the predicted, the following results are achieved. As shown in fig.5.1 above, the predicted cutting force is underestimated compared to forces measured from the experiments. In this work the focus was on the cutting force, because it is this force which typically is the most important regarding fixation in the lathes machines. It was also found in the fig.5.1 that the measured cutting force decreased with an increase in cutting speed up to 41m/min and beyond this speed it was increased. One possible explanation is that the strength of the workpiece decreases as the temperature increases with an increase in cutting speed. Another possible explanation is that if the shear strength is assumed to be uniform in the primary deformation zone, the shear force will be reduced because the chip thickness is less at higher cutting speeds. This will then decrease the cutting forces up to some cutting speed.

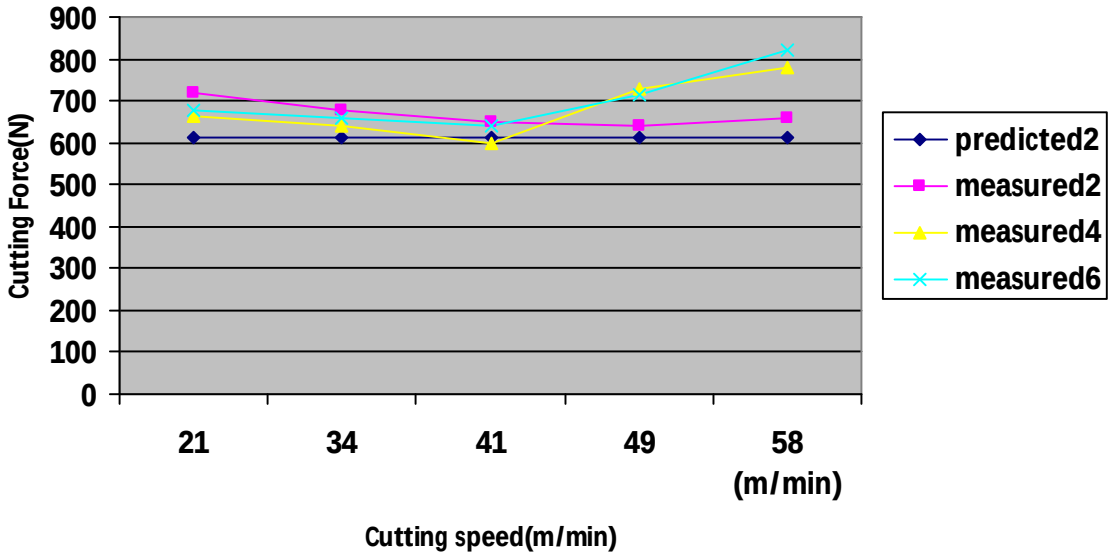

Figure 5.2: Cutting speed versus main cutting force & comparison of cutting force between experiments & analysis

The figure 5.2 show that orthogonal cutting with feed of 0.1mm/rev, depth of cut of 1.5mm, and cutting speeds of 21, 34, 41, 49, 58m/min. When average values of the measured force from the experiments are compared with the force from the predicted, the following results are achieved. The predicted cutting forces here are also underestimated, but a satisfactory match is observed when the predicted cutting forces are compared with experiments measurements. The measured forces in this study also decreases up to 41m/min as cutting speed increases. This decrease also assumed as the result of the thermal softening effect over the workpiece effect as cutting speed increases. Another observation in the experiments was, as the cutting speed increases surface finish of the work material also increases. The effect of cutting speed is only on the surface texture of the work material. The cutting force is dependent on depth of cut and feed of rate. The graph above show that as the cutting speed is increasing, the predicted force is constant but the measured force is variable. The possible explanation for the variable is that due to external influence, machining conditions, use of cutting tool repeatedly & machining without using of coolant.

The main cutting force was found maximum when the cutting speed reached at 58 m/min, feed rate of 0.1mmpr and rake angle of 25 degree. On the other hand, the minimum cutting force was observed when the cutting speed reached at 41m/min with feed rate of 0.05mm/rev for the rake angle of 20 degree. Thus, evaluating the results of machining conditions in respect to low cutting force, the optimum cutting speed was obtained for the rake angle of 20 degree.

5.1.2 The effect of rake angle on main cutting force

Main cutting force results were obtained with constant depth of cut of 1.5 mm, feed rate of 0.05 & 0.1 mm/rev, five different cutting speeds 21,34,41,49 and 58m/min and tool rake angles of 15, 20 & 25 degrees as given in table 3.3 (a-f). Based on values listed in table 3.3, main cutting force values for different rake angles were given. From the figure we can observe that rake angle has an important effect on all the measured cutting force components. Positive rake angle produces higher shear angle; therefore, it leads to reduction of cutting forces. It also leaves a better surface finish since it assists the chip to flow away from the work-piece. But, excessive rake angle

weakens the tool, thus causes to tool breakage. As a result, as the cutting forces and temperature were reduced considerably, and the optimum rake angle was obtained as 20 degree.

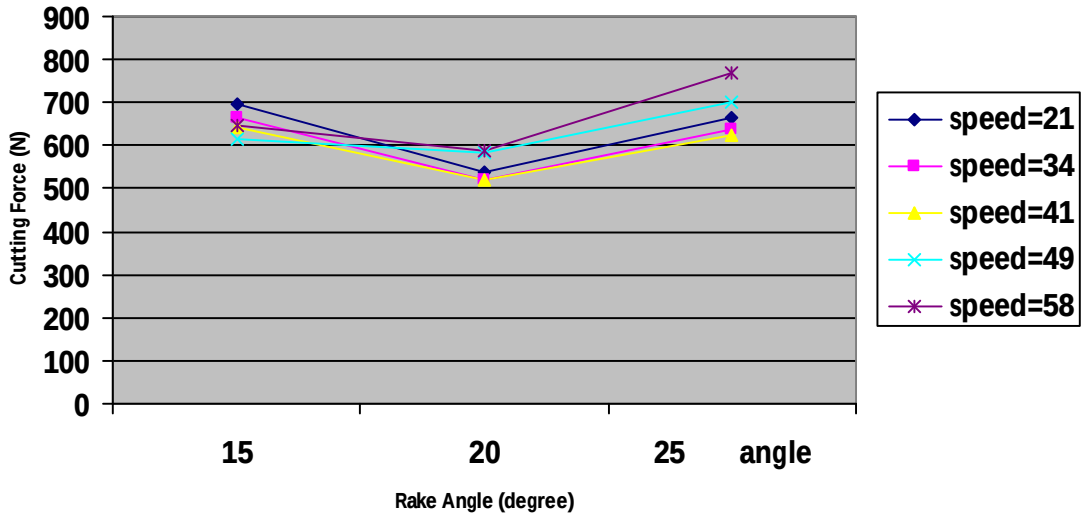

Fig.5.3: Main cutting force alteration due to rake angle with feed of 0.05mm/rev.

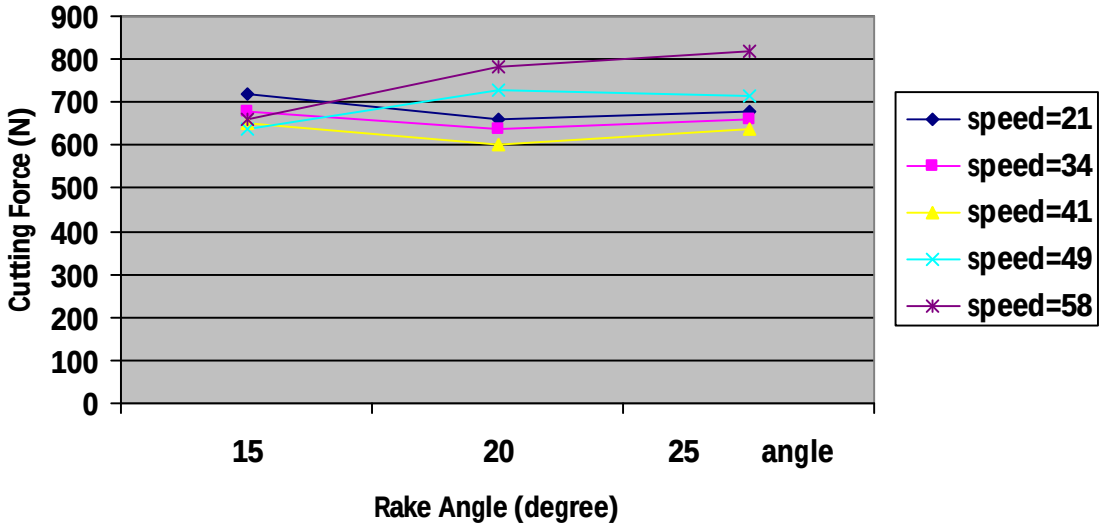

Fig.5.4: Main cutting force alteration due to rake angle with feed of 0.1mm/rev.

The most remarkable result concluded from fig.5.3 & fig.5.4 is that main cutting force was increased in the positive direction of rake angle, for all cutting speeds, while cutting force was decreased by given positive rake angle up to some value of cutting speed (41m/min). This is due to changing of tool/chip contact area. This result was identical with previous works. It was discussed that the change of rake angle in positive direction had positive influence on cutting forces. This situation attributed decreasing tool/chip contact area and friction force. In this way chip flows easier. Same situation was confirmed in this study and the results showed decreasing of cutting force with alteration of rake angle in the positive direction. The decrement of the main cutting force with respect to the increment of the rake angle holds good until some optimum value, that is, for cutting mild steel material, the optimum cutting tool rake angle was found to be 20 degree.

5.2 Analysis of Modeling of cylindrical hollow material with chip flow in ANSYS

The finite element analysis done on ANSYS by modeling the cylindrical hollow material structure having chip flow is to determine the stress and their distribution around the contact of chip and workpiece. In the model, the tool was pushed to penetrate through the workpiece to form the chip. The loading conditions applied are the main cutting forces which get from the experiment result of optimum rake angle of 20 degree. In the model with ansys, the left boundary nodes are fixed in x-direction, y-direction & z-direction while the right boundary nodes are applied by the main cutting force in the positive y- direction.

The main motive in this work is to investigate the distribution of stresses or strains around the Surface contact of chip and workpiece.

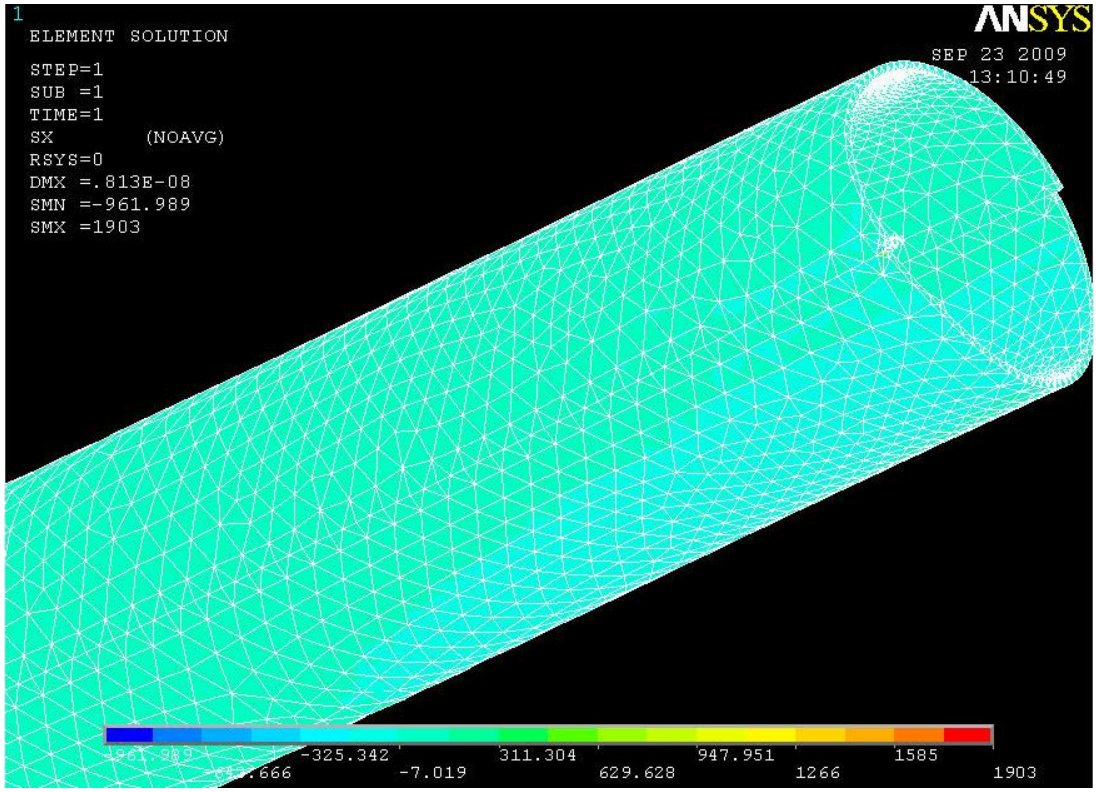

Figure 5.5(a) Distribution of X-component stress plot

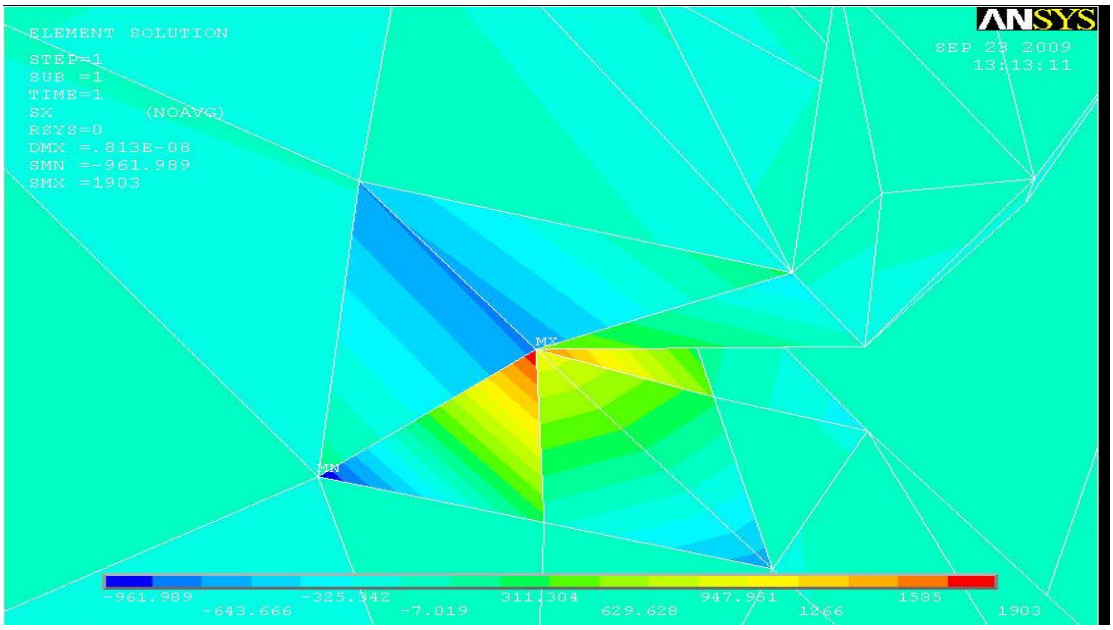

Figure 5.5(b) Distribution of X-component stress around the contact chip & workpiece, magnified view

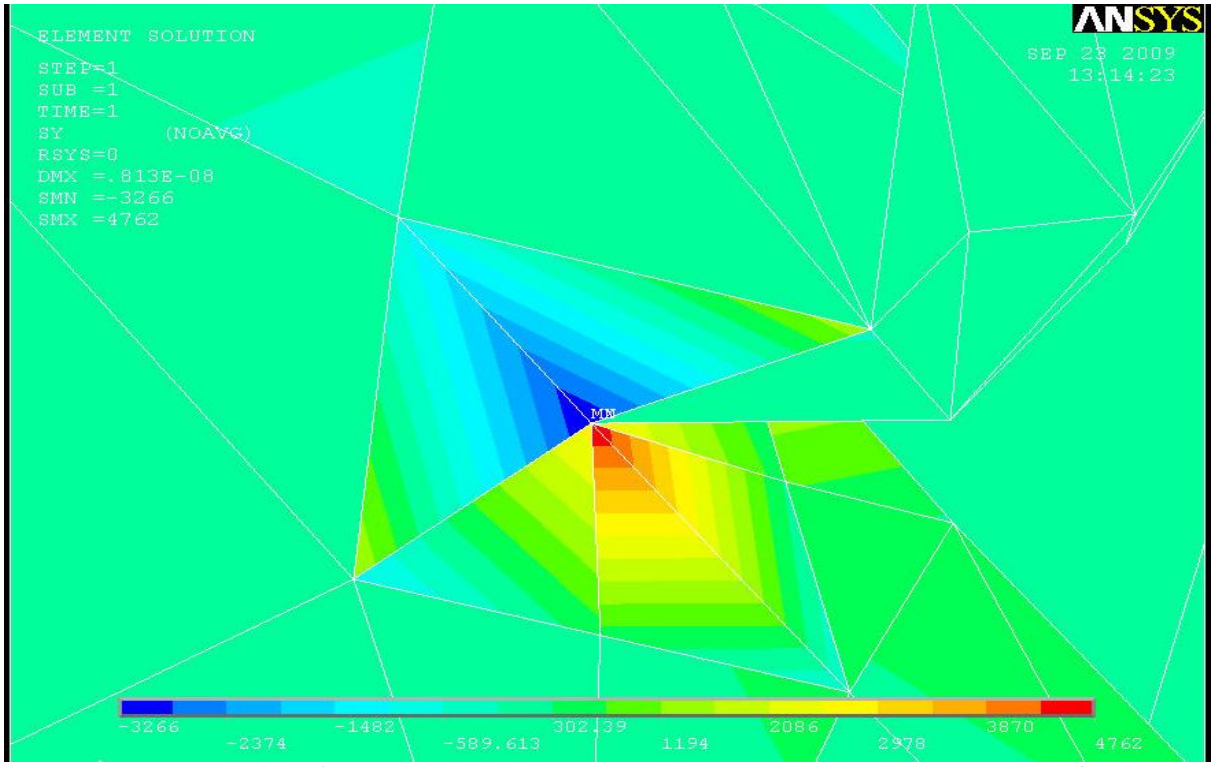

Figure 5.6 Distribution of Y-component stress around the contact chip & workpiece, magnified view

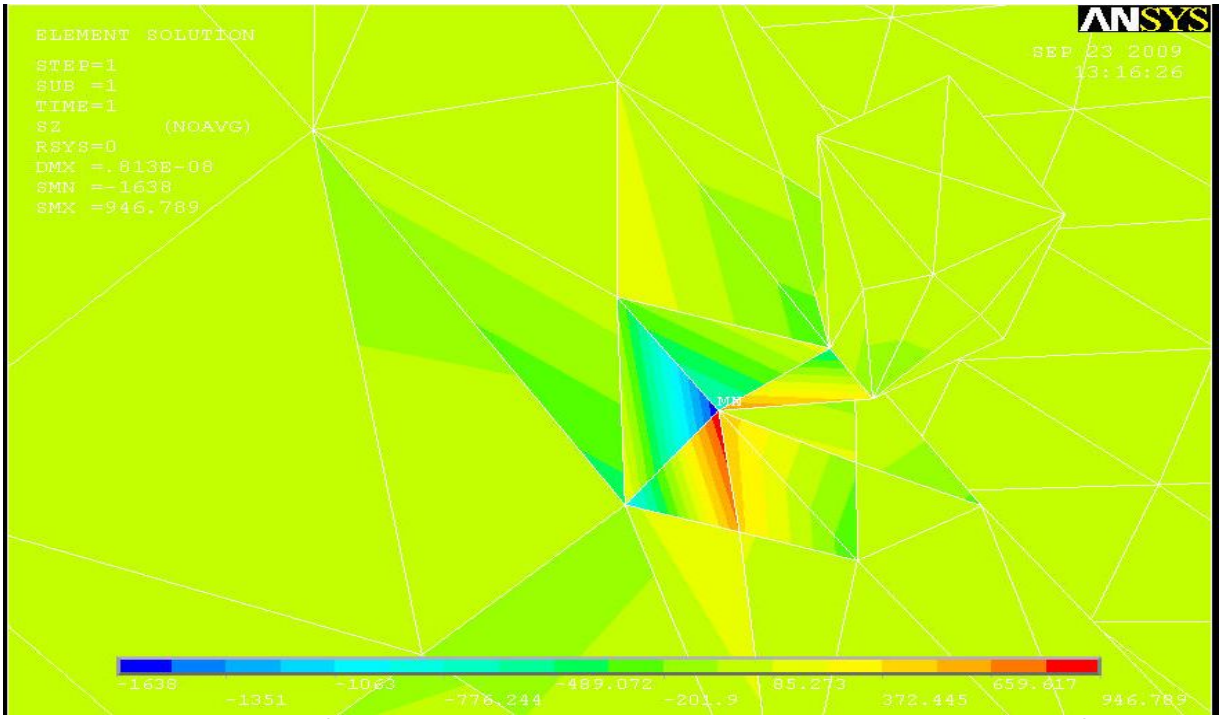

Figure 5.7 Distribution of Z-component stress around the contact chip & workpiece, magnified view

As seen clearly in the figures (5.5-5.7), the unidirectional stresses in the X, Y, and Z directions, the maximum stresses shown are distributed in the vicinity of the contact of chip flow and material but are not uniform around the contact of chip & material front rather localized somewhere near the contact face. On the other case, the shear stress distribution (figures 5.8-5.10) shows somewhat different orientation a slight localized near the contact of chip and material faces. Due to the main cutting force applied in the cutting edge of tool the deformation become narrow, then the shear stress distribution is high around the contact of chip and material, but not uniform a slight farthest away from the contact face.

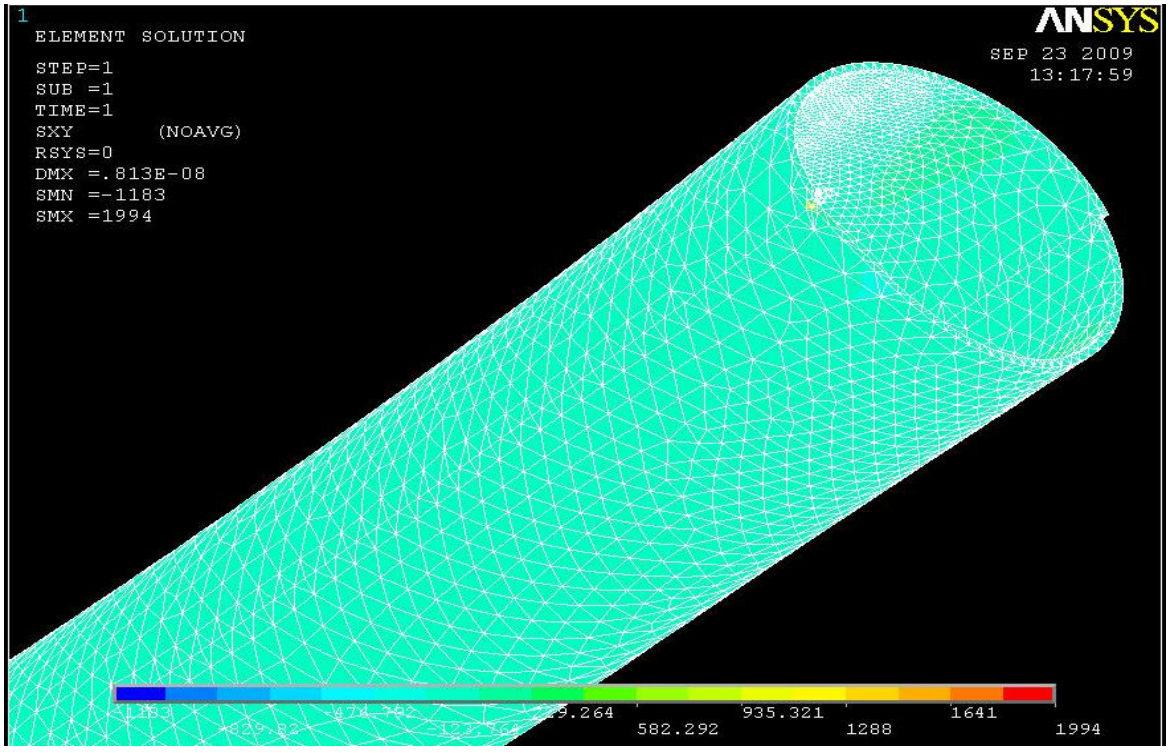

Figure 5.8(a) Distribution of XY-shear stress plot

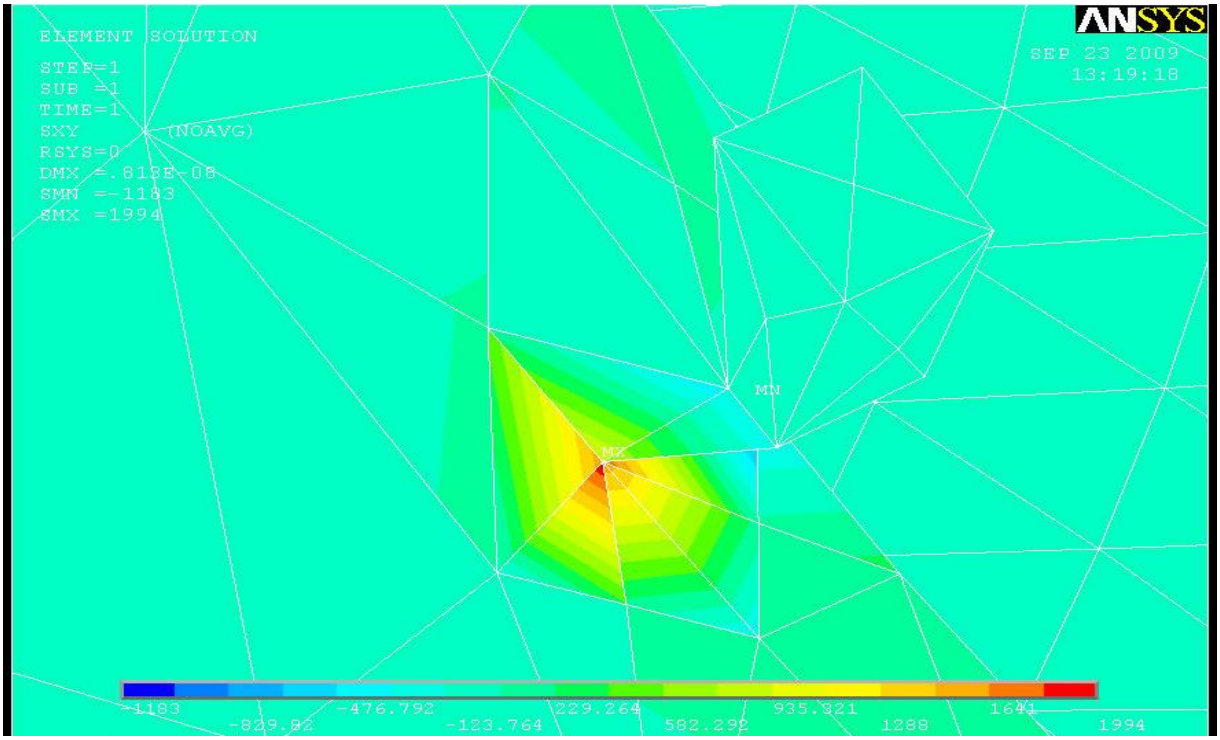

Figure 5.8(b) Distribution of XY-shear stress around the contact chip & workpiece, magnified view

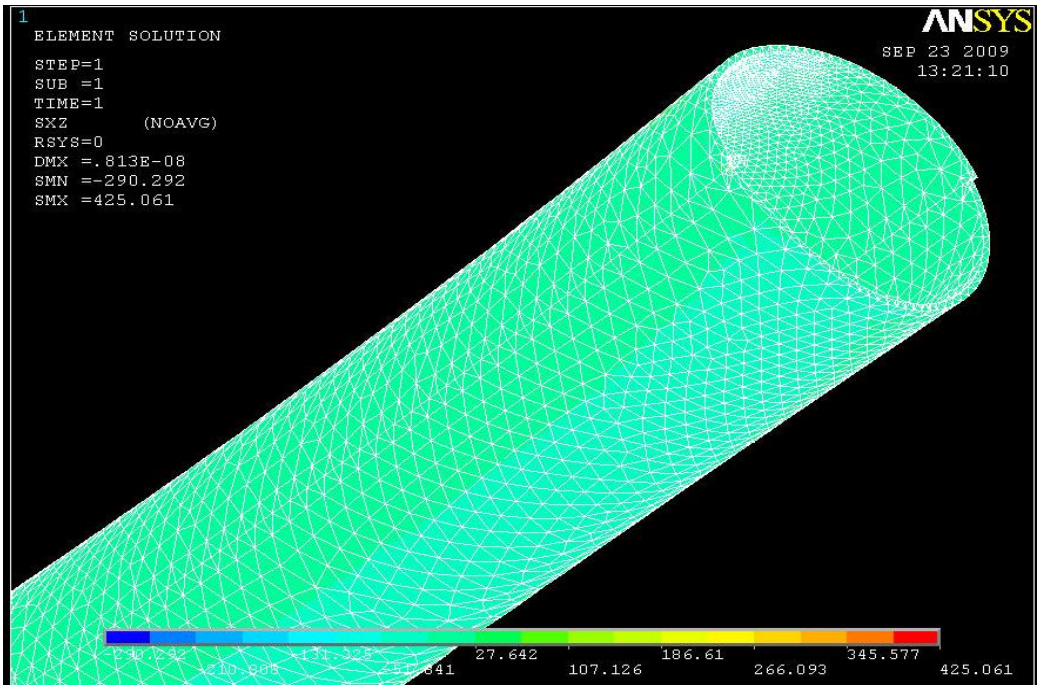

Figure 5.9(a) Distribution of XZ-shear stress plot

The stress effect in the material transfers the load applied in the tangential direction to the whole body of the material in axial and radial direction as seen in the shear stress plots. In addition the shear stress induced within the material is also showing some form of localized patterns that will have its own contribution for the advance of penetration the workpiece.

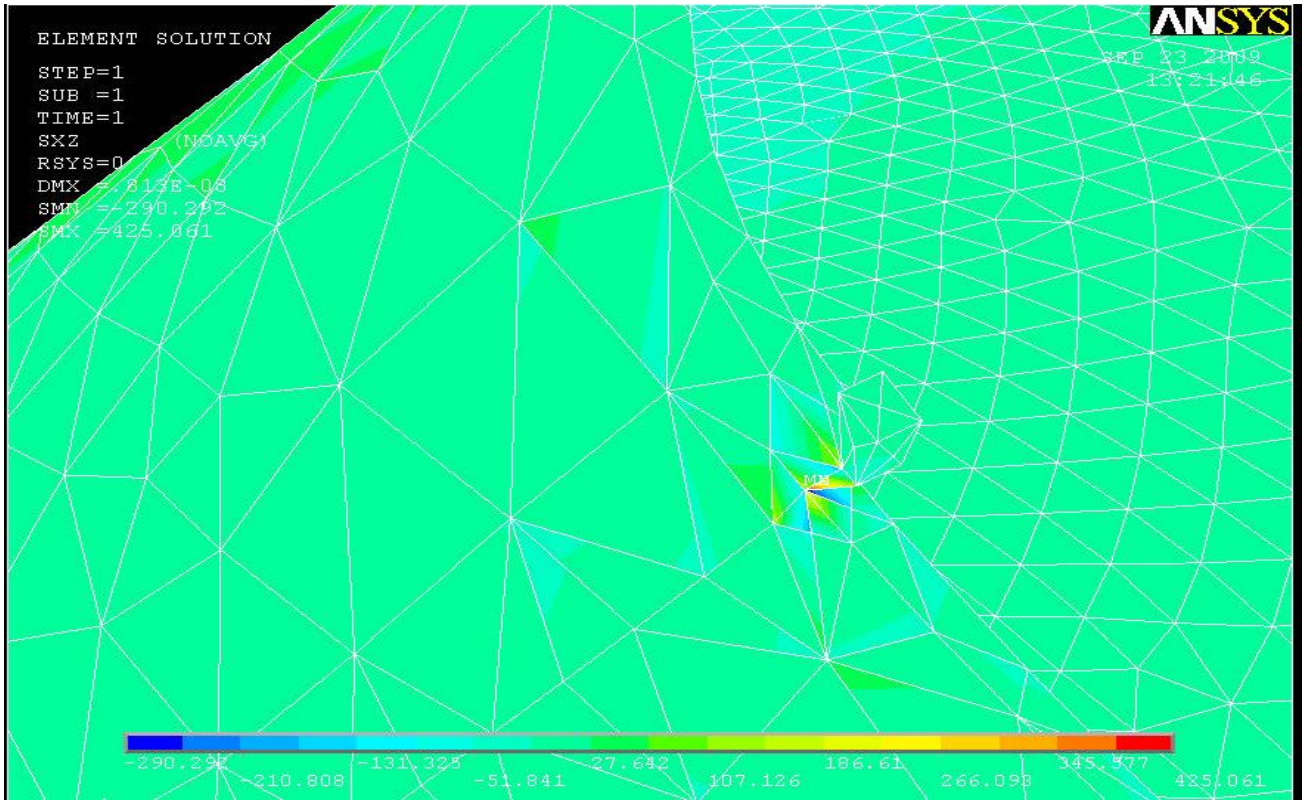

Figure 5.9(b) Distribution of XZ-shear stress around the contact chip & workpiece, magnified view

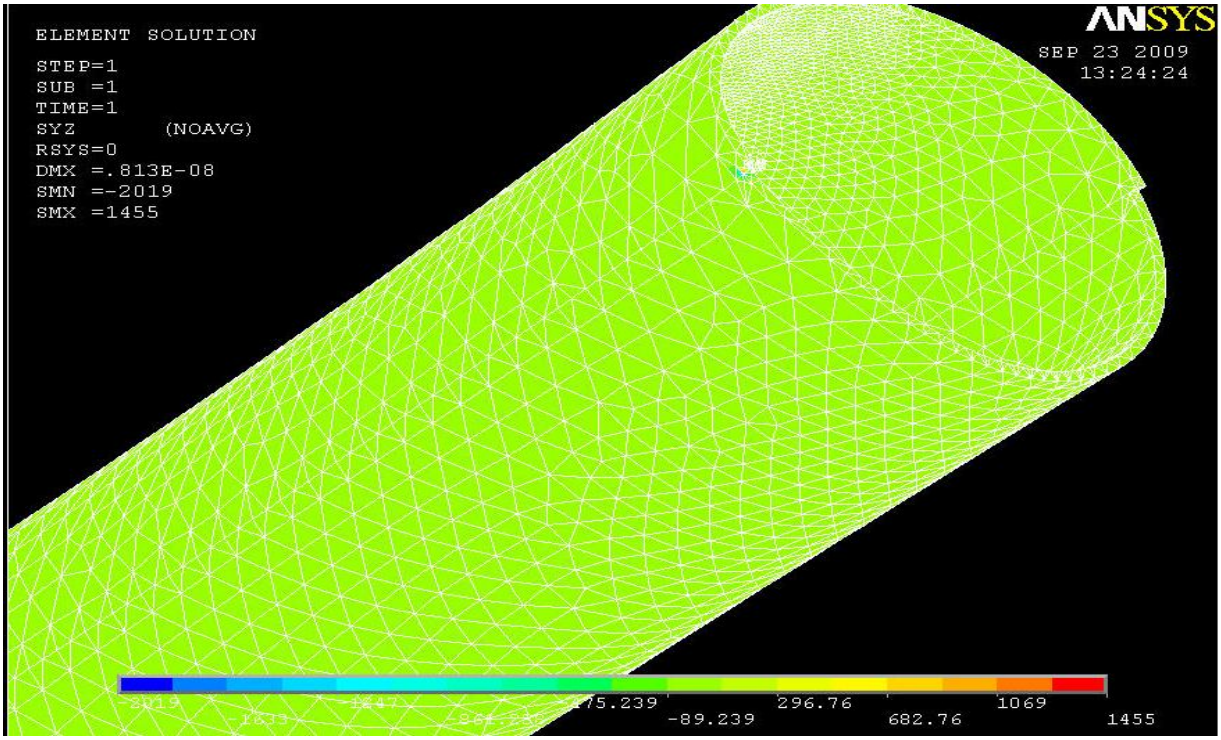

Figure 5.10(a) Distribution of YZ-shear stress plot

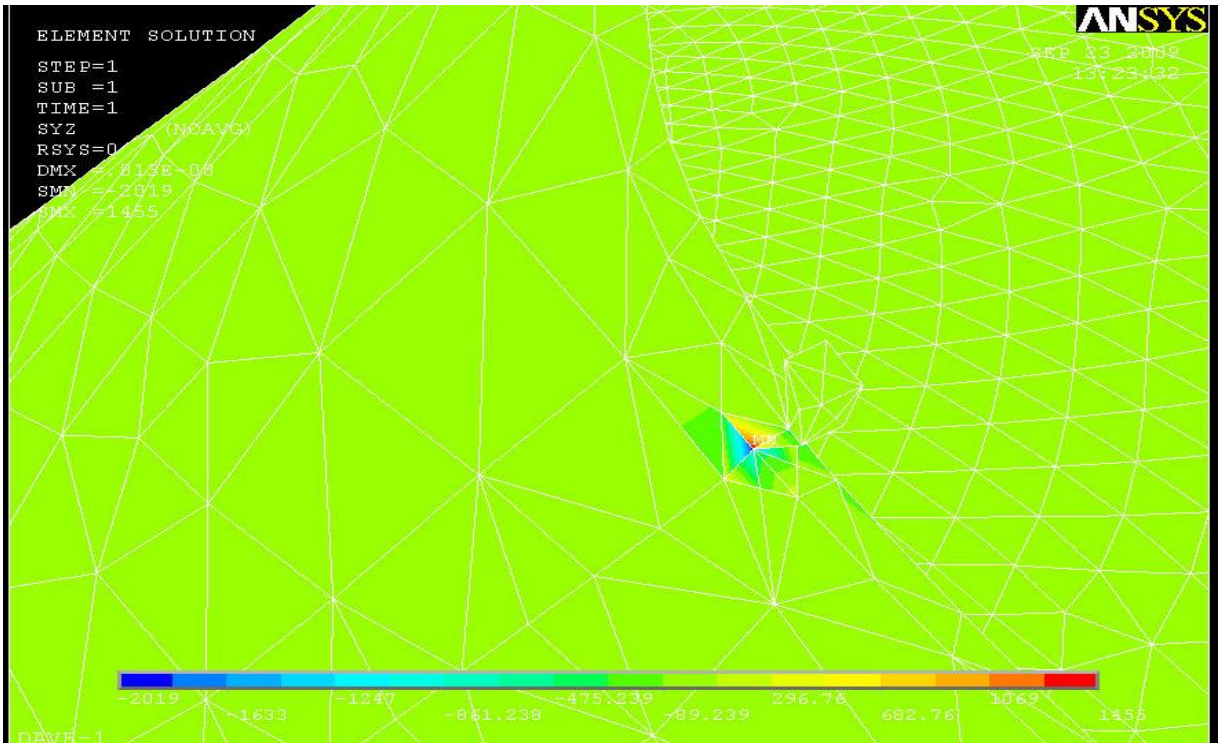

Figure 5.10(b) Distribution of YZ-shear stress around the contact chip & workpiece, magnified view

The localized stress intensity, von Misses stress and the von Misses total strain plots (figure 5.11-5.13) reveal that their maximum values are shielded in front of the maximum penetration line of the contact between chip and material. This is happening due to the greater resistance of the propagation of the localized stress in the material structure is faced at the narrowest part of contact between chip and material.

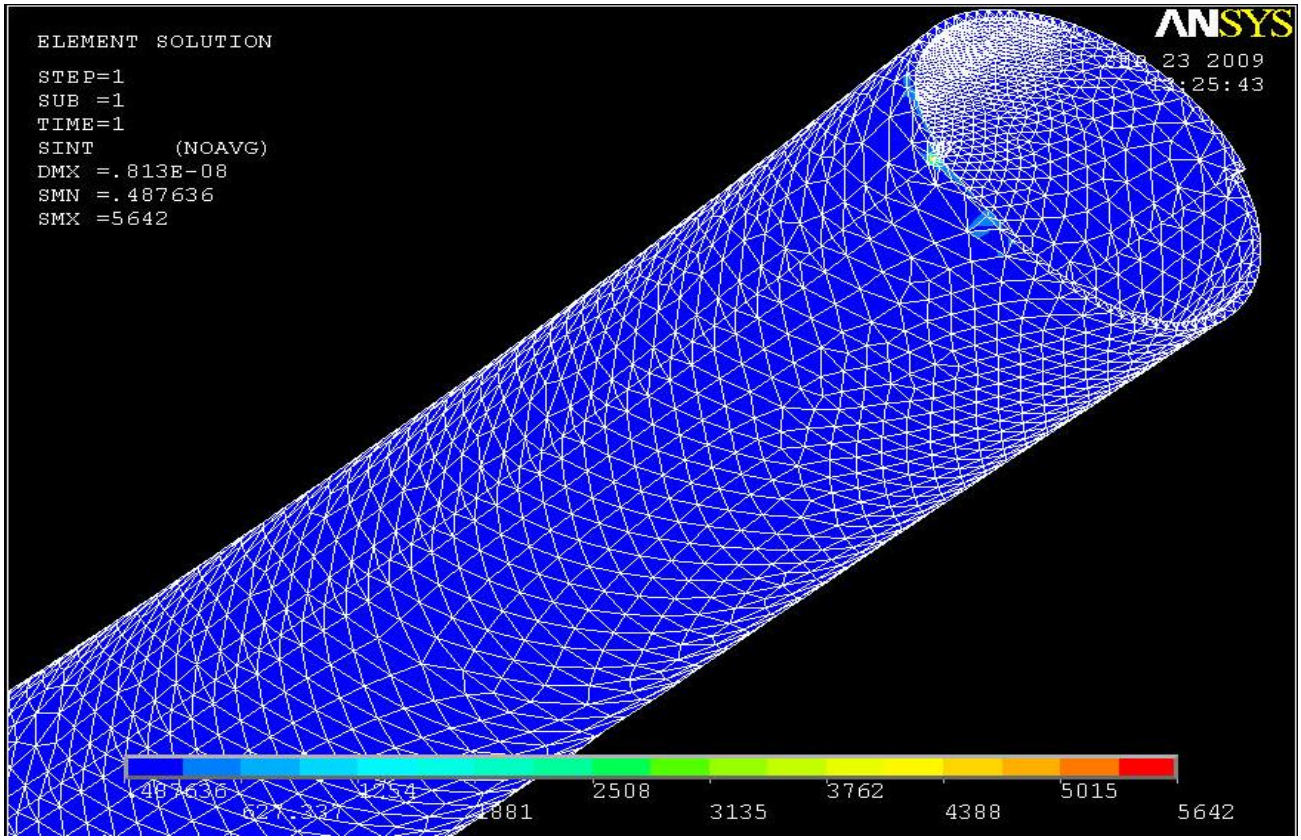

Figure 5.11(a) Distribution of stress intensity plot

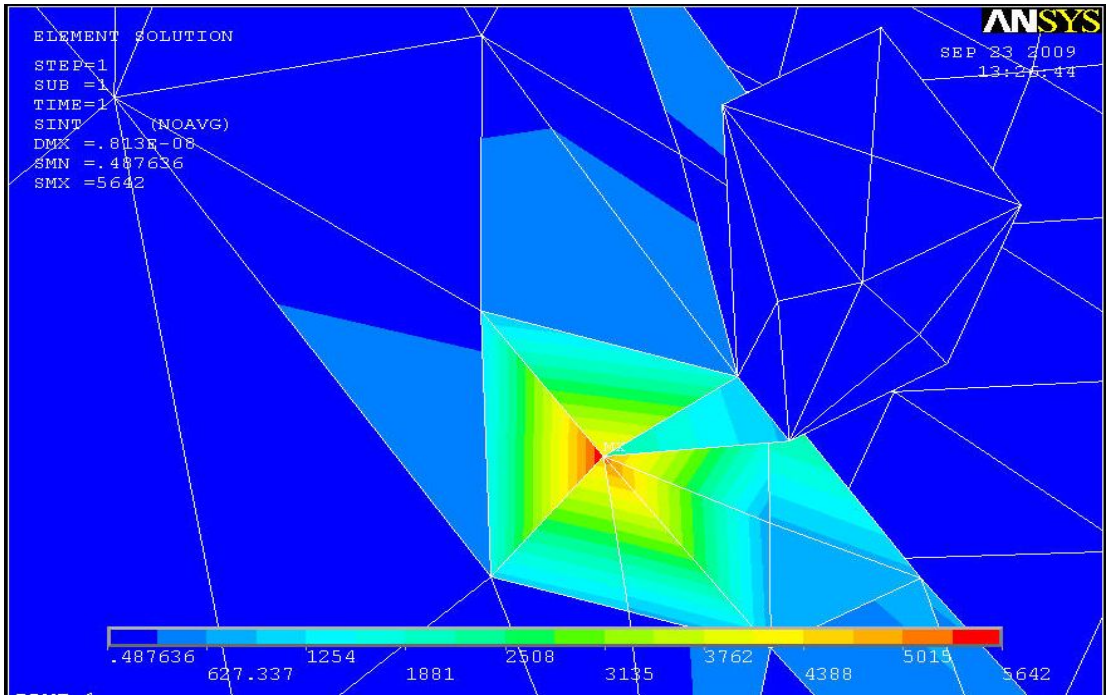

Figure 5.11(b) Distribution of stress intensity around the contact chip & workpiece, magnified view

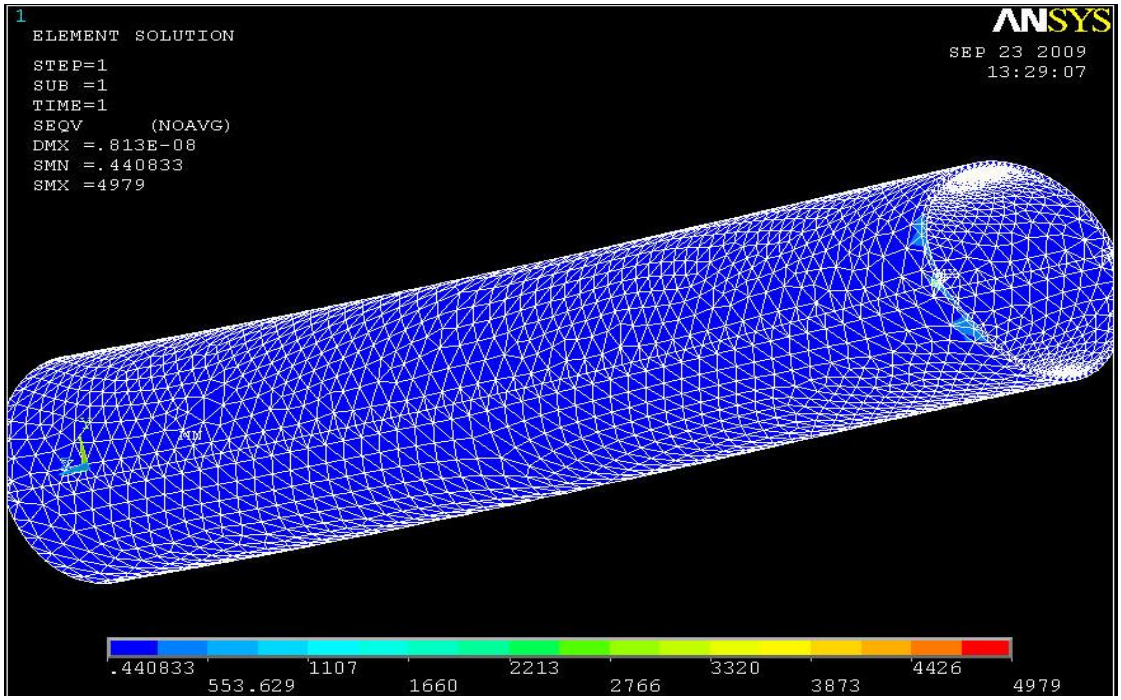

Figure 5.12(a) Distribution of von Misses stress plot

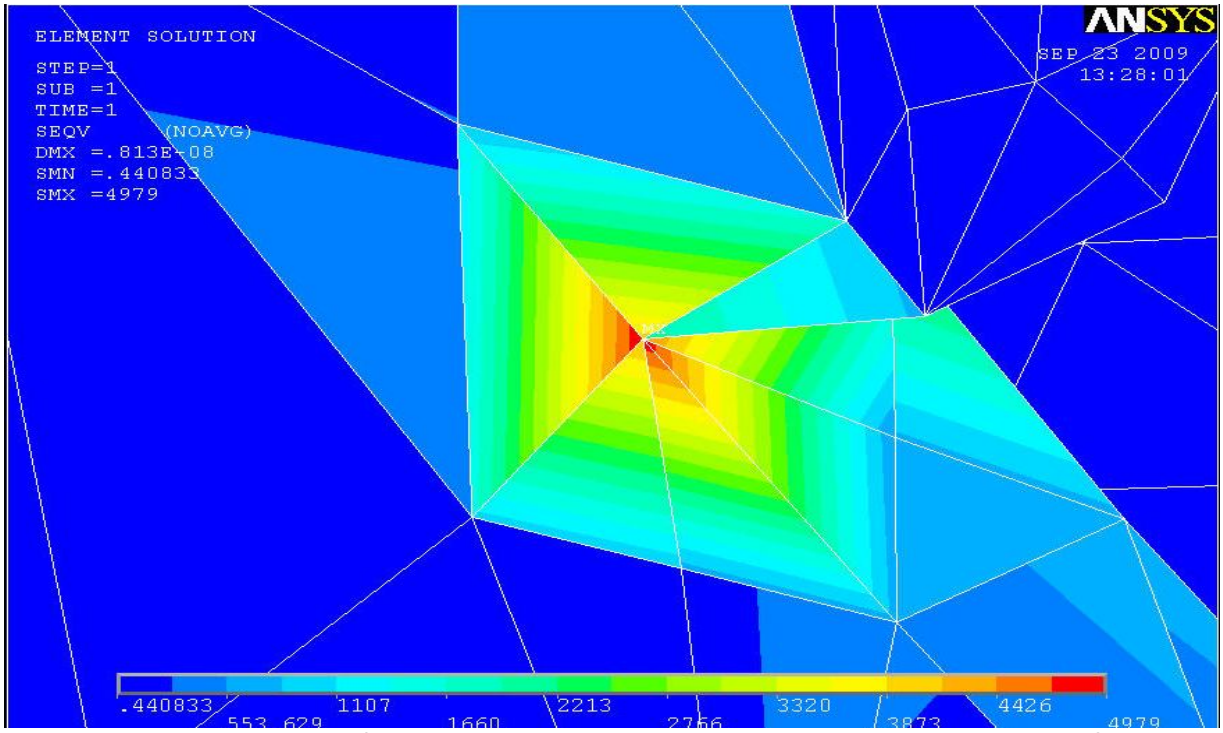

Figure 5.12(b) Distribution of von Misses stress around the contact chip & workpiece, magnified view

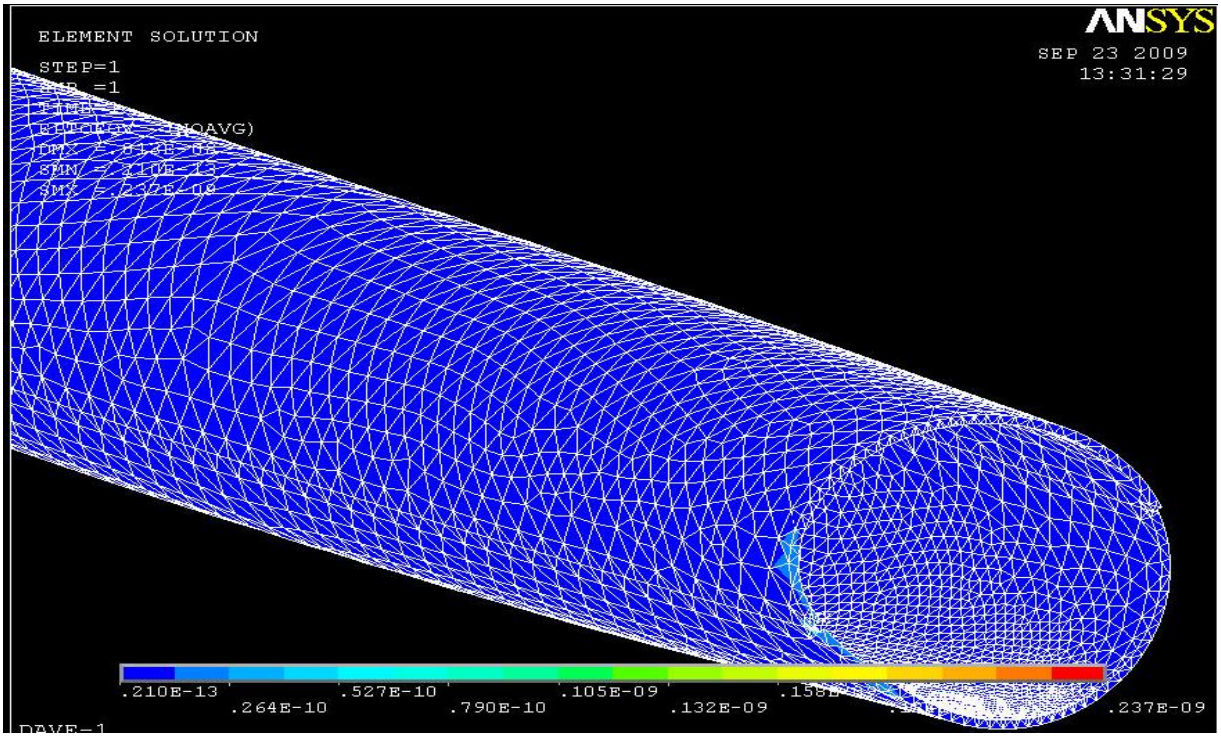

Figure 5.13(a) Distribution of von Misses total strain plot

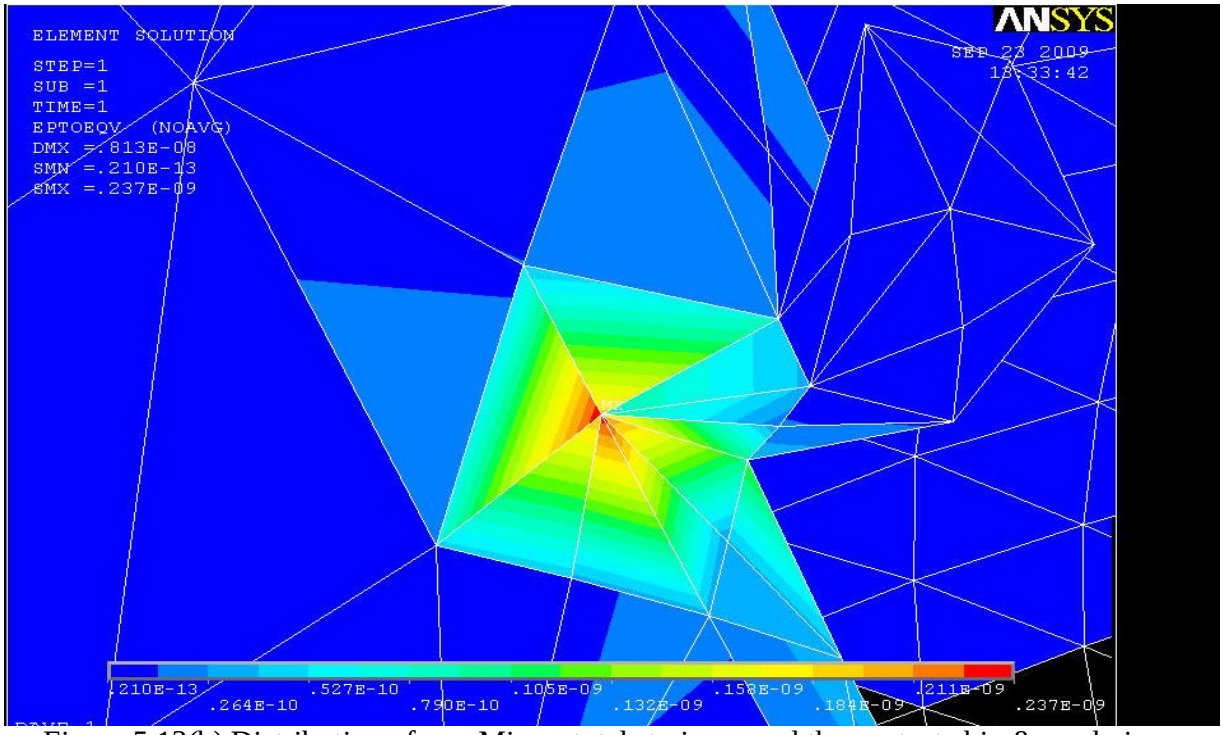

Figure 5.13(b) Distribution of von Misses total strain around the contact chip & workpiece, magnified view

Chapter 6

Conclusion and Recommendations

6.1 Conclusion

This study has showed the stress, shear stress and strain distribution in an isotropic material. The commercial finite element code ANSYS was used as a modeling tools. Predicted results of cutting forces were verified with experiments which is the end cutting of a tube on a lathe.

In this study, the main cutting force components of the three forces applied during an orthogonal cutting operation were measured with the help of FT102 Three Component Electronic Force Measuring Device. The effects of cutting speeds and tool geometry, i.e., rake angle on the main cutting force component were evaluated. The following conclusions and observations can be drawn from these investigations.

- ✓ The forces were measured by the FT102 Three Component Electronic Force Measuring Device. From the three force components we took the main cutting force only.
- ✓ Main cutting force for all cutting speeds was high for given positive rake angles.
- ✓ Positive rake angle produces higher shear angle; therefore, it leads to reduction of cutting forces. It also leaves a better surface finish since it assists the chip to flow away from the work-piece. But, excessive rake angle weakens the tool, thus causes to tool breakage. As a result, as the cutting force was reduced considerably, and the optimum rake angle for the given material, i.e., mild steel was obtained as 20 degree.

Methods and corresponding computer simulation for assessing of orthogonal metal cutting operation have been discussed. The orthogonal metal cutting was simulated via a finite element package (ANSYS). The approach described herein inclusive in that it integrates isotropic material with finite element analysis and incorporates the assessment of stress analysis around the contact of chip and material which have got the cutting force from the experimental results. As observed the results from the plots of stress and strain distribution around the surface contact between chip and material, the stress and strain shows a uniform distribution which can be predicted to be at the maximum penetration line contact surface of chip and material. This results show that the same result with that of literature survey part. The following conclusions and observations can be drawn from these modeling.

- ✓ The maximum stresses shown are distributed in the vicinity of the contact surface of chip and material.
- ✓ The stresses are uniform distributed near the contact face between chip and material.
- ✓ The maximum shear stresses are distributed around the contact of chip and material.
- ✓ The shear stresses are not uniformly distributed slightly away from the contact face.
- ✓ The stress intensity, von Misses stress and von Misses total strain are uniformly distributed infront of the contact zone between the chip and the material.

6.2 Recommendation and Future Works

After the discussions and conclusions, it might be said that the most important parameters affecting the results of process variable is the separation criterion. Different separation criterion give quite different results. Therefore a powerful separation criterion, which satisfies mechanics of the process and gives good agreement with experiment in terms of measurable variables, is needed to use in machining simulations.

In this paper the stress analysis of isotropic hollow cylindrical material with surface contact of chip and material is presented. Thus, one of the future continuation of this work could be extending it to other isotropic and composite materials.

In the current paper the stress analysis is carried out using the finite element method package ANSYS due its availability. In this case one of the future directions is to develop the solid model and its finite element discretization in a more versatile software package having these solid elements to have very good results.

References

[1] R. T. Pritchard , Workshop Processes, For Mechanical Engineering Technicians, Volume 1& 2.

[2] Mallock, A., The Action of Cutting Tool, Proceedings of Royal Society, 1881.

[3] Degarmo, E. P., Black, J. T. and Kohser, R. A., Materials and Processes in Manufacturing, Prentice-Hall International Inc., 1997.

[4] Merchant, M.E., Mechanics of Metal Cutting and Type 2 Chip, Journal of Applied Physics, 1945.

[5] Palmer, W.B. and Oxley, P.L.B., Mechanics of Orthogonal Machining, Proceedings of Institute of Mechanical Engineers, 1959.

[6] Lee, E.H. and Shaffer, B.W., Theory of Plasticity Applied to the Problem of Machining, Journal of Applied Mechanics, 1951.

[7] Shaw, M.C. and Mamin, P.A., Friction Characteristics of Sliding Surfaces Undergoing Sub-Surface Plastic Flow, Journal of Basic Engineering, 1960.

[8] Thomsen, E.G., Lapsey, J.T. and Grassi, R.C., Deformation Work Absorbed by the Workpiece During Metal Cutting, Transactions of American Society of Mechanical Engineers, 1953.

[9] Bacher, W.R., Marshall, E.R. and Shaw, M.C., The Size Effect in Metal Cutting, Transactions of American Society of Mechanical Engineers, 1952.

[10] Cotrell, A.H., Conference on the properties of metal at high rates of strain, Institution of Mechanical Engineers, 1957.

[11] Strenkowski, J.S. and Kyoung-Jim Moon, Finite Element prediction of chip geometry and tool/workpiece temperature, Journal of Engineering for Industry, 1990.

[12] Tyan, T. and Yang, W.H., Analysis of Orthogonal Metal Cutting Process, International Journal of Numerical Methods in Engineering, 1992.

[13] Iwata, K., Osakada, K. and Terasaka, Y., Process Modeling of Orthogonal Cutting by the Rigid Plastic Finite Element Method, Journal of Enginnering Materials and Technology, 1984.

[14] Liu, C.R. and Lin, Z.C., Effect of Shear Plane Boundary Condition on Stress Loading in Orthogonal Machining, International Journal of Mechanical Science, 1985.

[15] Komvvopoulos, K. and Erpenbeck, S.A., Finite Element Model of Orthogonal Metal Cutting, Journal of Engineering for Industry, 1991.

[16] Lin, Z. C. and Lin, S. Y., A Coupled Finite Element Model of Thermo Elastic Plastic Large Deformation for Orthogonal Cutting, International Journal of Engineering Materials and Technology, 1992.

[17] Caroll, J. T. and Strenkowski, J. S., Finite Element Model of Orthogonal Cutting with Application to Single Point Diamond Turning, International Journal of Mechanical Science, 1988.

[18] K.G. Chandiramani., Metal Cutting Technology and Experiments.

[19] Thomas Childs., Metal Machining Theory and Applications, 1999.

APPENDIX

Experimental data collected when turning (St. 37) mild steel.

No of test	Feed rate (mm/rev) 0.05	Rake Angle 15°	Cutting Speed (m/min)	Measured Cutting Force (N)			Average Measured Cutting Force (N)	Predicted Force (N)
				Case 1	Case 2	Case 3		
1			21	700	693	702	698.3	306.16
2			34	670	665	662	665.67	
3			41	640	642	641	641	
4			49	620	615	617	617.3	
5			58	650	643	646	646.3	

Table 3.3 (a) Results for experiment.1

No of test	Feed rate (mm/rev) 0.1	Rake Angle 15°	Cutting Speed (m/min)	Measured Cutting Force (N)			Average Measured Cutting Force (N)	Predicted Force (N)
				Case 1	Case 2	Case 3		
1			21	717	720	722	719.67	612.32
2			34	675	683	680	679.3	
3			41	650	652	651	651	
4			49	638	640	641	639.67	
5			58	660	662	661	661	

Table 3.3(b) Results for experiment.2

No of test	Feed rate (mm/rev) 0.05	Rake Angle 20°	Cutting Speed (m/min)	Measured Cutting Force (N)			Average Measured Cutting Force (N)	Predicted Force (N)
				Case 1	Case 2	Case 3		
1			21	540	538	541	539.67	306.16
2			34	520	520	522	520.67	
3			41	521	520	519	520	
4			49	580	585	582	582.3	
5			58	588	590	591	589.67	

Table 3.3 (c) Results for experiment.3

No of test	Feed rate (mm/rev) 0.1	Rake Angle 20°	Cutting Speed (m/min)	Measured Cutting Force (N)			Average Measured Cutting Force (N)	Predicted Force (N)
				Case 1	Case 2	Case 3		
1			21	660	665	662	662.3	612.32
2			34	635	640	642	639	
3			41	600	598	602	600	
4			49	727	728	730	728.3	
5			58	782	780	782	781.3	

Table 3.3 (d) Results for experiment.4

No of test	Feed rate (mm/rev) 0.05	Rake Angle 25°	Cutting Speed (m/min)	Measured Cutting Force (N)			Average Measured Cutting Force (N)	Predicted Force (N)
				Case 1	Case 2	Case 3		
1			21	665	670	667	667.3	306.16
2			34	640	638	640	639.3	
3			41	620	625	622	622.3	
4			49	702	700	703	701.67	
5			58	770	765	765	767.67	

Table 3.3 (e) Results for experiment.5

No of test	Feed rate (mm/rev) 0.1	Rake Angle 25°	Cutting Speed (m/min)	Measured Cutting Force (N)			Average Measured Cutting Force (N)	Predicted Force (N)
				Case 1	Case 2	Case 3		
1			21	680	678	677	678.33	612.32
2			34	658	660	662	660	
3			41	635	640	644	639.67	
4			49	715	710	720	715	
5			58	810	830	820	820	

Table 3.3 (f) Results for experiment.6

Table 5.1 (a) Modeling result for experiment of No. 1

Cutting force (N)	Displacement vector Sum for nodal solution (DMX)	Von Misses stress of nodal solution (SMX)	Von Misses stress of element solution (SMX)	Von Misses total strain of element solution (SMX)
698.3	0.125E-05	4743	7517	0.358E-07
665.67	0.108E-05	4539	7110	0.343E-07
641	0.101E-05	4336	6782	0.292E-07
617.3	0.978E-06	4200	6658	0.282E-07
646.3	0.103E-05	4398	6850	0.332E-07

Table 5.2 (b) Modeling result for experiment of No.2

Cutting force (N)	Displacement vector Sum for nodal solution (DMX)	Von Misses stress of nodal solution (SMX)	Von Misses stress of element solution (SMX)	Von Misses total strain of element solution (SMX)
719.67	0.128E-06	5978	6845	0.318E-07
679.3	0.112E-05	5825	6550	0.309E-07
651	0.101E-05	5598	6238	0.297E-07
639.67	0.958E-06	5515	6128	0.292E-07
661	0.103E-05	5650	6320	0.301E-07

Table 5.1 (c) Modeling result for experiment of No. 3

Cutting force (N)	Displacement vector Sum for nodal solution (DMX)	Von Misses stress of nodal solution (SMX)	Von Misses stress of element solution (SMX)	Von Misses total strain of element solution (SMX)
539.67	0.839E-06	2638	4041	0.192E-07
520.67	0.813E-06	4510	4979	0.192E-07
520	0.813E-06	4510	4979	0.192E-07
582.3	0.906E-06	5031	5554	0.264E-07
589.67	0.922E-06	5117	5649	0.269E-07

Table 5.1 (d) Modeling result for experiment of No.4

Cutting force (N)	Displacement vector Sum for nodal solution (DMX)	Von Misses stress of nodal solution (SMX)	Von Misses stress of element solution (SMX)	Von Misses total strain of element solution (SMX)
662.3	0.938E-06	5204	5745	0.274E-07
639	0.100E-05	5551	6128	0.292E-07
600	0.103E-05	5725	6320	0.301E-07
728.3	0.130E-05	7199	7947	0.378E-07
781.3	0.138E-05	7633	8426	0.401E-07

Table 5.1 (e) Modeling result for experiment of No. 5

Cutting force (N)	Displacement vector Sum for nodal solution (DMX)	Von Misses stress of nodal solution (SMX)	Von Misses stress of element solution (SMX)	Von Misses total strain of element solution (SMX)
667.3	0.968E-06	4201	6658	0.317E-07
639.3	0.999E-06	4336	6873	0.327E-07
622.3	0.105E-05	4539	7195	0.343E-07
701.67	0.109E-05	4743	7517	0.358E-07
767.67	0.125E-05	5420	8591	0.409E-07

Table 5.1 (f) Modeling result for experiment of No. 6

Cutting force (N)	Displacement vector Sum for nodal solution (DMX)	Von Misses stress of nodal solution (SMX)	Von Misses stress of element solution (SMX)	Von Misses total strain of element solution (SMX)
678.33	0.839E-06	4336	6873	0.327E-07
660	0.813E-06	4404	6980	0.332E-07
639.67	0.813E-06	4607	7302	0.348E-07
715	0.906E-06	4878	7732	0.368E-07
820	0.922E-06	6775	10739	0.511E-07